**Passive Acoustic Detection and Measurement of Rainfall at Sea and an Empirical Ocean Ambient Sound Model**

Bin-Bing Ma

A dissertation submitted in partial fulfillment

of the requirements for the degree of

Doctor of Philosophy

University of Washington

2004

Program Authorized to Offer Degree: Oceanography

University of Washington

Graduate School

This is to certify that I have examined this copy of a doctoral dissertation by

Bin-Bing Ma

and have found that it is complete and satisfactory in all respects,

and that any and all revisions required by the final

examining committee have been made.

Committee Members:

Chair of Supervisory Committee

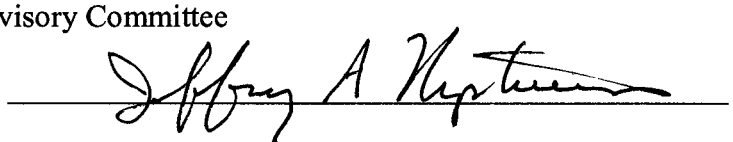

Jeffrey A. Nystuen

Reading Committee

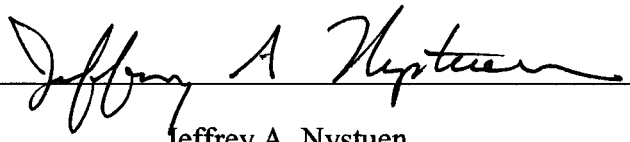

Jeffrey A. Nystuen

Eric D'Asaro

Ren-Chieh Lien

Date: 9 December 2004

In presenting this dissertation in partial fulfillment of the requirements for the doctoral degree at the University of Washington, I agree that the Library shall make its copies freely available only for scholarly purposes, consistent with "fair use" as prescribed in the U.S. Copyright Law. Requests for copying or reproduction of this dissertation may be referred to Proquest Information and Learning, 300 North Zeeb Road, Ann Arbor, MI 48106-1346, to whom the author has granted " the right to reproduce and sell (a) copies of the manuscript in microform and/or (b) printed copies of the manuscript made from microform."

Signature 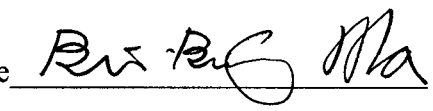

Date December-10-2004

University of Washington

**Abstract**

**Passive Acoustic Detection and Measurement of Rainfall at Sea and an Empirical Ocean Ambient Sound Model**

Bin-Bing Ma

Chair of the Supervisory Committee:

Associate Professor Jeffrey A. Nystuen

School of Oceanography

Rainfall over the ocean is one of the most important climatic parameters for both oceanic and atmospheric science. Traditional accumulation-type rain gauges are difficult to operate at sea, and so an alternate technique for measuring rain using underwater sound has been developed. Over 90 buoy-months of ambient sound spectra have been collected on the Tropical Atmosphere Ocean Project (TAO) array since 1998. By applying the Vagle et al. (1990) wind speed algorithm, the instrument noises and sensitivity bias for the absolute calibration of each Acoustic Rain Gauge (ARG) are obtained. An acoustic discrimination process is developed to retrieve the pure geophysically generated signals. A new single frequency rainfall rate algorithm is proposed. The acoustic rainfall accumulation comparisons with ancillary data show the comparable results for both long (seasonal) and short (hours) time scales. By identifying the characteristics of sound spectra generated from wind and rain, an empirical ocean ambient sound model is constructed. This model has five components for different frequency bands, each physically based on the physical interaction of the sound generating mechanisms for wind and rain. The results show significant improvements predicting sound levels from 1 to 50 kHz when compared with a previous model, APL-UW 9407. Using the temporal separation of rainfall detection to define an individual rainfall event, a typical rainfall event in the study region (at 10°, 12°N, 95°W) has a mean duration of 30 minutes and a mean accumulation of 8mm, respectively. However, large events with durations over than an hour, contribute 50% of

the total accumulation. In contrast, events in the Western Tropical Pacific Ocean (at 0°, 165°E) are smaller and of shorter duration, 4.6 mm and 18 minutes, respectively, with fewer large events present. The mean rainfall rate when it is raining is the same for both locations, 15mm/hr. Locally, rainfall events produce patchiness of relatively cool and fresh water that is mixed vertically. The fresh patch of water is also advected horizontally. The mean rate of vertical mixing is 25-200 cm/hr to a depth of 1 meter and 65 cm/hr to depths of 5 and 10 meters.

## TABLE OF CONTENTS

## LIST OF FIGURES

## LIST OF TABLES

## ACKNOWLEDGEMENTS

I would like to express my gratitude to Professor Jeffrey A. Nystuen for providing me the opportunity to work on the project of acoustic detection on oceanic rainfall. His inspiration and encouragement made this dissertation possible. I would like to thank my entire supervisor committee members for advise and comments on this work. I would like to thank Dr. McPhaden who led the NOAA-PMEL–TAO, and Dr. Cronin who led the NOAA-PMEL-EPIC programs for providing the comparison buoy data. I like to thank Dr. Cifelli of Colorado State University for providing the RV Ron Brown radar data. I also like to thank the Taiwanese Navy for the funding and support of my study.

## DEDICATION

*To my family*

# Chapter 1: Passive Acoustic Detection and Measurement of Rainfall at Sea

## 1.1 Introduction

The ocean ambient noise has often been treated as "unwanted" background sound at any given location and time. Different sources of ambient sound contribute to the overall sound level at different frequency ranges and time spans. Some of the sources are also heavily depend on the location. For example, at some continental shelf regions, biological sounds can be the dominant ambient noise source. Sites near ocean shipping lanes are much noisier than other locations at the low frequencies. For the higher frequencies (50 kHz plus), thermal noise is a dominant source whereas the other sources are often attenuated. For the frequency range from 1 to 30 kHz, wind generated noise is the major persistent noise source component, characterized by a spectrum with a uniform negative slope. However when rain is present, the rain generated sound usually dominates all the other sources in this frequency band. In summary, the ocean ambient sound is time, frequency, and location dependent. If one can detect when a particular dominant source is present (e.g. rain), then that "unwanted noise" can be treated as a "wanted signal" and be used to quantify its presence. The temporal and frequency distribution of typical sources of ocean ambient sound are illustrated in figure 1.1.

Rainfall measurement over the ocean is very difficult to achieve because of its inhomogeneity in both time and space. Furthermore, the natural roughness of air-sea interface produces a potentially catastrophic environment for surface instruments on moorings, and this is reflected in the data quality from physical collection-types of rain gauges on moorings. Other techniques for measuring the rainfall over the ocean use satellite- based instruments. These should provide a large-scale coverage for the measuring different parameters associated with rainfall. However, the satellite's temporal resolution is usually very low (e.g. eight satellite passes per day). Surface truth measurements are needed for the various satellite-based rainfall measurements. Luckily,

rain is also one of the principal natural sources of underwater sound (Nystuen, 2001). This allows acoustic measurements of rainfall. Although there are sometimes man-made or biological noises that are loud and could potentially interfere with the acoustical measurement of rain, these noises are generally intermittent or geographically localized.

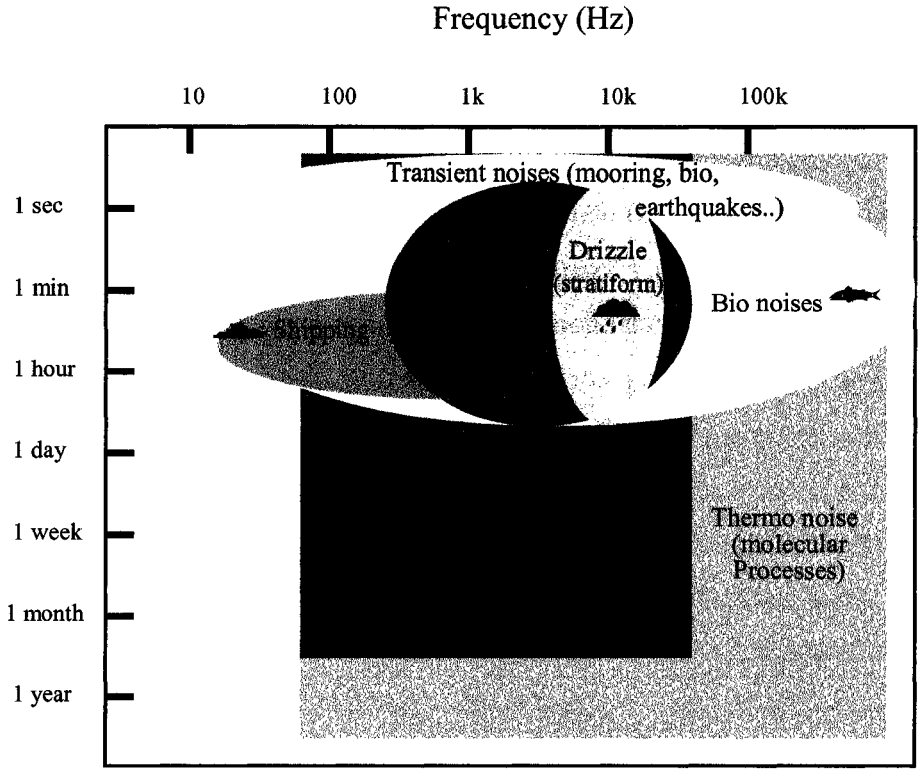


*Figure 1.1 The temporal and frequency distribution of typical sources of ocean ambient sound.*

This chapter first describes some background information and other ancillary data used in this study. A new method is proposed using the Vagle et al. (1990) wind speed algorithm to determine the frequency-dependent instrument noise and sensitivity bias to achieve the hydrophones' absolute calibration. The acoustic discrimination process for the qualification of wind and rain generated geophysical signals is described. For quantification of rainfall rate, an orthogonal least squares regression between the ARG acoustic data and a subset of 1-minute interval R.M. Young self-siphoning rain gauges

data during the rainfall events is used to produce an empirical algorithm. The acoustic discrimination process and rainfall algorithm is tested on the acoustic data from other deployments (10° N, 95°W and 12°N, 95°W), and compared with the satellite-based Tropical Rain Measuring Mission (TRMM) rainfall product 3B42 and R.M. Young rain gauges co-located on the surface moorings.

## 1.2 Background

Naturally occurring raindrops range in size from about 300 microns diameter (a drizzle droplet) to over 5 mm diameter (often at the beginning of a heavy downpour). As the drop size changes, the shape of the splash changes and so does the subsequent sound production. Laboratory and field studies (Medwin et al., 1992; Nystuen 1996, 2001) have been used to identify five acoustic raindrop sizes (Table 1.1). For tiny drops (diameter < 0.8 mm), the splash is gentle, and no sound is detected. On the other hand, small raindrops (0.8 - 1.2 mm diameter) are remarkably loud. The impact component of their splash is quiet, but the geometry of the splash is such that a bubble is generated by every splash in a very predictable manner (Pumphrey et al., 1989). These bubbles are relatively uniform in size, and therefore frequency, and are very loud underwater. Small raindrops are present in almost all types of rainfall, including light drizzle, and are therefore responsible for the remarkably loud and unique underwater "sound of drizzle" heard between 13-25 kHz, the resonance frequency for bubbles created by the small raindrops. Interestingly, the splash of the next larger raindrop size, medium (1.2-2.0 mm diameter), does not trap bubbles underwater, and consequently medium raindrops are relatively quiet, much quieter than the small raindrops. The only acoustic signal from these drops is a weak impact sound spread over a wide frequency band. For large (2.0-3.5 mm diameter) and very large (> 3.5 mm) raindrops, the splash becomes energetic enough that a wide range of bubble sizes are trapped underwater during the splash, producing a loud sound that includes relatively low frequencies (1-10 kHz) from the larger bubbles. For very large raindrops, the splat of the impact is also very loud with the sound spread over a wide frequency range

(1-50 kHz). Thus, each drop size produces sound underwater with unique spectral features that can be used to acoustically identify the present of that drop size within the rain.

In any given time, the local hydrophone pressure, $P_a$, at the measurement site can be expressed as the sum of all sound sources around the hydrophone in micropascals,

$$P_a = P_r + P_w + P_{ss} + P_{ml} + P_{st} + P_{other} \tag{1.1}$$

where *r, w, ss, ml*, and *st* denote rain, wind, sea state, marine life and ship traffic, respectively (Black et al., 1997). The sound pressure level (SPL) in decibels (dB) can be expressed as

$$SPL\ (f) = 10\ \log_{10}\left(\frac{P_a^{\ 2}}{P_{ref}^{\ 2}}\right) \quad dB\ re\ 1\mu Pa^2 / Hz \tag{1.2}$$

where $P_a^2$ is the variance of the pressure fluctuations in the 1 Hz bandwidth, and $P_{ref}$ is a reference pressure density level at 1 $\mu Pa^2$ /Hz. The contribution to the pressure fluctuation from different sources cannot be separated since they are indistinguishable. But if different sources have unique frequency spectra *SPL(f)*, then times with only particular sources present can be identified, for example, $P_w$ (wind only), $P_r$ (rain only), and $P_r + P_w$ (rain and wind combined).

The pressure signal due to wind and rain comes from the ocean surface. If the sound source is assumed to be uniformly distributed, then the sound intensity at source depth, $h$, below the surface can be related to the sound intensity at the surface, $I_0$, by

$$I(h) = \int I_0 \cos^2\theta \quad atten(p)\, dA \tag{1.3}$$

where $\theta$ is the zenith angle and *atten(p)* describes the attenuation due to geometric spreading and absorption along the acoustic path, $p$. By relating $I_0$ to rainfall rate,

acoustic measurements at rainfall rate can be obtained (Nystuen, 2001). If absorption and refraction are neglected, the measurement should be independent of depth. For any particular deployment, the attenuation along the acoustic path can be complicated, but have only resulted in minor corrections in other studies, e.g., Vagle et al., 1990.

*Table 1.1 Acoustic raindrop sizes and types of bubble generated. The raindrop sizes are identified by different physical mechanisms associated with the drop splashes*

| Drop Size | Diameter | Sound | Frequency range (kHz) | Bubbles generated | Splash character |
|---|---|---|---|---|---|
| Tiny | < 0.8 mm | Silent | | No | Gentle |
| Small | 0.8-1.2 mm | Loud bubble | 13 - 25 | Type I | Gentle<br>with bubble every splash |
| Medium | 1.2-2.0 mm | Weak impact | 1 - 30 | No | Gentle,<br>No bubbles |
| Large | 2.0-3.5 mm | Impact,<br>Loud bubbles | 1 - 35<br>2 - 35 | Type II, III | Turbulent<br>Irregular bubble entrainment |
| Very Large | >3.5 mm | Loud impact<br>Loud bubbles | 1 - 50<br>1 - 50 | Type II, III | Turbulent<br>Irregular bubble entrainment<br>Penetrating jet |

## 1.3 The instrument - Acoustic Rain Gauges (ARGs)

The Acoustic Rain Gauges (ARGs) consist of an ITC-8263 hydrophone, signal pre-amplifiers and a recording computer (Tattletale-8) (Fig. 1.2). The nominal sensitivity is -160 dB relative to 1 V/μPa and the pre-amplifier instrument noise has the equivalent oceanic background noise level of about 28 dB relative to 1 $\mu Pa^2/Hz$. Band-pass filters are present to reduce saturation from low frequency sound (high pass at 300 Hz) and aliasing from above 50 kHz (low pass at 40 kHz). The ITC-8263 hydrophone sensitivity also rolls off above its resonance frequency, about 40 kHz. A data collection sequence consists of four 1024 point time series collected at 100 kHz (10.24 ms each) separated by

5 seconds. Each time series is fast Fourier transformed (FFT) to obtain a 512-point (0-50 kHz) power spectrum.

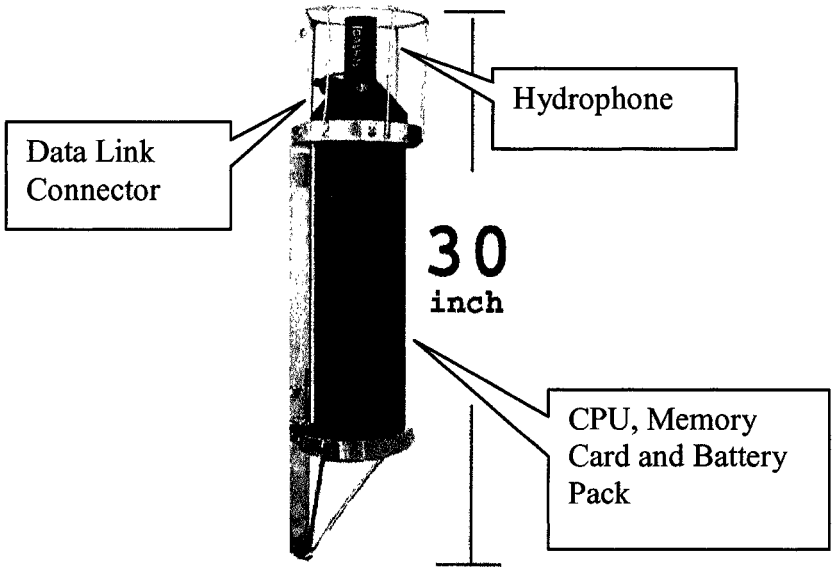


*Figure 1.2 Acoustic Rain Gauge*

These four spectra are averaged together and spectrally compressed to 64 frequency bins, with frequency resolution of 200 Hz from 100 to 3,000 Hz and 1 kHz from 3 to 50 kHz. These spectra are evaluated individually to detect the acoustic signature of rainfall and then are recorded internally. Two algorithms are used for initial rainfall classification.

The rain-detection algorithm is:

$$SPL_{21kHz} > 194\text{-}2.35*SPL_{5.4kHz}$$

or

$$SPL_{21kHz} > 48\ dB\ and\ SPL_{5.4kHz} > 53\ dB \qquad (1.4)$$

The drizzle-detection algorithm is

$$SPL_{21kHz} > 44 \text{ and } SPL_{21kHz} > 14 + 0.7 * SPL_{8.3kHz} \quad (1.5)$$

These detection algorithms, are designed to detect all possible rainfall situations. However, loud noises are also detected. This noise component of the data needs to be removed by a further classification analysis. The partition of detection algorithms are shown in figure 1.3.

The ARGs have been deployed on the Tropical Atmosphere Ocean project (TAO) moorings since 1998 at different locations with depths from 28 to 98 meters (McPhaden et al., 1998). The depth was chosen to be above the thermocline, lessening the effects of acoustic refraction, and to maximize sampling area, so that the buoy itself does not occupy a significant portion of the effective listening area. Equation 1.3 can be used to estimate the effective sampling area at the surface. Neglecting refraction and absorption, 90% of the signal is arriving from a sampling area equal to:

$$\text{Surface sampling area} \cong \pi(3h)^2 \quad (1.6)$$

where $h$ is the depth of the hydrophone. The integrating area of the hydrophone is important for two reasons. First, rainfall is inhomogeneous on all scales, but rainfall measurements are needed on large temporal or spatial scales. An instrument with a large inherent sampling area should produce a better "mean" rainfall statistic. Second, the large spatial sampling allows the short temporal sampling periods being used for each data sample to include many individual raindrop splashes (Nystuen, 2001), and therefore record a statistically smooth spectrum.

The temporal sampling strategy is designed to allow the instrument to record data for up to one year and yet detect the relatively short time intervals of associated with rainfall (Nystuen, 1998). In order to achieve this goal, the ARG enters a low power mode "sleep mode" between each data sample. For these deployments, the ARGs "sleep" for 8-9 minutes and then sample the sound field. If "rain" is detected, the sampling rate

changes to 1-minute (or 3-4 minutes if "drizzle" is detected) and stays at the higher sampling rate until rain is no longer detected. For the rain or drizzle detected condition, four spectra are stored (separated by 5 seconds). For no-rain condition, one averaged spectrum is stored.

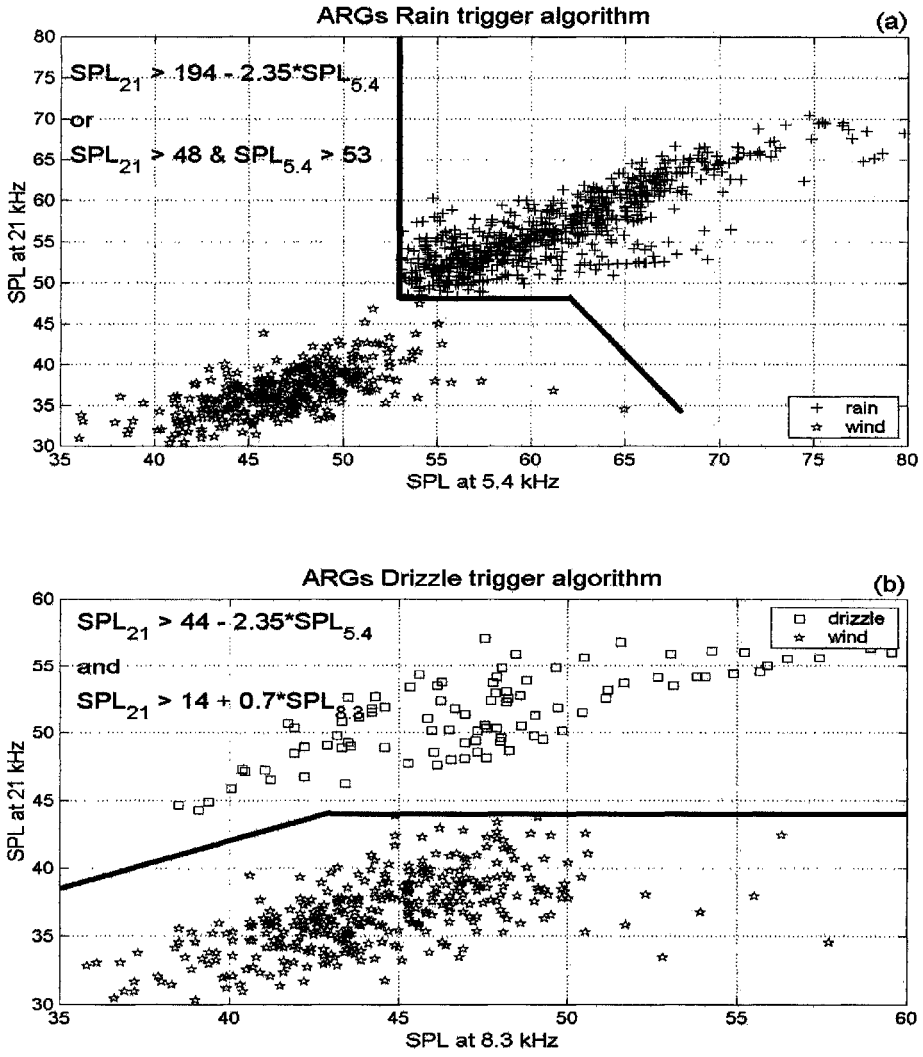


*Figure 1.3. The scatter diagram of rain detection (top), and drizzle detection (bottom) are the examples from ARG "K" which was deployed at 0, 165°E in Year 2000. These algorithms are used for the initial screening of potential precipitation event and trigging the data logging sequence on the ARGs.*

ARGs have been deployed in several different climate regions as shown in figure 1.4. Two climate regions, the Western Pacific warm pool and Inter-tropical Convergence Zone (ITCZ), have been chosen for this study. These open ocean locations should have less contribution of biological sources than continental shelf regions, and not be affected by bottom reverberation. About 90 buoy-months of acoustic data are available for the analysis. The acoustic data sets used in this study are listed in table 1.2.

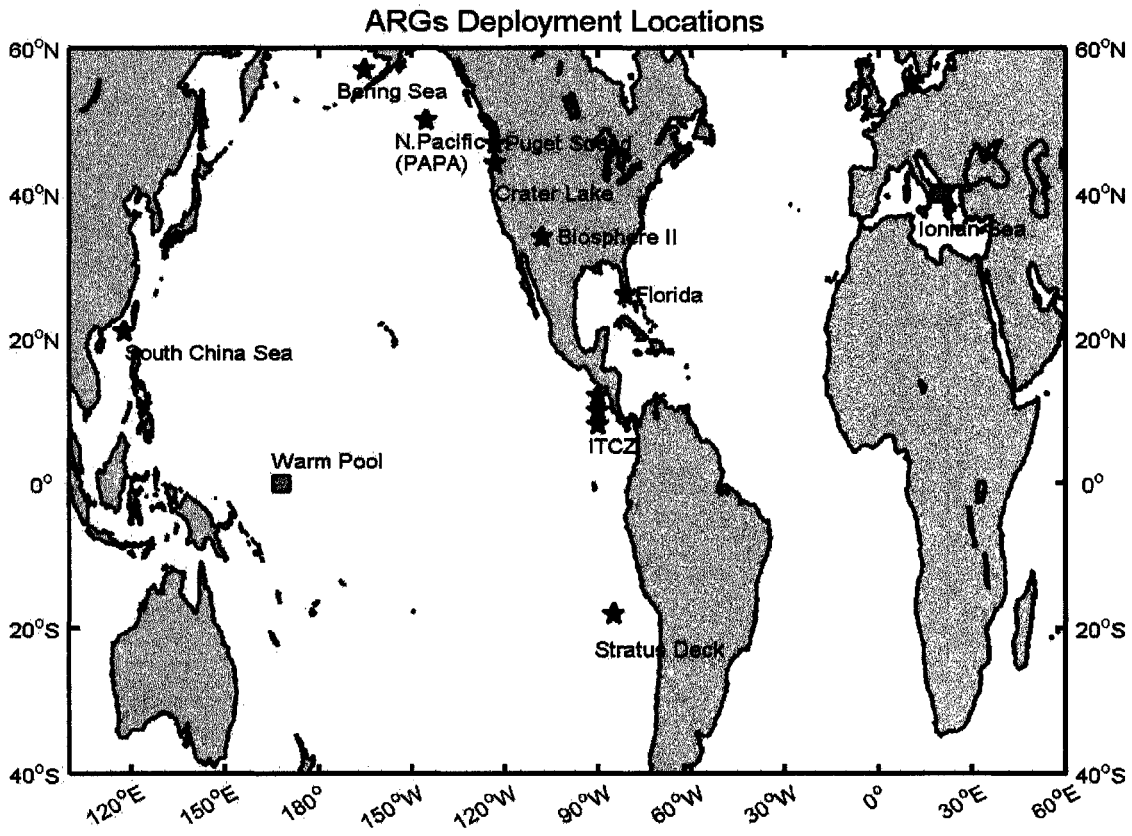


*Figure 1.4 The deployment of ARGs in different climate regions since 1996. The data at the Western Pacific warm pool and Intertropical Convergence Zone (ITCZ), which have about 90 buoy-months acoustic record are used in this study. The "□" represents multiple depths deployment.*

*Table 1.2. The acoustic data sets used in this study. * indicates the data set used in produce the rainfall rate algorithm. Note that the "B" and "K" ARGs are deployed in the same mooring but at different depths.*

| Location | Deployment | | | | | |
|---|---|---|---|---|---|---|
| | **ARG** | **Log** | **Depth** | **Record Setting** | **Deploy Period** | **Note** |
| 0, 165 E | * "B" | 4 | 20m | R-1 min D-4 min W-9 min | Mar 1, 2000 -Jul 20, 2000 | The wind estimate higher than R.M. Young anemometer by 0-2m/s |
| 0, 165E | * "K" | 1 | 50m | R-1 min D -3 min W -9min | Mar 1, 2000 -Jul 20, 2000 | Wind speed conversion well match with R.M. Young anemometer. |
| 0, 165E | "A" | 4 | 8m | R -0.5 min D- 4 min W -9 min | July 23, 2000 -Nov 20, 2000 | Noisy sample |
| 0, 165 E | * "D" | 1 | 98m | R-1 min D -3 min W -9min | Jul 23, 2000 -Nov 20, 2000 | Successful |
| 0, 165E | "A" | 5 | 28m | R -0.5 min D -4 min W -9 min | Jul 2001 -Jan 2002 | Successful |
| 0, 165E | "G" | 2 | 98m | R -1 min D -3 min W -9min | Jul 2001 -Nov 2001 | Hydrophone Malfunction after November |
| 8N, 95W | "G" | 1 | 38m | R -1 min D -3 min W -9min | Dec, 1999 Mar, 2000 | Not much precipitation in this period. |
| 8N, 95W | "L" | 1 | 38m | R -1 min D -3 min W -9min | Apr 22, 2000 - Nov10, 2000 | Successful |
| 10N, 95W | "E" | 1 | 38m | R -1 min D -3 min W -9min | Dec, 1999 -Apr, 2000 | Not much precipitation in this period |
| 10N 95W | "I" | 1 | 38m | R -1 min D -3 min W -8min | Apr21, 2000 -Nov, 2000 | Strong local noise |
| 10N, 95W | * "C" | 1 | 38m | R -1 min D -3 min W -8min | Nov 10, 2000 -Apr 16, 2001 | Acoustic data at first 100day, than noise present in two 10-20day periods. |
| 10N, 95W | "L" | 2 | 38m | R -1 min D -3 min W -9min | Apr, 2001 -Mar 31, 2002 | Successful |
| 12N, 95W | "F" | 1 | 38m | R -1 min D -3 min W -9min | Dec, 1999 -Apr, 2000 | Not much precipitation in this period |
| 12N, 95W | "H" | 1 | 38m | R -1 min D -3 min W -8min | Apr 23, 2000 -Dec 2, 2000 | Periodical local noises present. |
| 12N, 95W | "D" | 2 | 38m | R -1 min D -3 min W -9min | Mar 27, 2001 -Apr 1, 2002 | Successful |

[1] *ARGs settings for difference condition; R: Rain trigger; D: Drizzle trigger; W: Wind only.*

[2] *The ARG "A" and "B" record 36 frequency channels with one spectrum for rain, drizzle, and wind in every sampling interval. The other ARGs record 64 frequency channels with 4 spectra for rain and drizzle (each separated by 5 second), and one spectrum for wind.*

## 1.4 Ancillary data from mooring and satellite

Pacific Marine Environmental Laboratory (PMEL) ocean moorings data (http://www.pmel.noaa.gov/tao) and Tropical Rain Measuring Mission (TRMM) satellite data (http://trmm.gsfc.nasa.gov) are used in the intercomparison of ARGs data for algorithm development and validation.

### *a. Data from ATLAS mooring*

The Next Generation Autonomous Temperature Line Acquisition System (ATLAS) buoys (Milburn et al., 1996; McPhaden et al., 1998) are deployed on the TAO array of the tropical Pacific Ocean. ARGs were mounted on the mooring lines at the various locations. Selected ancillary data sets from the moorings are used in the study.

1) R.M. YOUNG ANEMOMETER DATA

A R.M. Young (RMY) Company anemometer is mounted on the ATLAS mooring at 4 meters height. The data values are 10-minute averaged wind vectors. The error estimate is ±0.3 m/s or 3% of the wind speed, whichever is greater (Freitag et al., 2001). By using the Coupled Ocean-Atmosphere Response Experiment (COARE) V2.5 flux algorithm (Fairall et al. 1998), these values are converted to equivalent 10 meters height wind speed. The 10 meters winds are slightly stronger than 4m winds values by factors 1.010~1.0217. This is smaller than the error estimate of R. M. Young anemometer. The surface anemometer wind speed data are used to predict the ambient sound level at 8 kHz. This allows the sensitivity bias and instrument noise of the hydrophone to be identified.

2) R.M. YOUNG RAIN GAUGES DATA

Precipitation measurements on ATLAS buoys are made using R.M. Young Company Model 50203-34 self-siphoning rain gauges mounted 3.5 meters above the ocean surface. The instruments have a 100-$cm^2$ (11.3-cm diameter) catchment cylinder mounted on top of a fill tube. The measuring tube has a maximum capacity of 500mL, equivalent to 50 mm of rainfall accumulation, after which it automatically drains via a siphon. Siphon events take about 30 seconds, and are typically identified by sharp declines in volume for two consecutive samples. In real-time processing, these events are ignored. The 1-minute volume samples are stored on board the mooring while at sea, and are available for postprocessing after recovery. In post-deployment processing, data associated with siphon events are flagged, typically removing three minutes worth of data centered on the event. Once the mooring is recovered, the 1-minute accumulations are first flagged for obviously erroneous data. A 16-min Hanning filter is then applied to these data to generate smoothed 10-minute accumulations. The estimated instrumental error for 10-minute derived rainfall rates is 0.4 mm/hr when the rain present, and is 0.1 mm/hr when there is no rain (Serra et al., 2001).

***b. TRMM precipitation product 3B42***

TRMM is a satellite dedicated to the measurement of precipitation in the tropics. TRMM satellite was launched on November 27, 1997 and is maintained an altitude approximately 350 km and an inclination of 35 degrees to the Equator. The satellite acquires approximately 16 orbits of data per day for mapping tropical rainfall between latitudes of 38 degrees north and south of the equator. Rainfall sensors include a precipitation radar (PR), a microwave imager (TMI) and a visible/infrared sensor (VIRS). Data from these instruments are combined in a variety of ways to produce rainfall products which are available through the NASA Goddard Distributed Active Archive Center (DAAC). Several levels of process are used in producing different products. The rainfall product 3B-42 is a daily precipitation product which produced from spatially averaged on a 1° by 1° grid which combined rain structure (2B-31) and VIRS calibration (1B-01) to adjust IR estimates from geosynchronous IR observations. Global estimates

are made by adjusting the GEOS Precipitation Index (GPI) to the TRMM estimates.

## 1.5 Sensitivity correction for Deep Ocean Geometry

### *a. Background noise removal – power summation method*

The ocean ambient sound measuring sites in the ITCZ and Pacific warm pool are away from coastal regions with the depths over 3,700 m minimizing bottom reflection effects and biological sources associated with continental shelves. At the times when all other sources ($P_r$, $P_w$, $P_{ss}$, $P_{ml}$, $P_{st}$) are absent, the only source left will be background noise. For a given time period the background noise can be defined as minimum of the measured records $P_{bk} = min(P_a(t))$. Because the background noise is smallest contributor to the overall sound pressure, removing the $P_{bk}$ from the signal will be important only if the other sources are also small. To eliminate $P_{bk}$ from acoustic measurement, we note that

$$P_c^2 = P_a^2 - P_{bk}^2 - 2\langle P_a P_{bk} \rangle \tag{1.7}$$

where the $P_c^2$ is the *root-mean-square* pressure without background. Since the $P_{bk}$ is assumed to be independent of the other pressure sources, the cross term is assumed to be zero. This leads to

$$P_c^2 = P_a^2 - P_{bk}^2 \tag{1.8}$$

Thus, the background noise can be eliminated by the following manipulation:

$$10\log_{10}\left(P_c^2\right) = 10\log_{10}\left(P_a^2 - P_{bk}^2\right) \tag{1.9}$$

$$P_a^2 - P_{bk}^2 = 10^{(SPLa/10)} - 10^{(\min(SPLa)/10)} \tag{1.10}$$

*Table 1.3 The measured sound pressure level (db re 1μPa$^2$/Hz) vs. corrected value which use the 27.5 dB as background noise reference.*

| Measured SPL | Corrected SPL | Difference |
|---|---|---|
| 30 dB | 26.41 dB | 3.59 dB |
| 40 dB | 39.74 dB | 0.26 dB |
| 50 dB | 49.97 dB | 0.03 dB |

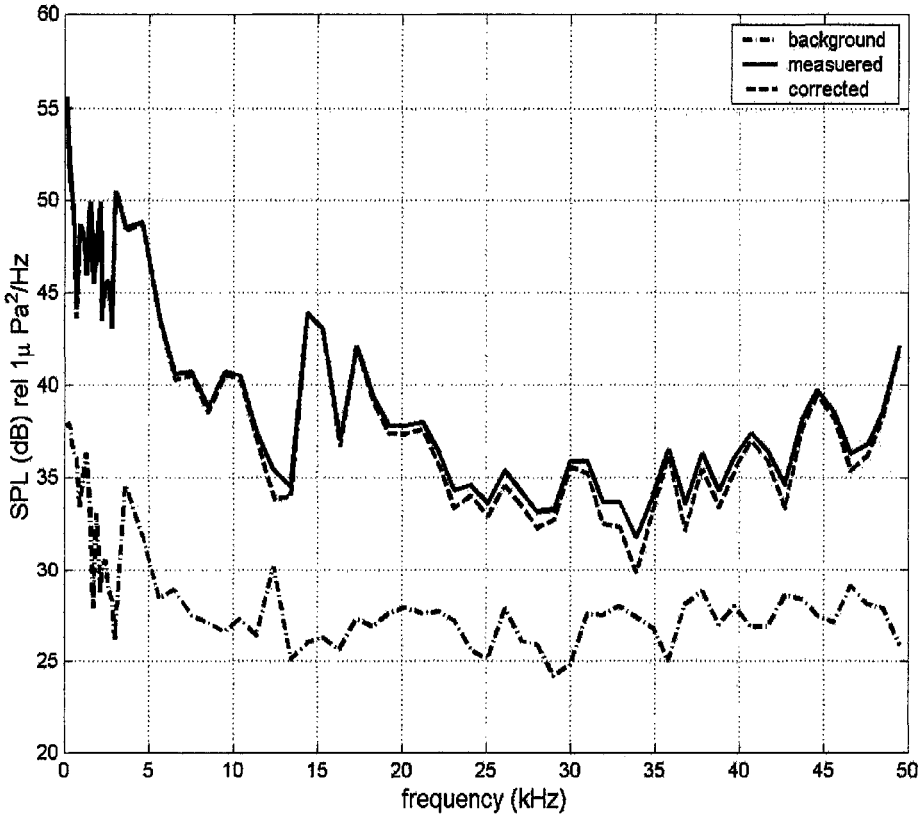


*Figure 1.5 Example of background noise removal. The dash-dotted line is the background noise which is the lowest spectrum from a week-long record. The solid line is an arbitrary sample spectrum, and the dash is the corrected spectrum which applying equations 1.9 and 1.10 to remove the background noise contribution.*

The ARGs only record the power spectrum density data in order to save on-board storage space. Equation 1.10 provides a means to remove the background noise from the data. The typical background level at 8.5 kHz is about 27.5 dB relative to 1μPa$^2$/Hz and

the corresponding correction for different measured sound levels is shown in table 1.3. An example of full spectral correction before and after background noise removal is shown in the figure 1.5. The background noise removal is only important when the background noise level is close to the sampled level.

***b. Sensitivity bias and instrument noise***

The frequency-dependent sensitivity correction is an important process which needs to be addressed before further data analysis, especially if the SPL will be used to quantify the geophysical signal. The hydrophone manufacturer provides a receiver sensitivity correction that is produced from a single point source. But the geometry of the open-ocean is very different from the confined lab environment. The ambient sound source is from a broad surface area. If one applies a known uniform source in the laboratory, and then integrates the receiver sensitivity correction for multiple paths, the sensitivity correction can be acquired for the geometry of ambient sound measurement. But this is very difficult to achieve even in an environment-controlled laboratory. Thus a new approach is tried, which assumes that the sensitivity correction $SC(f)$ of the open ocean is the sum of the receiver sensitivity correction, sensitivity bias and the instrument noise. It has the following form:

$$SC(f) = SC_b + SC_i(f) \tag{1.11}$$

where $SC_b$ is the sensitivity bias, $SC_i$ is the instrument noise (frequency dependent), and the units is in $dB\ re\ 1\mu Pa^2 / Hz$.

The wind generated noise is produced by agitation of the surface water and includes bubble noise created by breaking waves and surf. Wind spectra have a constant negative slope versus logarithmic frequency with sound levels decreasing above 500Hz at a rate of about 6 dB per octave (Kundsen et al., 1948; Wenz, 1962; Urick, 1983). Vagle et al. (1990) proposed an algorithm between wind speed and SPL at 8 kHz, and they

suggested that averages greater than at least three hours are needed to obtain reliable wind estimates from the ambient sound.

$$W = \left[ 10^{\left(\frac{SPL_{8\,kHz}}{20}\right)} + 104.5 \right] / 53.91 \qquad (1.12)$$

*W: wind speed at 10 meters height (m/sec)*

The surface anemometers were co-located on all of the moorings. Thus an expected "wind only" sound level can be predicted by applying equation 1.12. The $SC_b$, the sensitivity bias, is the offset from measured SPL values at 8 kHz. The frequency-dependent instrument noise, $SC_i$, is found by assuming a uniform slope for the wind spectra and using a linear regression to find deviations. The corrected signal is given by:

$$SPLc(f) = SPL(f) - SC(f) \qquad (1.13)$$

where *SPLc(f)* is the corrected acoustic signals in dB relative 1 $\mu Pa^2$ /Hz. A flow diagram for this process is shown in figure 1.6 with further details described in Appendix A.

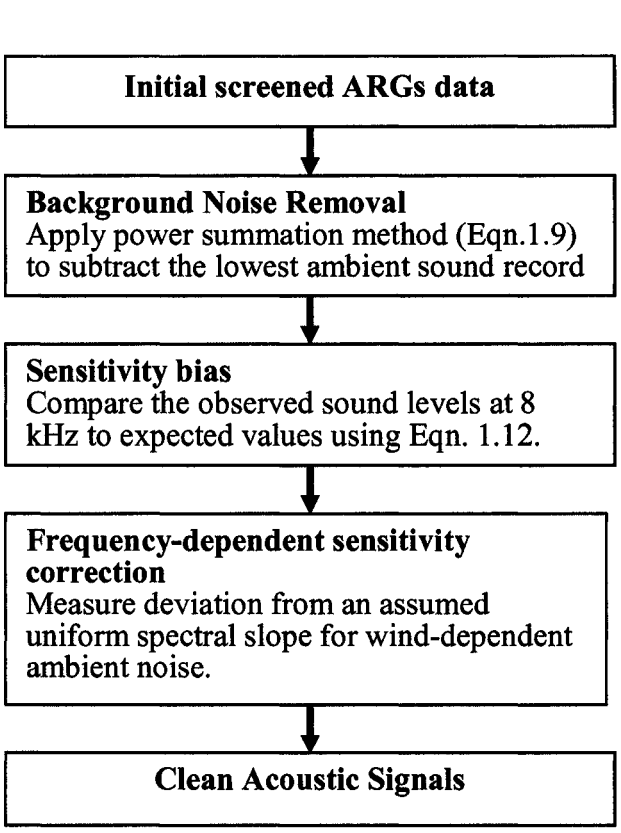


*Figure 1.6 The sensitivity correction flowchart*

## 1.6 Acoustic discrimination process

The basic concept of the acoustic discrimination process is to use the unique spectral and temporal characteristics of different types of rainfall to detect the present of precipitation. Spectra not consistent with expected geophysical signals are assumed to be "noise" and are removed from the data. The acoustic data are divided into wind detection and precipitation (rain and drizzle) detection according to the initial screening (Eqn. 1.4 and 1.5) and are treated separately. For the wind detection data, one spectrum was stored during initial screening at the data collection, five different types of spectral shape tests are applied, see Appendix B for details.

For data initially classified as precipitation (Eqn. 1.4 and 1.5), sets of four spectra are stored and each separated by five seconds. The discrimination process removes two types of noise. The first is associated with "bangs", when one of the spectra in the group of four is much louder than the other three spectra. For example, a wave slap on the hull of the surface buoy would produce a loud noise detected by just one of the measured spectra. Assuming that the rainfall signal is continuous over at least 20 seconds, then such a transient noise is inconsistent with rainfall and the record is flagged as noise. The second test is similar to the wind detection noise test and uses the shape at the recorded spectrum to eliminate sound spectra that are not consistent with known rainfall signals. Three sample spectra which represent drizzle, light rain and strong rain are used for comparing with observed spectra in all frequency bands. If the observed spectra are inconsistent with these sample spectra, the spectrum will be flagged and rejected. Finally, there is a continuity check. This assumes that real geophysical events (rainfall) are longer than a single data point. Any isolated measurement is removed by checking the reoccurrence of rainfall signals. The sequence of overall discrimination process is shown in the figure 1.7, and details and illustrations are given in Appendix B.

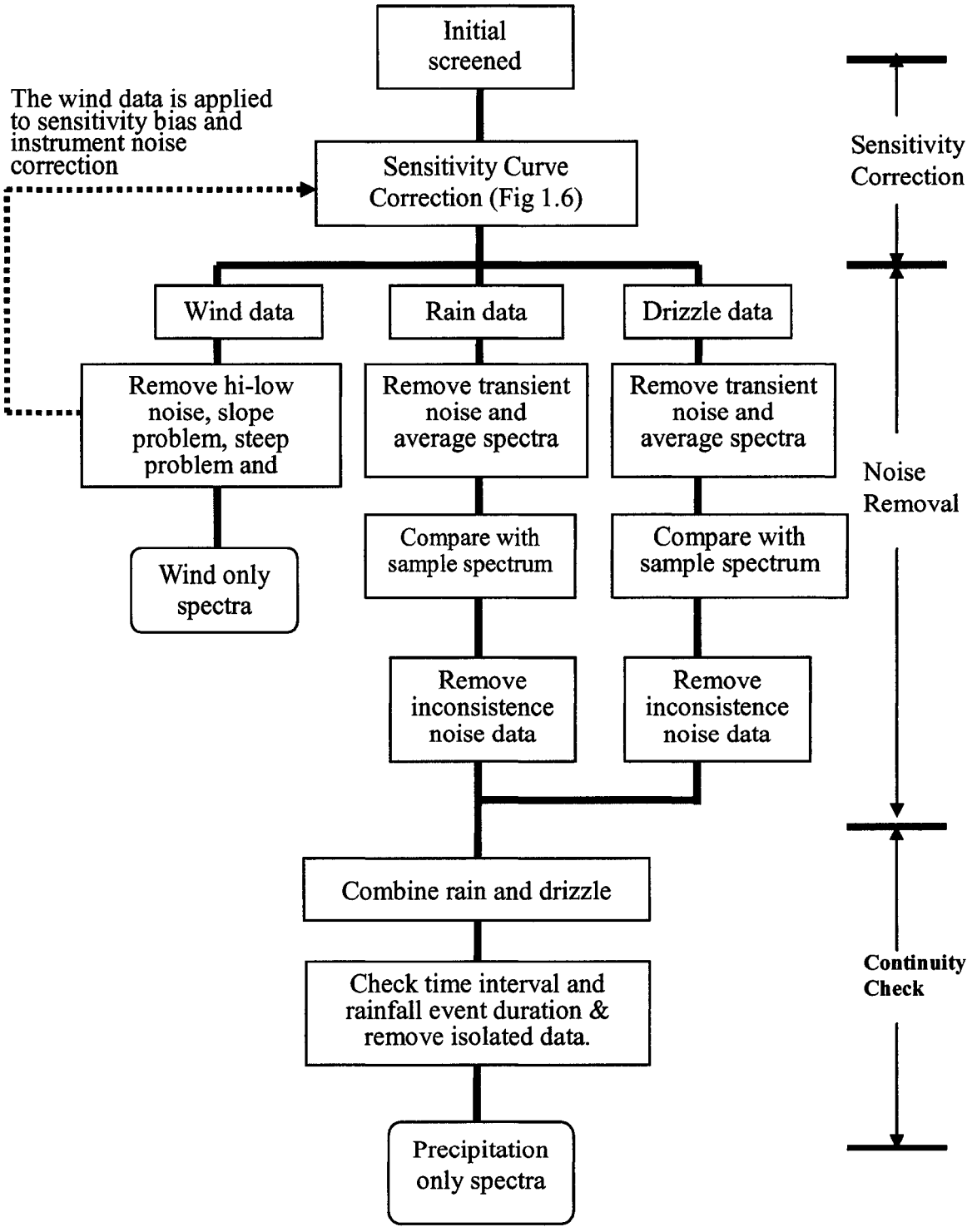


Figure 1.7 Acoustic Discrimination Process

**1.7 Evaluation of acoustic discrimination process in rainfall**

To evaluate the success of the acoustic discrimination process for individual spectra, a simple optimal decision matrix, the binary decision statistic (Urick, 1983) is adopted (Fig. 1.8). The input data are the R. M. Young surface rainfall rates for 10-minute intervals, and with a "positive" detection threshold set at 0.4 mm/hr. The ARG rain detection is set as the output decision. Correct detection, missed detection, and false alarm categories are further binned into rainfall rates with bin width 5mm/hr (Fig. 1.9). Three different process stages: 1) initial screening (solid line), 2) noise removal (dotted line), and 3) continuity check (dashed line), are shown in this evaluation. Initially the false alarm rate is very high. After the discrimination process the false alarm rate becomes acceptable. The trade-off to this reduction in false alarm is the shift of "correct decisions" to "missed detections". However for rainfall rates higher than 15 mm/hr, the discrimination process does not shift any correct decisions to missed detections, while the false alarm rate drops to nearly zero. This is illustrated again in figure 1.10. The probability of detection is calculated from the ratio of correct to "missed" detection. The probability of detection increases as the rainfall rate increases and reaches 100 % when the rainfall rate is over 15 mm/hr. The probability of false alarms is calculated from the ratio of false alarm and null decision (no rain in both instruments). Through the discrimination process, the probability of false alarm is reduced from 19.5 % to 7.3 % (after noise removal) to the final 0.4 % (after continuity check). The discrimination process has eliminated most of the false alarms and still maintained a high probability of detection, at least for rainfall rate over 5mm/hr. The sources of errors in this analysis will be the detection errors from both instruments since the true rainfall is unknown and errors are possible for both instruments. The probability of false alarm from several ARG deployments is shown in table 1.4.

| Rainfall rate (mm/hr) Every 10 minutes | | Decision (ARGs spectra) | |
|---|---|---|---|
| | | **Rain** | **No Rain** |
| **Input RMY R: Rainfall rate (mm/hr)** | **Rain** | **Correct**<br>Pd(R)<br>Criteria: RMY ≥ 0.4 mm/hr;<br>ARG detected at least one precipitation spectra. | **Missed**<br>Pm(R)<br>Criteria: RMY ≥ 0.4 mm/hr;<br>No ARG detection at all. |
| | **No Rain** | **False Alarm**<br>Criteria: RMY < 0.4 mm/hr.<br>ARG detected at least one precipitation spectrum. | **Correct**<br>(Null decision)<br>Criteria: RMY < 0.4 mm/hr;<br>No ARG detection at all. |

*Figure 1.8 The binary optimal decision matrix scheme. The input is RMY self-siphoning rain gauge 10-minute rainfall. The output decision is the ARG precipitation detection.*

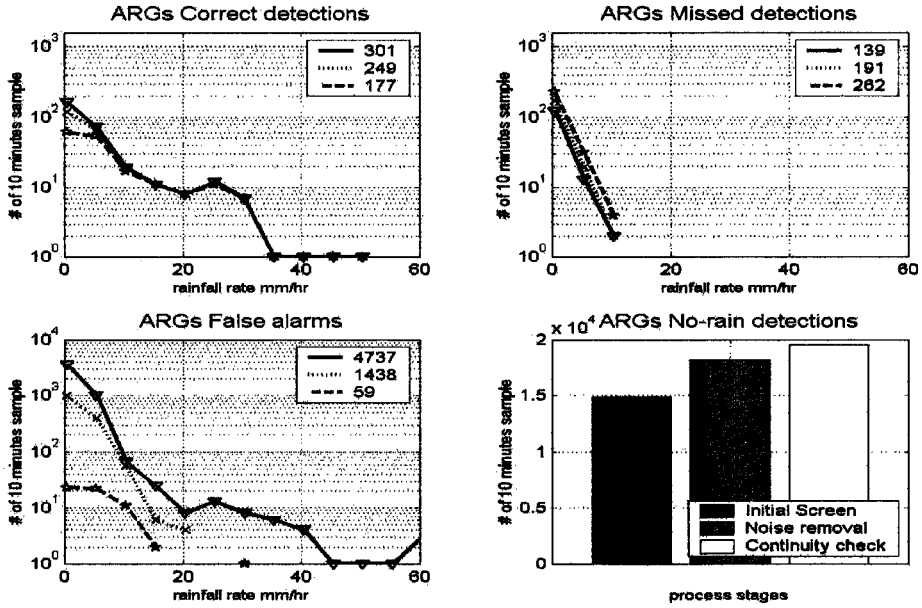


*Figure 1.9 Optimal decision matrix of detection in different discrimination process stages. The solid line is the initial screening using equations 1.4 & 1.5. The dotted line is after Noise removal but before the continuity check, and the dashed line is the final product after the continuity check. The number in the legend boxes represents overall number of samples in each category. The data are separated into 5mm/hr bin-width bins. The rainfall rate used for the "correct" and "missed" detection categories are from the R.M. Young surface rain gauge, while the rainfall rate for the "false alarm" category is from the ARG data using equation 1.17.*

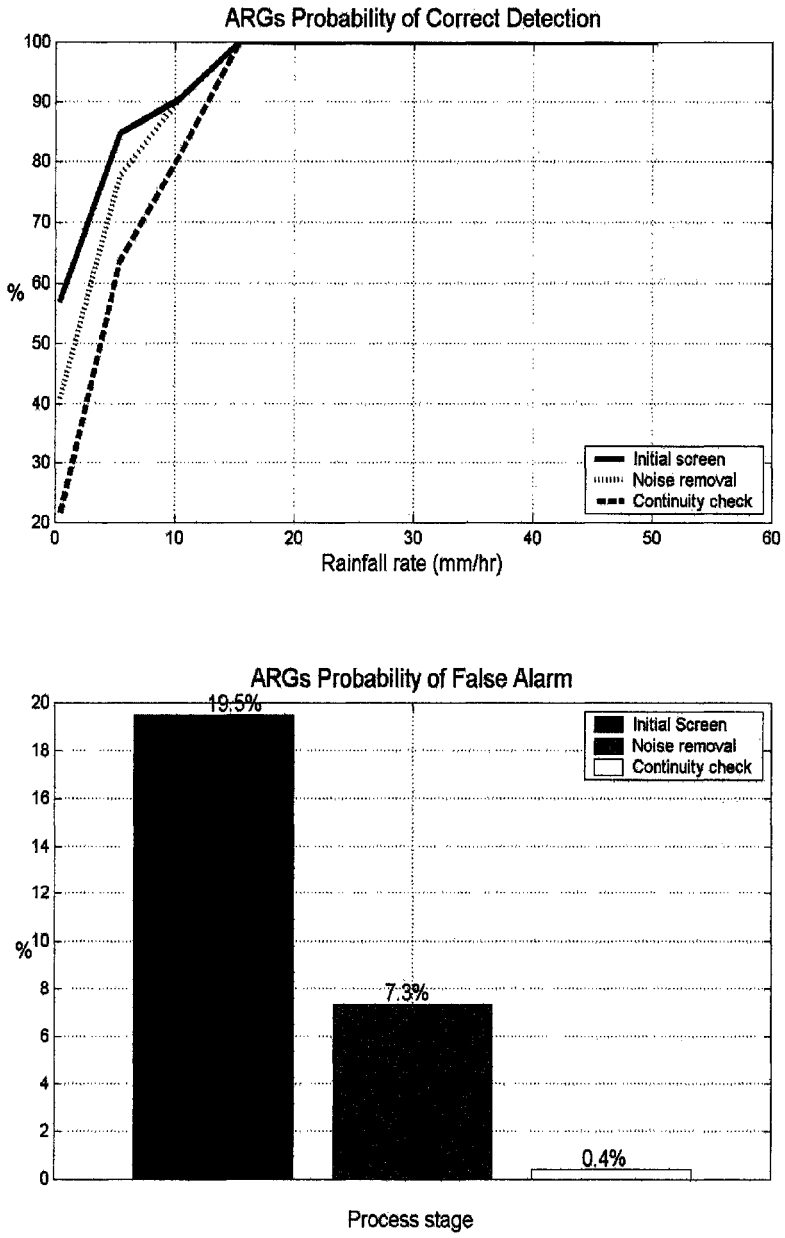


*Figure 1.10 The probability of correct detection is calculated from the "correct" and "miss" categories in the binary decision matrix. The probability of false alarm is calculated from the "false alarm" and "null decision" categories.*

*Table 1.4 Probability of false alarm after discrimination process*

| ARG name | Deployment period | Probability of false alarm |
|---|---|---|
| K | 5 months | 0.4 % |
| C | 5.5 months | 0.2 % |
| D | 5 months | 0.3% |
| B | 5 months | 0.5 % |

## 1.8 Rainfall quantification - empirical algorithm for deep open-ocean

A simple relationship between sound intensity and rainfall rate (mm/hr) can be written in the form of

$$I = aR^b \tag{1.14}$$

where $I$ is the sound intensity and $R$ is the rainfall rate.

Taking $10\log_{10}$ of equation 1.14 at 5 kHz, this becomes

$$dBR/10 = (SPL_{5kHz} - a')/b' \tag{1.15}$$

where $dBR = 10\log_{10}(R)$, $a'$ represents the intercept and $b'$ is the slope. The acoustic rainfall signal at 5 kHz is chosen because it has a large dynamic range and is in a part of the acoustic spectrum not thought to be affected by wind speed (Nystuen, 2001). Similar empirical algorithm of rainfall rate conversion was proposed by Nystuen (1996) based on observations from a shallow brackish pond near Miami, FL:

$$dBR/10 = (SPL_{5kHz} - 50)/17 \tag{1.16}$$

where $R$ is the rainfall rate in mm/hr. Using the R. M. Young data as a guide for rainfall rate and the acoustic sound pressure level (dB) at 5 kHz, a new empirical algorithm for rainfall rate versus sound pressure level can be produced. Nominally, the R.M. Young

rainfall product is the rainfall rate (mm/hr) for 10 minutes intervals. This product is the result of smoothing 1-minute rainfall rate data with a 16-point Hanning filter. From figure 1.11 it is clear that this smoothing has removed part of the dynamic range associated with heavy rainfall. In order to produce acoustic algorithm that includes a large dynamic range, a subset of the original 1- minute sampling interval of R.M. Young data is used after obvious errors (negative values and siphoning events) are removed (Fig. 1.12). The outliers shown in figure 1.12 with "+" signs are data points from ARGs either trigged only by "K" or "B" which were deployed in the same location but at different depth (Table 1.2). These data points are not simultaneous from both instruments and thus are thought to be due to the acoustic discrimination process errors (about 1 %). The points with R. M. Young rainfall rate smaller than 0.4 mm/hr, which are smaller than then the instrument error (Serra, 2001), are also removed ("Δ" signs). Statistical outliers, defined by the last 10% of the density distribution are removed before the orthogonal linear regression is calculated. The surface sampling area for the ARG is about 7,069 $m^2$ when deployed at 50-meter deep. This is roughly seven orders of magnitude larger than the R. M. Young rain gauge 100-$cm^2$ catchment area. When rain cell is approaching from the distance, the ARG will detect the rainfall generated sound before the R. M. Young rain gauge catches any raindrops, and similarly when the rain cell is moving away.

The new rainfall rate algorithm is

$$dBR/10 = (SPL_{5kHz} - 42.4)/15.4 \qquad (1.17)$$

The standard deviation for the difference between ARG estimate rainfall rate using equation 1.17 and R. M. Young rainfall rate is of order of 0.25. This is quite large and most likely due to time mismatch, instrument performance, the sampling area covered, and natural variability of rainfall. This algorithm is also quite different from the previous study. In particular, the sound levels reported from the open ocean locations appear to be nearly 10 dB quieter than in the Miami, FL data. Presumably, the bottom reverberation of the shallow fresh water pond versus the deep open ocean condition is responsible for the

changes in the empirical algorithm.

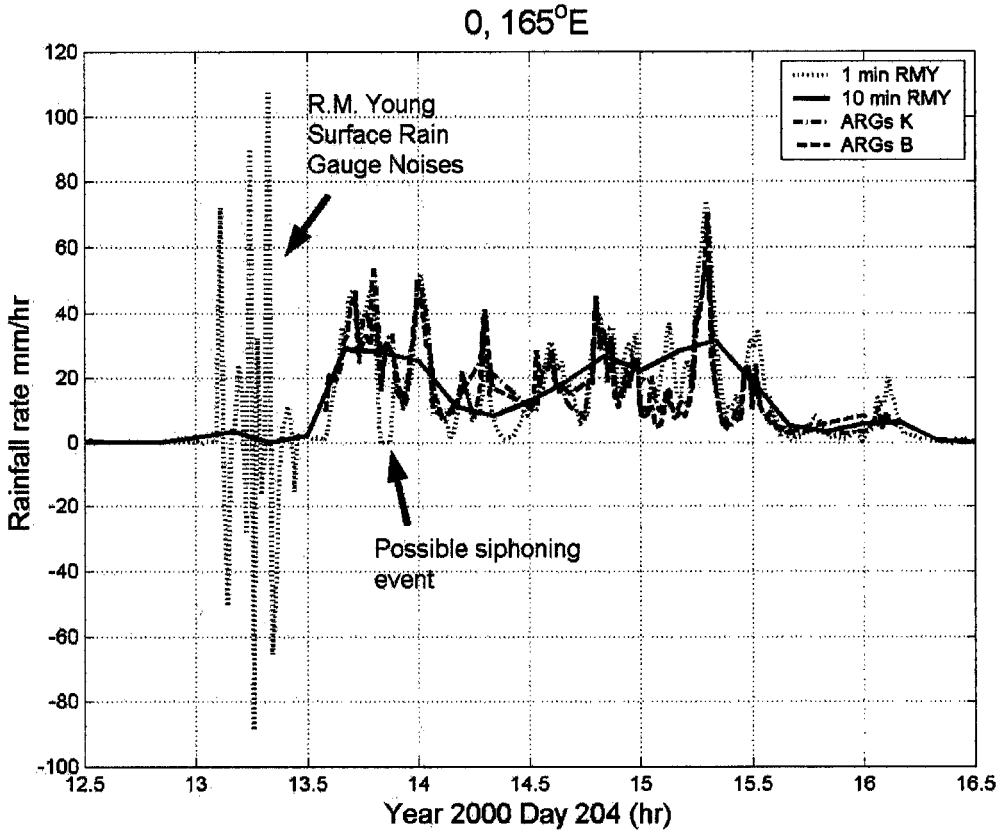


*Figure 1.11 The rainfall rate comparison between two ARG "K", ARG "B", 1 and 10-minute R. M. Young surface rain gauge. The ARGs rainfall conversion is using equation 1.17. The ARGs "K" and "B" are co-located on the same mooring at 0°, 165°E which were deployed at the depth of 50 m and 20 m respectively.*

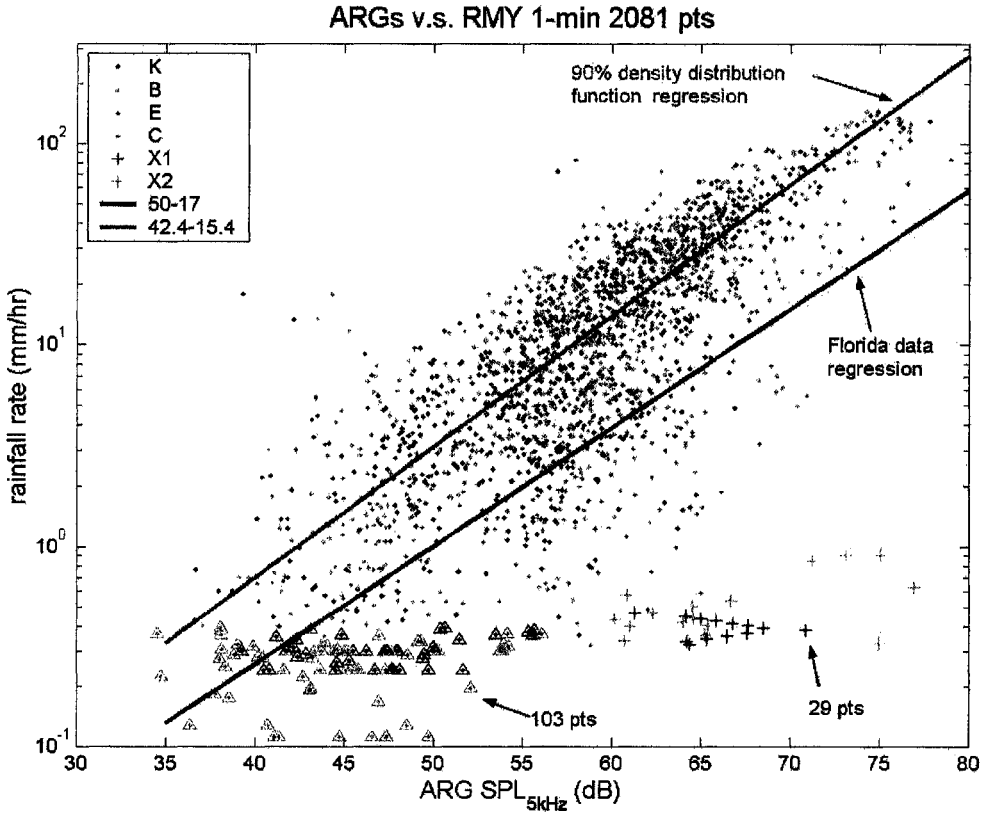


*Figure 1.12 The linear regression of rainfall rate versus $SPL_{5kHz}$. ARGs (K,B,C, and D) and R. M. Young 1-min sampling interval rainfall data are shown. The outliers shown as "+" are acoustic data triggered by "K" or "B" ARG but not both instruments, although these two ARGs were deployed at the same location. The data have the "Δ" symbol shows R.M. Young less than 0.4 mm/hr, smaller than the instrument's sampling error. The black- line is the regression from Nystuen (1996), and the red- line is the regression of R.M. Young 1-minute vs. ARGs 1-minute after removing the outliers. The numbers in the legend box represent a' and b' in equation 1.15 for each regression line.*

## 1.9 Validation of rainfall rate algorithm

Rainfall accumulations for the Year 2001 at the 10° N, 95°W and 12 °N, 95°W TAO moorings are shown in figure 1.13. The acoustic rainfall accumulation is calculated by applying the rainfall rate algorithm (Eqn. 1.17) and is compared with the co-located R.M. Young rain gauge and TRMM satellite rainfall product 3B42. This part of the ocean has a distinctive rainy season beginning in May and lasting into October. Exact

agreement between the satellite estimate and the surface instruments should not be expected, since the sampling strategies are very different (spatial averaging versus high temporal resolution). However, seasonal agreement should be expected. The comparison shows that the R.M. Young gauge and ARG at the 10°N, 95°W has excellent agreement for both individual events and for the annual accumulation (Fig. 1.13 top). At 12°N, 95°W, the R.M. Young gauge did not function properly during several time periods (Fig. 1.13 bottom). The accumulation measurement of R.M. Young data is shifted to match the ARG accumulation after each period of non-performance. The R.M. Young and ARGs are in good agreement when both instruments were functioning properly. The ARGs also have very good seasonal agreement with TRMM. The difference in annual rainfall estimate is less than 5 %. The scatter plots for daily accumulation are shown in figure 1.14. The ARGs and R.M. Young shows very good agreement (Fig. 1.14 top), but the ARGs and TRMM (Fig. 1.14 bottom) shows the satellite measurement does not have any daily rainfall accumulation over 50mm. This probably reflects the spatial sampling limitations of satellite rainfall estimation compared to the more localized acoustic measurement of rainfall. The satellite measurement always spatially smooths intense local rainfall events, whereas a point measurement will occasionally measure an intense local events. Apparently, at season time scales of months, this difference becomes small, suggesting that both measurements are correct at the longer time scales.

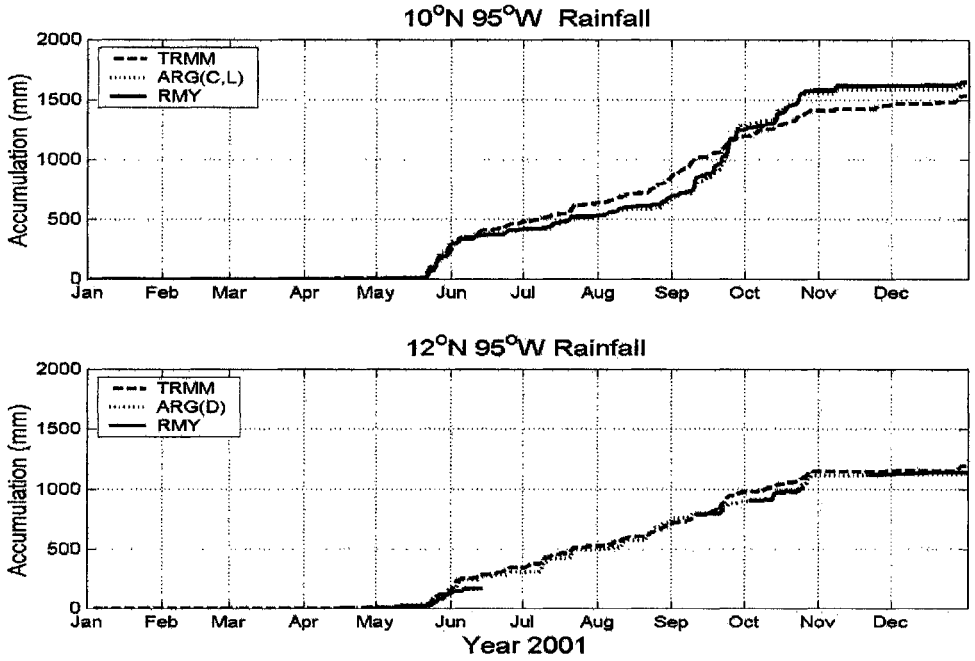


*Figure 1.13 The rainfall accumulation in 10° and 12°N, 95°W in 2001. The dotted line is the ARGs, solid line is R. M. Young, and dash line is TRMM rainfall accumulation (mm).*

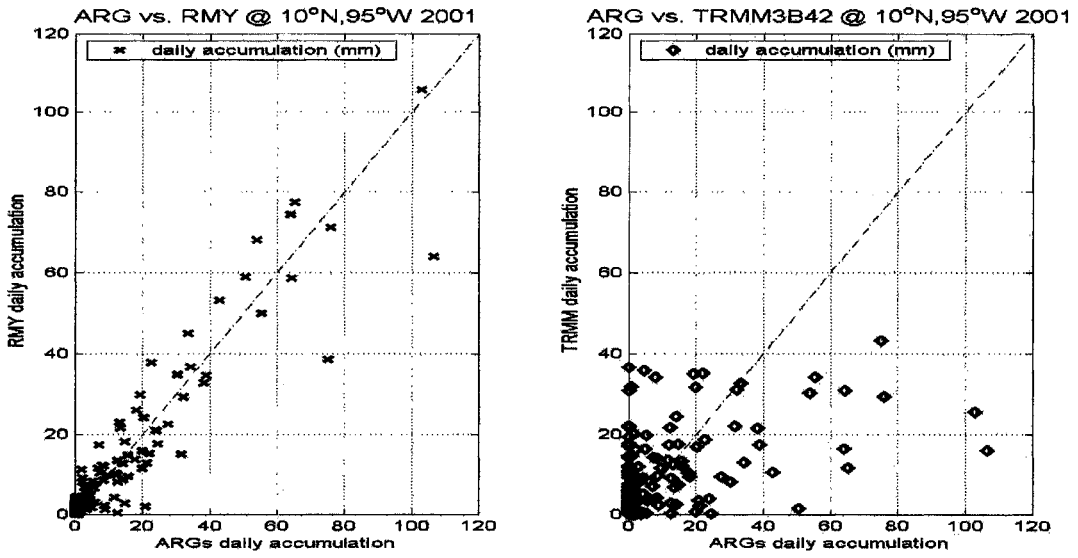


*Figure 1.14 The daily rainfall accumulation scatter plots.*

## 1.10 Wind contamination and rainfall rate conversion error estimates

At low frequencies, as the rainfall rate decreases, the signal is gradually replaced by wind-generated sound (from breaking waves). Or alternatively, as the wind speed increases, the sound pressure levels due to rainfall will become "contaminated" by wind. Figure 1.15 attempts to predict when this will happen. The component of sound at 5 kHz due to wind can be predicted using equation 1.12 and adjusted to 5 kHz (+3dB) using the observed spectral slope for wind. Figure 1.15 shows the relative amplitude of the sound due to rainfall rate (Eqn. 1.17) and due to wind. Thus the separation line on the plot is an indication of when the rainfall rate algorithm is valid. This prediction assumes that rain does not affect the sound generated by wind, and that the sound produced by each process is independent, at least at 5-8 kHz. In fact, it is "known" that rain suppresses wave breaking, and so the sound present in heavy rain and high-wind conditions needs further investigation.

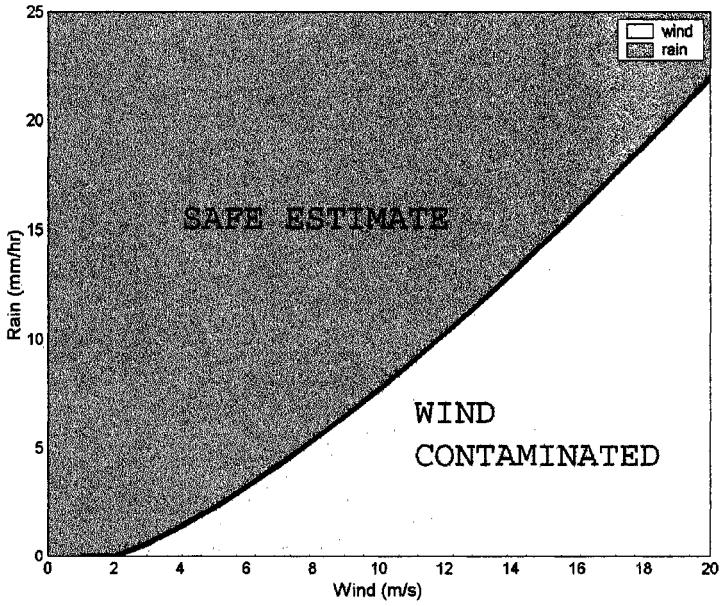


*Figure 1.15 Possible wind contamination of rainfall rate conversion. The likelihood of the rainfall rate estimate using equation 1.17 will be contaminated by the wind generated sounds.*

The error bars of 95 % confidence interval for a 1 minute acoustic sample are shown in the figure 1.16. This is evaluated using chi-square cumulative distribution given the number of independent measurements. The difference between error bars at 0.1-3 kHz and 3-50 kHz are due to different means of spectrally compressed method used (2 adjacent frequencies averaged for 0.1-3 kHz, and 10 adjacent frequencies averaged for 3-50 kHz). The rainfall conversion (Eqn. 1.17) using SPL at 5 kHz can be interpreted from the error bar at 5 kHz. Figure 1.17 shows the logarithmic scale of rainfall rates versus the SPL at 5 kHz. Since the rainfall rate regression is a logarithmic relation (Fig. 1.12), larger rainfall rates will have larger absolute error bars.

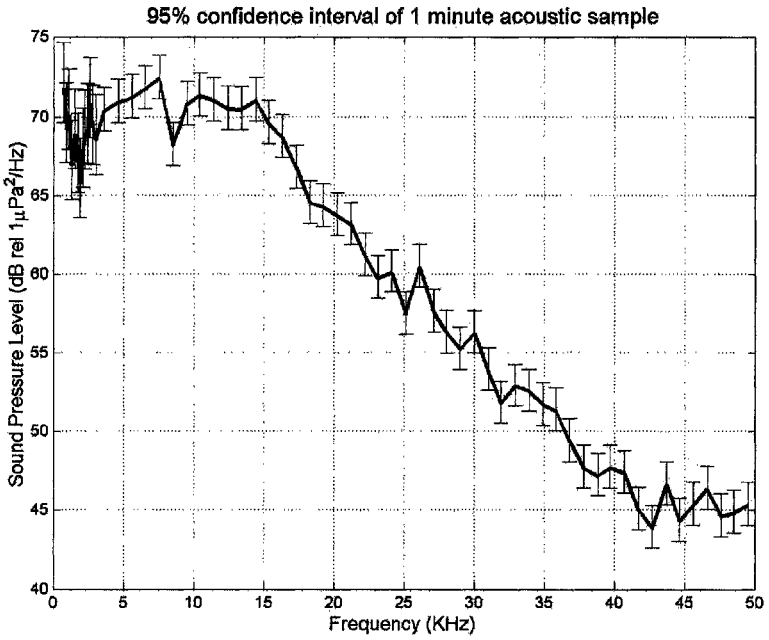


*Figure 1.16 The error estimates of 1 minute acoustic measurement.*

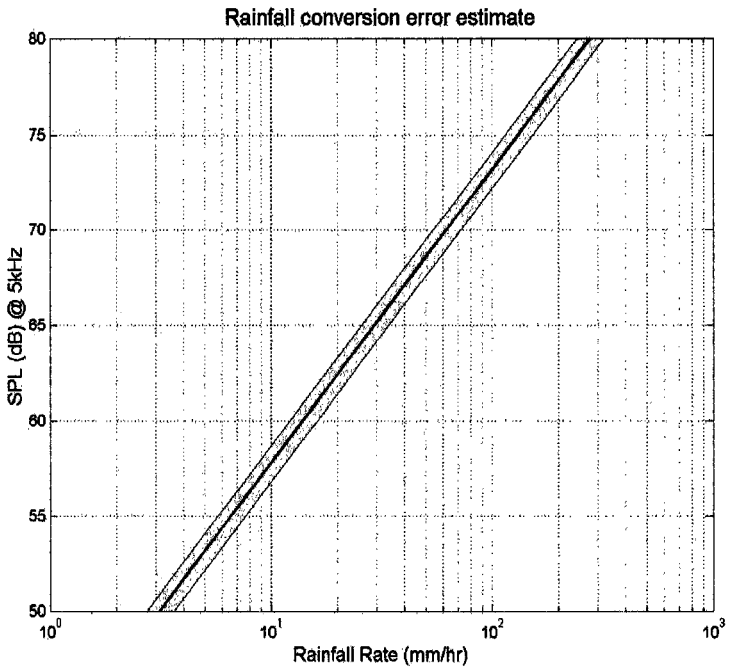


*Figure 1.17 The error estimates of acoustic rainfall conversion.*

# Chapter 2: Empirical Ocean Ambient Sound Model

## 2.1 Introduction

The ocean ambient sound received by an omnidirectional hydrophone can be partitioned into signals from non-geophysical and geophysical sources. The geophysical sounds are mainly caused by the physical processes on the ocean surface, in particular wind and rain. Because the geophysical ambient noise serves the baseline of the sound level in the ocean, the study of geophysical generated ocean ambient sound is not only important to the ocean physicists interested in understanding the rainfall and wind over the ocean, but is also important for military applications of sonar, and for biologists in studying noise impact on marine mammals. The marine mammals are one of the main sources of biologic noises, since they utilize sound for hunting, communication and social activities. The impact of anthropogenic produced noise pollution on the marine ecosystem is of increasing interest.

The geophysical signals can be distinguished from non-geophysical sources by comparing the known spectral and temporal characteristics of each sound source. Distinct ambient sound spectra for various rainfall rates and wind speeds are identified through a series of discrimination processes (see, chapter 1). Individual contributions from the rainfall and the wind to the overall sound production are separated by inspecting the frequency and temporal characteristics. Several physical processes have been identified as responsible for the production and absorption of sound. These include 1) wind generated breaking waves producing sound through sound generated by individual bubbles (over 500Hz) (Medwin and Beaky, 1989), and 2) bubbles trapped by raindrop splashes (Nystuen, 2001; Medwin et al., 1992). These processes lead to the generation of sound with particular spectral characteristics. By developing empirical algorithms for each of these characteristics, the ocean ambient sound level can be predicted given wind and rainfall conditions.

## 2.2 Characteristics of rain and wind generated ambient sound spectra

Summary spectra of the rain and wind generated sounds are shown in figure 2.1 for all the available data from ITCZ and Western Pacific warm pool (chapter 1). These spectra are grouped and averaged according to the co-located surface sensors' data, and provide a climatological view of the ocean ambient sound. There are some distinctive features of sound generated by wind and rain. The wind-only spectra are shown for the wind speeds at 2-4 m/s, 4-6 m/s and 6-8 m/s. These spectra (dash lines) have a constant negative slop from 1 to 50 kHz with, sound level decreasing at about 15.7 dB per decade. The rainfall spectra (solid lines) are averaged from the rainfall rate 2-5 mm/hr, 5-10 mm/hr, 10-20 mm/hr and above 20 mm/hr, respectively. Light rain (< 10 mm/hr) has a unique signal from 13 to 25 kHz, due to the 1-mm raindrops present in most drizzles. Heavier rainfall containing larger drops produces very loud sound levels across a wider frequency range. In the frequency band from 1 to 10 kHz the spectrum level increases with rainfall rate, but for frequencies above 10 kHz there is less dependence on the rainfall rate. This figure shows a coherent picture of the acoustic spectral dependency on wind alone and rain averaged over all wind conditions.

### *a. Wind influence on light rain - drizzle (2-10 mm/hr)*

In figure 2.1, no wind dependence of the rain generated sound is shown. To examine the wind influence on the rainfall generated sound, the surface anemometer data are used to further classify rainfall spectra. Figure 2.2 shows the spectra for rainfall rate 2-5 mm/hr and 5-10 mm/hr decomposed into various wind speeds. For these lighter rainfall rates (rainfall rate 2-5 mm/hr and 5-10 mm/hr), the signal at 15 kHz is inversely proportional to the wind speed. This is because the bubble trapping mechanism for small raindrops is sensitive to the impact incident angle of the raindrop as it hits the ocean surface. Laboratory studies show the probability that an individual drop will produce a bubble decreases linearly from 100% at normal incidence to 10% for oblique incidence 20° from the vertical (Medwin et al., 1990; Nystuen, 1993). On the other hand, the sound level

generated by rain in the frequency band from 2 to 8 kHz is relatively invariant with wind speed.

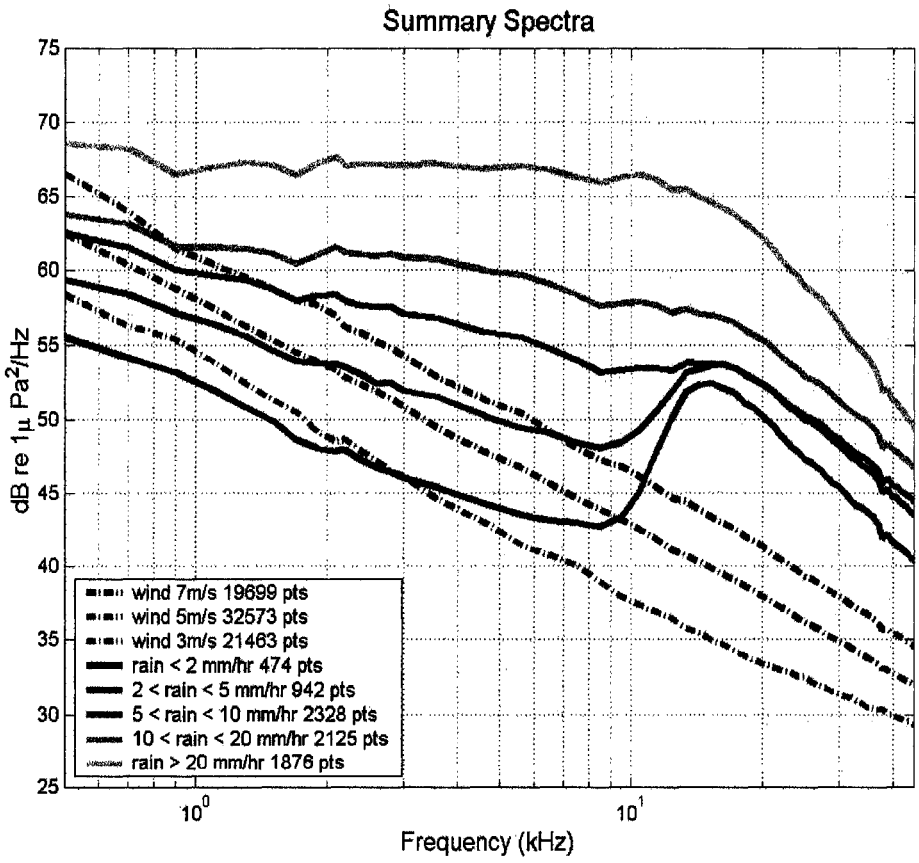


*Figure 2.1 Summary acoustic spectra on ran, drizzle and wind. The numbers in the legend box indicate how many spectra have been averaged to produce each spectrum.*

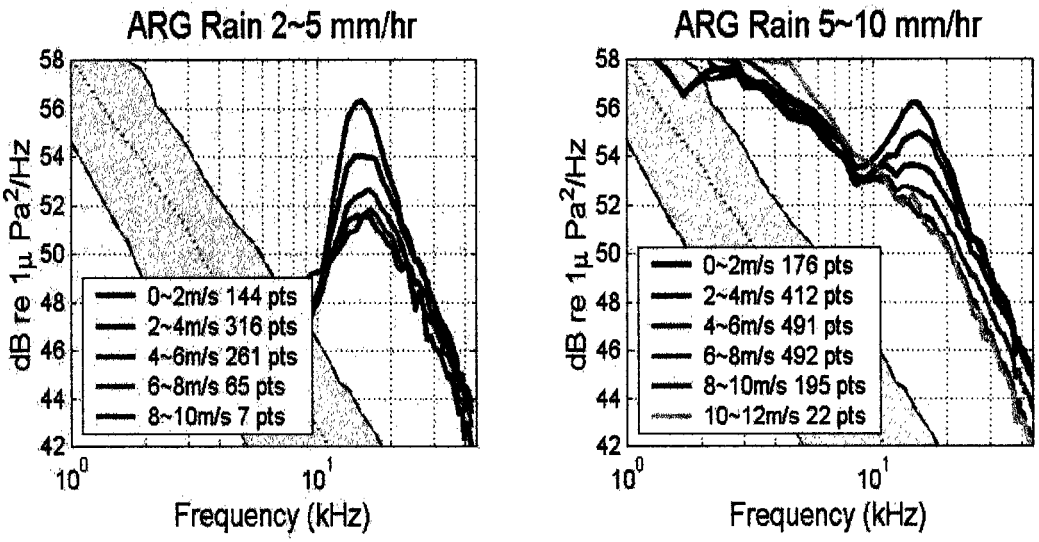


*Figure 2.2 The average sound spectra for rainfall rates 2-5 mm/hr and 5-10 mm/hr are decomposed into various wind speeds. The shaded area represents the wind-only spectra where the dash-dotted, dotted, and dash lines are the average wind-only spectra for wind speeds at 2-4 m/s, 4-6 m/s, and 6-8 m/s respectively. The numbers in the legend box indicate how many spectra have been averaged to produce each spectrum.*

***b. Large raindrops signals in heavy rainfall (10-30mm/hr)***

Figure 2.3 shows the sound spectra for the rainfall rate from 10 to 30 mm/hr in various wind speed conditions. The acoustic energy sharply drops off at below 2 kHz. This is likely due to a limitation of the largest bubble sizes that can be produced by the naturally occurring large raindrops splashes that are present in such heavy rainfall (Table 1.1). Figure 2.3 shows that below 2 kHz the spectra level increases as the wind speed increases. This is a summation effect, as the rainfall signal is relatively weak, while the wind signal is strongest in this frequency band and increases as wind speed increases. Again, from 2 to 8 kHz the spectral level is relatively invariant to the wind speed. As the large raindrop population increases, the sound level from 10 to 20 kHz is also elevated and gradually dominates the sound generated from small raindrops. Thus the wind effect observed for light rain sound production can no longer be detected. At frequency band

20-50 kHz, it appears that the sound levels decreases as the wind speeds increases. Presumably, a thin layer of bubbles has formed near the surface and its effect is to attenuate subsequent sound produced on the surface both from wind and rain.

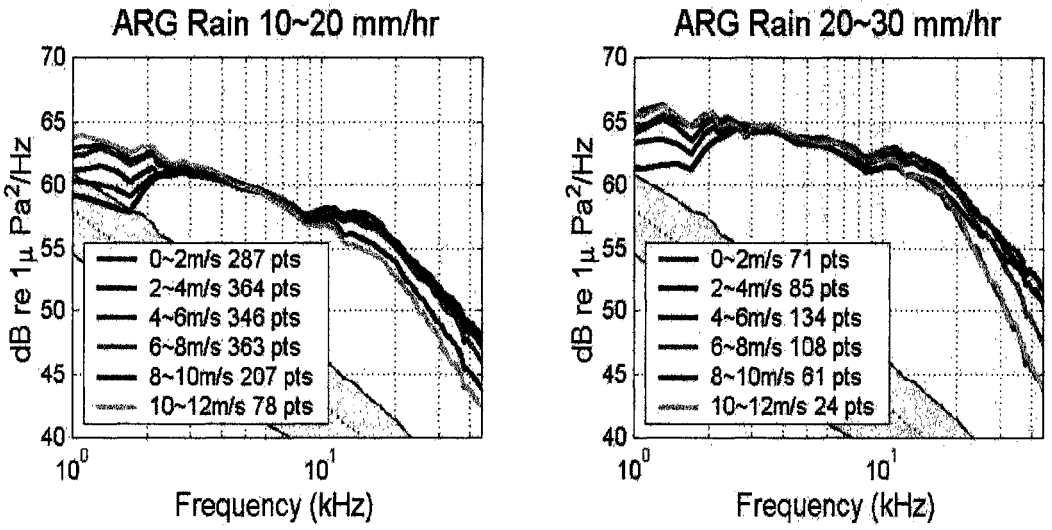


*Figure 2.3 The average sound spectra from rainfall rates 10-20 mm/hr and 20-30 mm/hr are decomposed into various wind speeds. Shaded areas are the wind-only spectra (see Fig. 2.2 caption for details).*

***c. Extremely heavy rainfall (30 mm/hr above)***

Once extremely heavy rainfall (> 30 mm/hr) is present, very large raindrops are usually present in the rain. These drops generate broadband sound (< 1 kHz to > 40 kHz) and little effect of wind is observed. In fact, the only wind dependence appears above 20 kHz where the sound level decreases as the wind speed increases (Fig. 2.4). This sound reduction effect has been observed in high wind speed conditions (Farmer and Lemon, 1984), and also during extremely heavy rainfall (> 150 mm/hr) (Nystuen et al., 1993). The detail of the interaction between these two types of bubble layer generating mechanisms is unknown. The influence of this bubble layer is observed for frequencies above 15 kHz. These are small bubbles that can be stirred down to form a "layer", while

larger bubbles rise to the surface more quickly and consequently are not present to reduce sound levels at lower frequencies.

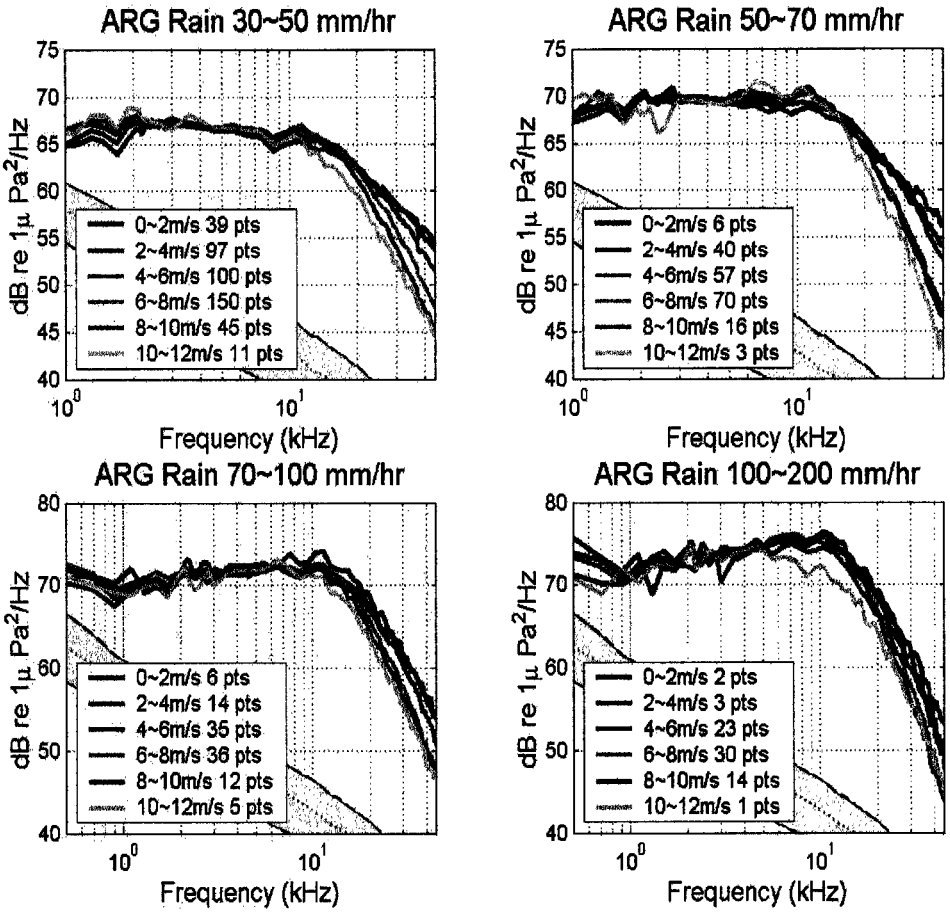


*Figure 2.4 The average rainfall 30-50 mm/hr, 50-70 mm/hr, 70-100 mm/hr, and 100-200 mm/hr in various wind speeds. Shaded areas represent wind-only spectra (see Fig. 2.2 caption for details).*

## 2.3 The Empirical Algorithms

Five spectral sections associated with the different dominant sound generating and suppression mechanisms for wind and rain can be identified and used to form an empirical model to predict geophysically generated sound levels given the rainfall and

wind speed conditions (Fig. 2.5). For section I, the wind-only spectra levels have the character of decreasing linearly as frequency increases. For section II, sound is produced by large raindrops and is invariant with respect to wind. For section III, between 8-25 kHz, sound is generated by small raindrops. This part of the spectrum is highly sensitive to the wind speed. For section IV, sound is produced by a combination of small and large raindrops. Finally for section V, there is a sound masking effect during high wind or extreme rainfall rates, due to a layer of bubble clouds which form just below the surface.

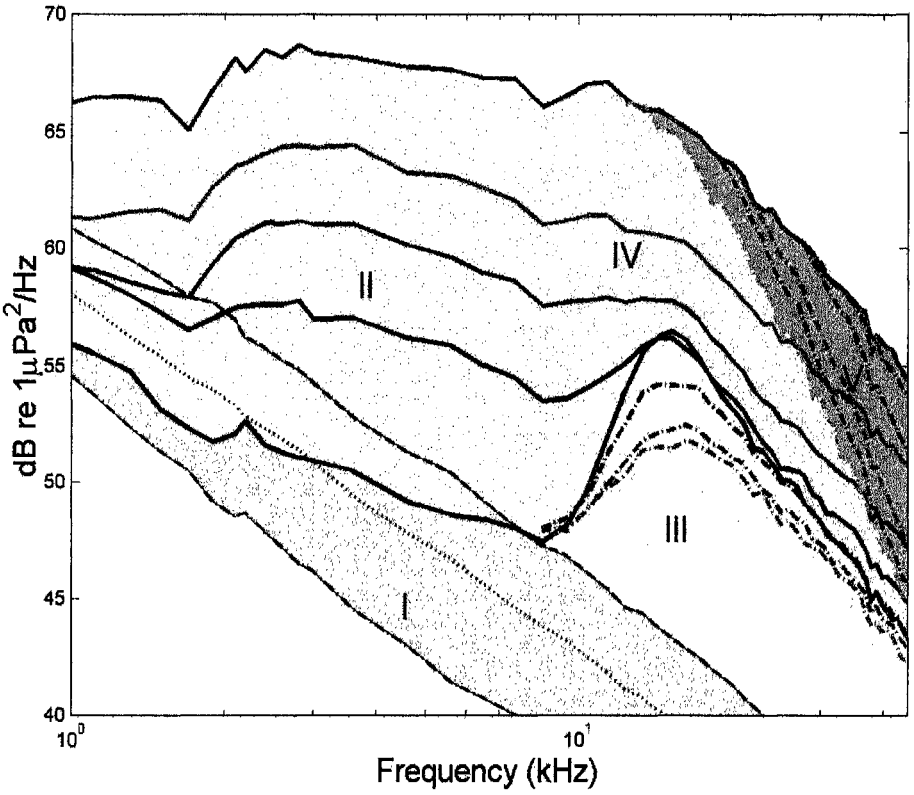


*Figure 2.5 The ocean ambient sound generated from wind and rain can be categorized into five sections with different sound producing and reduction mechanisms in the frequency band 1-50 kHz. I. Wind-only. II. Large raindrops. III. Light rain (drizzle). IV. Both small and large raindrops. V. The masking effect due to layer of bubbles near the surface. The dash-dotted lines on the section III and V represent wind-dependent rainfall spectra.*

***Section I. Wind generated noise from 1 to 50 kHz***

Vagle et al. (1990) proposed an algorithm relating wind speed and sound pressure level (SPL) at 8 kHz.

$$U = \left[ 10^{\left(\frac{SPL_{8\,kHz}}{20}\right)} + 104.5 \right] / 53.91 \tag{2.1}$$

where $U$ is wind speed at 10 meters height (m/s), $SPL$ is the sound pressure level in *dB re 1 $\mu Pa^2/Hz$*. The data from the ITCZ and Western Pacific warm pool show that the wind-only spectra have a uniform slope from 1 to 50 kHz, and this uniform slope is held to at least 14 m/s (Limited high wind speeds data are recorded during the observation period, but it is known that high wind can induce a bubble layer near the surface which can mask the sound production at higher frequency [20 kHz plus] (Farmer and Lemon, 1984). Thus, the uniform slope would not be valid in this condition). Linear regressions are applied to determine the slope of these wind-only spectra. This value is -15.7 dB/decade (Fig. 2.6). Using Vagle's wind speed algorithm at 8 kHz and slope deduced from the wind-only spectra, the empirical algorithm from wind-only sound can be written as follow:

$$SPL_{wind\,1\sim50khz}(f) = slope_{wind}[\log(f) - \log(8)] + SPL_{8kHz} \tag{2.2}$$

where $slope_{wind}$ = *-15.7 db/decade, and* $f$ is the frequency in *kHz.*

$$SPL_{8kHz} = \log(U \cdot 53.91 - 104.5) \times 20 \tag{2.3}$$

where $U$ is the wind speed in *m/s.*

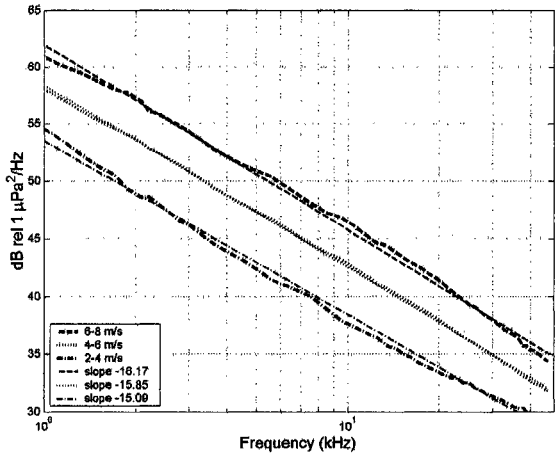


*Figure 2.6 The wind-only spectra and linear regressions for the wind speeds 2-4, 4-6, and 6-8 m/s. This uniform slope -15.7 dB/decade is validated at frequency band 1-50 kHz and wind speeds from 2 to14 m/s.*

***Section II. Rainfall signal at frequency band from 1 to 10 kHz***

The sound for this part of spectrum is mainly generated from large raindrops (2.0-3.5 mm diameter). The population of 2-3.5 mm drops is highly correlated with rainfall rate and therefore can be used to quantify rainfall. The study of the data collected from the ITCZ (chapter 1) shows the sound level at 5 kHz is proportional to the rainfall rate and relative invariant to the wind speed. The relation between the rainfall rate and sound pressure level at 5 kHz can be expressed as:

$$dBR/10 = (SPL_{5kHz} - 42.4)/15.4 \tag{2.4}$$

where $dBR = 10\log_{10}(R)$, $R$ is the rainfall rate (mm/hr) and $SPL_{5kHz}$ is the sound level at 5 kHz in *dB re* $1\mu Pa^2Hz^{-1}$.

The average spectra for a series of discrete rainfall rates are shown in figure 2.7. The slopes from 1 to 10 kHz as a function of rainfall rate are shown in figure 2.8. It

indicates that the slope increases linearly with logarithmic rainfall rate. Thus, the empirical algorithm for rain generated sound in this frequency band (1-10kHz) is:

$$SPL_{1-10khz}(f) = [\log(f) - \log(5)] \cdot slope_{rain} + SPL_{5kHz}(R) \tag{2.5}$$

$$SPL_{5khz} = 15.4 \times \log(R) + 42.4 \tag{2.6}$$

$$slope_{rain} = 8.33 \times \log(R) - 14.3 \tag{2.7}$$

where the $R$ is the rainfall rate in *mm/hr*, $f$ is the frequency in *kHz*, and $slope_{rain}$ is the slope for rainfall spectrum from 1 to 10 kHz. The coefficients for equation 2.7 are from the linear regression line shown in figure 2.8. Equations 2.5-2.7 are valid for rainfall rates from 2 to 200 mm/hr in the frequency band 1-10 kHz.

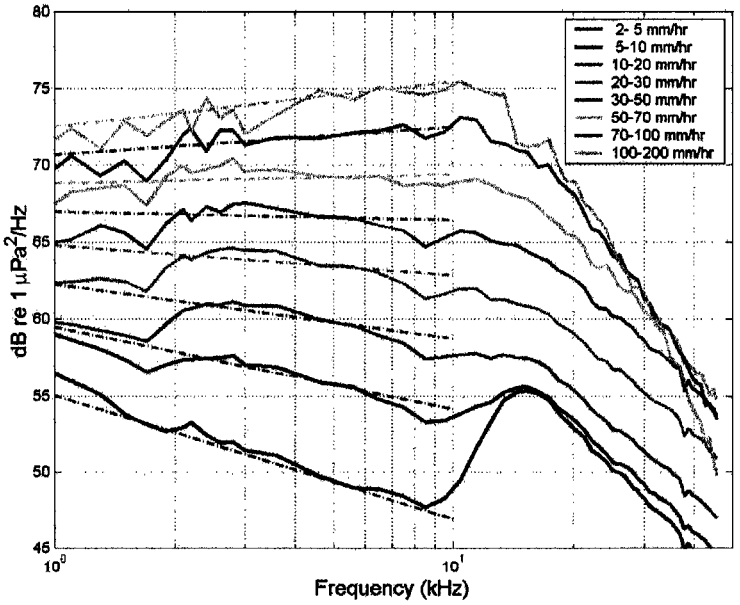


*Figure 2.7 The average rainfall spectra from discrete rainfall rate bins. The dash lines are linear regressions for frequencies from 1 to10 kHz. The slope of each linear regression line is given in figure 2.8.*

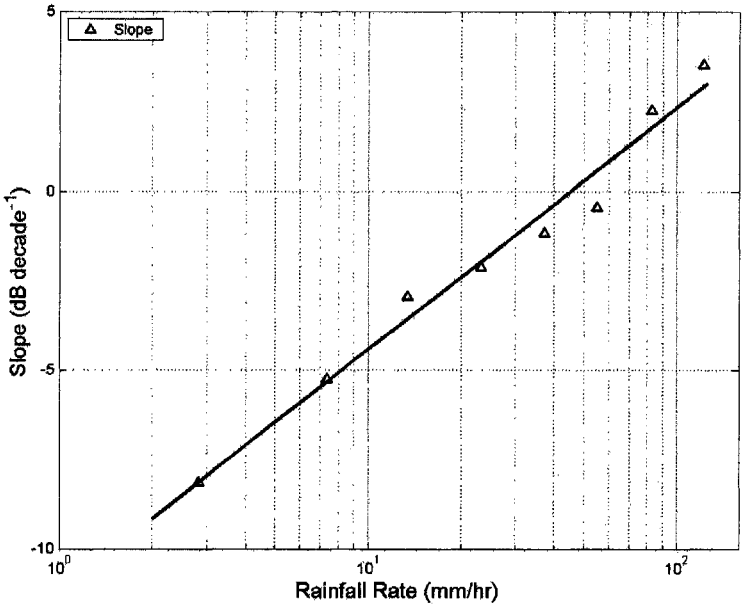


*Figure 2.8 The slope versus logarithmic rainfall rate ("Δ" signs) from the average rainfall spectrum for 1-10 kHz (Fig 2.7). The rainfall rate is calculated using equation 1.17. The coefficients of the linear regression (solid line) is given in the equation 2.7.*

***Section III. Light rain (drizzle) 10-50 kHz (wind-dependant)***

During the light rain, the main sources of sound generated are from small raindrops (diameters 0.8 - 1.2 mm). Small raindrops populations are poorly correlated with total water content and the influence of wind affects the magnitude of the signal. The analysis from ITCZ indicates that the sound generating mechanism from light rain exists at all rainfall rates above 2 mm/hr. Below 2 mm/hr, the signal is often contaminated by the wind. Above 10 mm/hr, the drizzle signals are masked by sound generated from the large raindrops. A three-coefficient non-linear equation (Eqn. 2.8) is designed to reproduce the observed spectra levels in various wind speeds by assuming the wind speed is the only variant in this section of the spectrum.

$$SPL_{10-50kHz} = \frac{A}{\left(1+\left(\frac{f}{f_o}\right)^{lslope}\right)\cdot\left(1+\left(\frac{f}{f_o}\right)^{hslope}\right)} \tag{2.8}$$

where $f$ is the frequency in kHz, $f_o$ is 15.5 kHz, $A$ is amplitude, *lslope* is low-frequency-slope and *hslope* is high-frequency-slope. The least squares fits shown in figure 2.9, are applied to identify coefficients for each wind speed category. These coefficients are shown in figure 2.10, and their numerical values are given in the table 2.1. Equation 2.8 is a discrete algorithm, rather than the continuous algorithms developed for section I and II. The absolute value of the high and low frequency slope decreases as wind speed increases and the peak amplitude is inversely proportional to the wind speed. In other words, the peak in the spectrum is suppressed as wind speed increases. Equation 2.8 is only good for frequencies up to 25 kHz. Above 25 kHz, the three-coefficient algorithm (Eqn. 2.8) is insufficient to estimate observed spectrum levels.

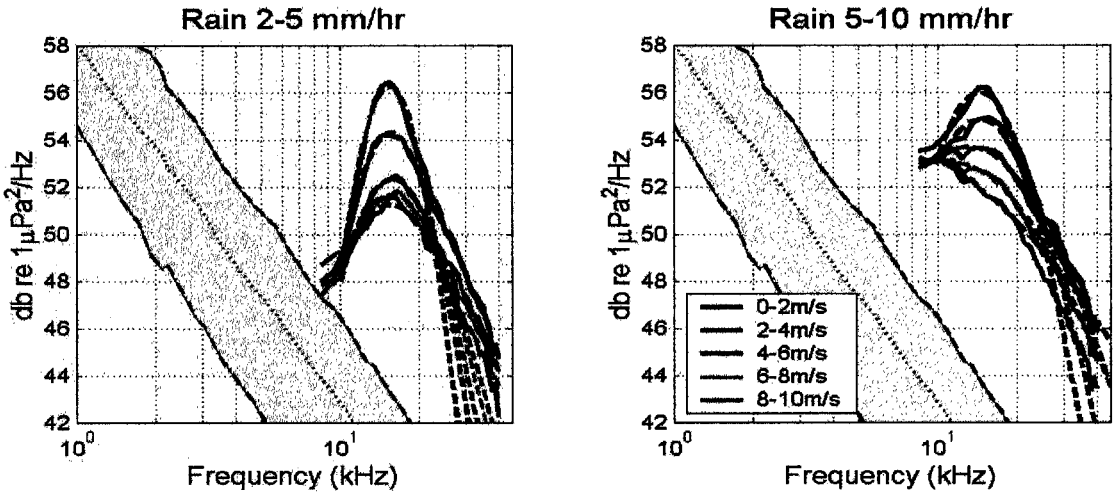


*Figure 2.9 The rainfall 2-5 mm/hr (left) and 5-10 mm/hr (right) in various wind speeds. The dash lines are the least squares fits using equation 2.8. The grey shaded area represents wind-only spectra for reference.*

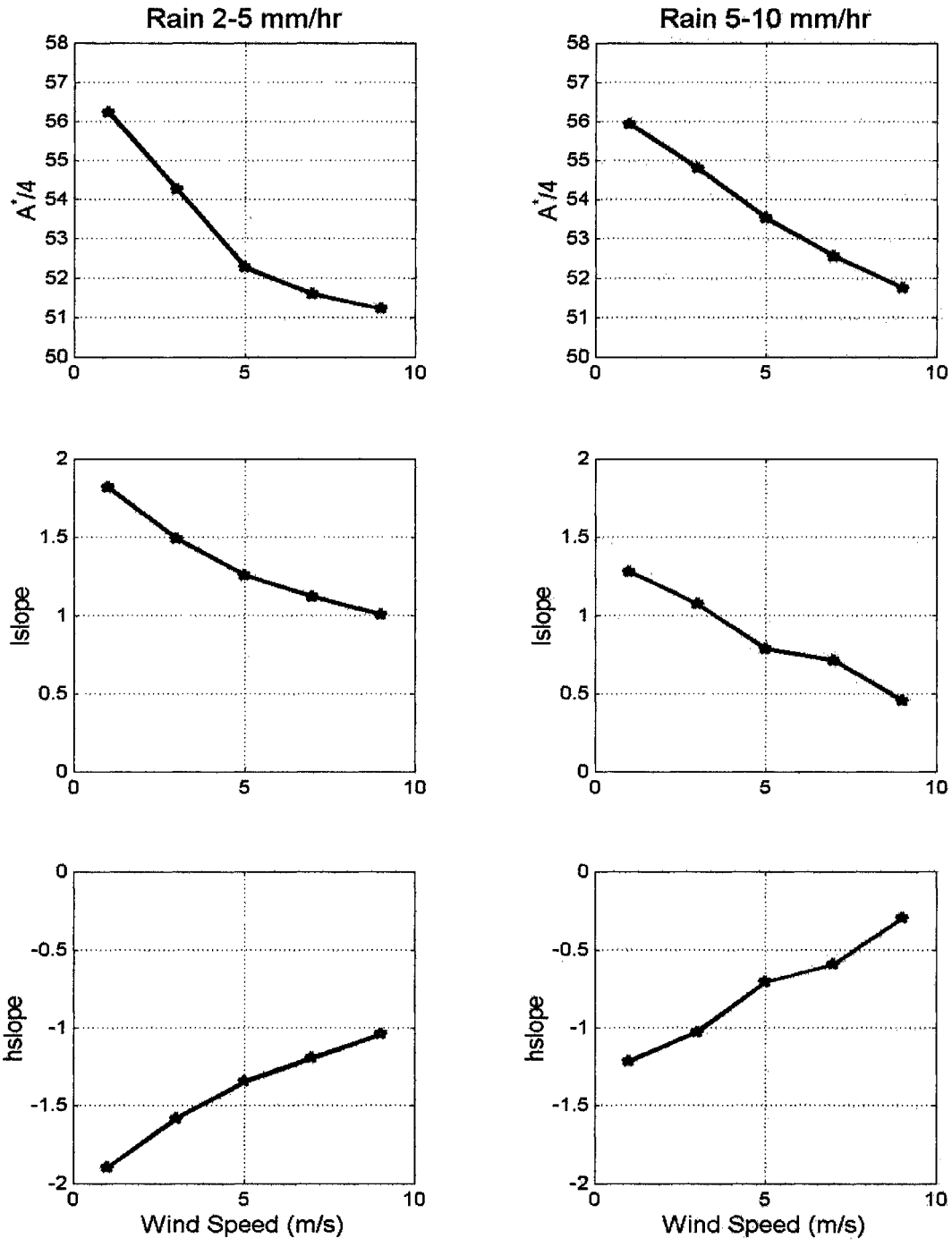


*Figure 2.10 The coefficients from equation 2.8 versus wind speeds for rainfall rate 2-5 mm/hr bin (left) and 5-10 mm/hr bin (right).*

*Table 2.1 The numerical values for three coefficients in equation 2.8.*

| Rainfall rates 2-5 mm/hr | | | | | |
|---|---|---|---|---|---|
| **Wind speed** | **0-2 m/s** | **2-4 m/s** | **4-6 m/s** | **6-8 m/s** | **8-14 m/s** |
| **A** | 224.9443 | 217.0343 | 209.0711 | 206.3746 | 204.8878 |
| **Lslope** | 1.8199 | 1.4904 | 1.2577 | 1.1173 | 1.0084 |
| **Hslope** | -1.8993 | -1.5843 | -1.3486 | -1.1938 | -1.0421 |
| Rainfall rates 5-10 mm/hr | | | | | |
| **Wind speed** | **0-2 m/s** | **2-4 m/s** | **4-6 m/s** | **6-8 m/s** | **8-14 m/s** |
| **A** | 223.7316 | 219.2085 | 214.1092 | 210.2187 | 207.0281 |
| **Lslope** | 1.2810 | 1.0731 | 0.7853 | 0.7121 | 0.4557 |
| **Hslope** | -1.2137 | -1.0274 | -0.7070 | -0.5934 | -0.2976 |

In order to produce a better result for frequency band above 25 kHz, a five-coefficient function (Eqn. 2.9) is proposed.

$$SPL_{10-50kHz} = \frac{A}{\left(1+lc\left(\frac{f}{f_o}\right)^{lslope}\right)\cdot\left(1+hc\left(\frac{f}{f_o}\right)^{hslope}\right)} \tag{2.9}$$

where $f$ is the frequency in kHz, $f_o$ is 15.5 kHz, and *A, lc, hc, lslope,* and *hslope* are five wind-dependent variables for this non-linear equation. These numerical numbers are given in table 2.2. The fitting result is shown in figure 2.11. We can try to assign physical means to the coefficients, but in fact these variables are statistically generated and may not have physical meaning, though the results show a better fit for frequencies > 25 kHz.

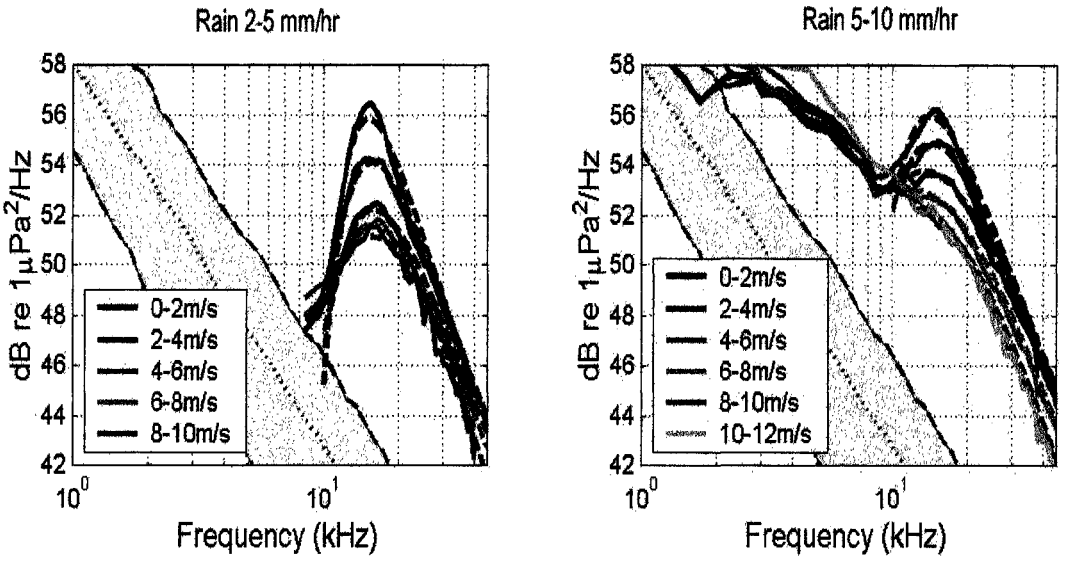


*Figure 2.11 The rainfall 2-5 mm/hr (left) and 5-10 mm/hr (right) in various wind speeds. The dash lines are the least squares fits using equation 2.9. The grey shaded area represents wind-only spectra for reference.*

***Section IV and V Heavy to extremely heavy rainfall signals at frequency band 10- 50 kHz***

During heavy to extremely heavy rainfalls (rainfall rates above 10 mm/hr), the rainfall generated sounds at frequency band from 10 to 20 kHz are proportional to the rainfall rate and relative invariant to wind. For the high wind speed (10m/s above) and/or extremely heavy rainfall (over 150 mm/hr) conditions, a decrease in the sound levels in the frequency band from 20 to 50 kHz is observed. This is evidence of a subsurface bubble layer as previously described. The interaction mechanism of bubble formation from strong wind and/or heavy rain is not well understood. Consequently, the ambient sound data from ITCZ are sorted empirically according to the wind speeds and decomposed into various rainfall rates (Fig. 2.12). The least-squares-fit is used to find the five coefficients for equation 2.9 (as rain-dependent variables this time). This gives a rain-dependent function to estimate the sound level at frequencies 10-50 kHz for four

discrete wind speed bins (0-4, 4-6, 6-8, 8-12 m/s) when rainfall rate is greater than 10 mm/hr. The values for these five coefficients in the equation 2.9 are given in table 2.2.

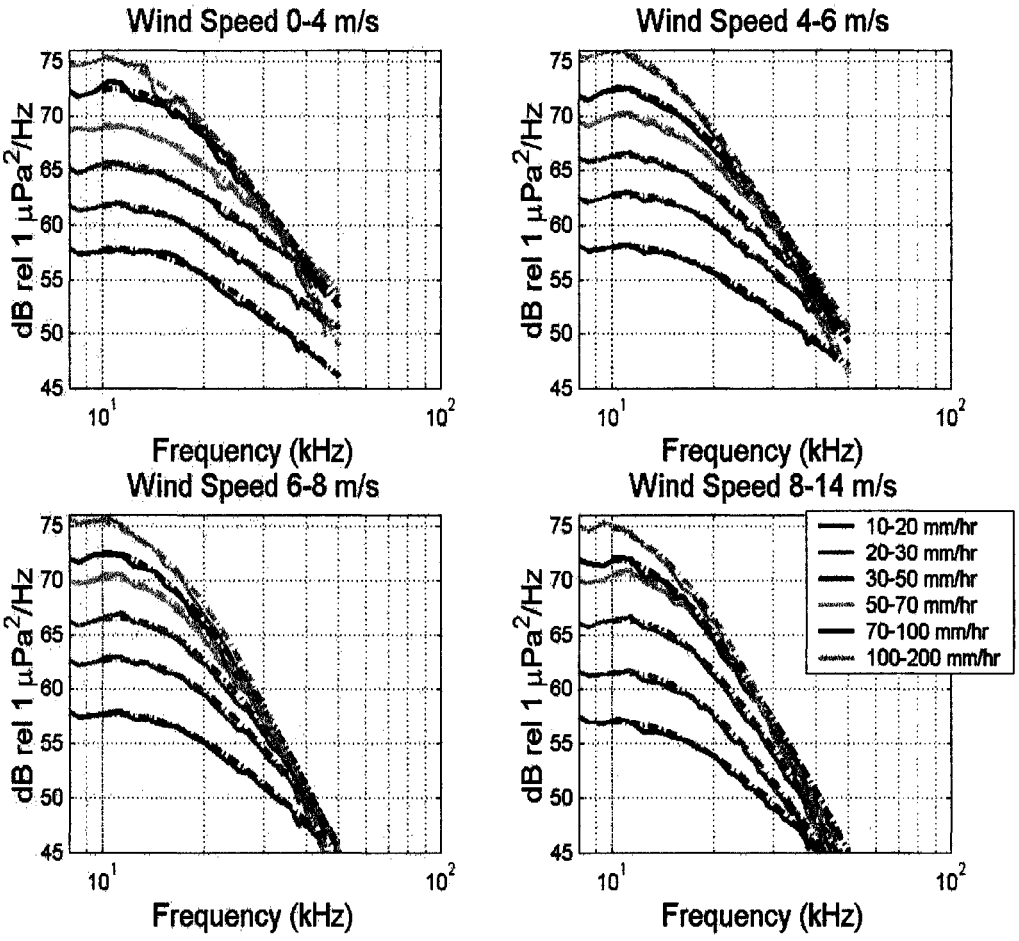


*Figure 2.12 The least squares fits at frequency band 10 to 50 kHz for rainfall rates 10 mm/hr and above. The least squares fits are shown in dash-dotted lines using Eqn 2.9. The numerical values of these five coefficients are given in the table 2.2a-e.*

*Table 2.2 The coefficient values for equation 2.9*

*Table 2.2a.* **log(A)**

| Rainfall Rate / Wind Speed | 2-5 mm/hr | 5-10 mm/hr | 10-20 mm/hr | 20-30 mm/hr | 30-50 mm/hr | 50-70 mm/hr | 70-100 mm/hr | 100-200 mm/hr |
|---|---|---|---|---|---|---|---|---|
| **0-2 m/s** | 14.1957 | 13.8391 | 15.0699 | 12.3104 | 2.0785 | 1.9197 | 2.5930 | 1.9049 |
| **2-4 m/s** | 2.1813 | 11.0307 | 15.0699 | 12.3104 | 2.0785 | 1.9197 | 2.5930 | 1.9049 |
| **4-6 m/s** | 2.2325 | 2.4076 | 2.1078 | 2.2131 | 2.7322 | 1.8805 | 1.8933 | 1.9209 |
| **6-8 m/s** | 12.5647 | 2.5482 | 2.3779 | 2.1635 | 1.9345 | 2.4050 | 1.9077 | 2.4000 |
| **8-10m/s** | 14.6970 | 2.2080 | 2.2181 | 2.2769 | 2.3827 | 1.9199 | 1.9263 | 2.0665 |
| **10-12m/s** | -- | 2.2563 | 2.2181 | 2.2769 | 2.3827 | 1.9199 | 1.9263 | 2.0665 |

*Table 2.2b.* **log(lc)**

| Rainfall Rate / Wind Speed | 2-5 mm/hr | 5-10 mm/hr | 10-20 mm/hr | 20-30 mm/hr | 30-50 mm/hr | 50-70 mm/hr | 70-100 mm/hr | 100-200 mm/hr |
|---|---|---|---|---|---|---|---|---|
| **0-2 m/s** | 12.4299 | 12.0739 | 13.1704 | 10.4903 | -0.1058 | -0.6776 | 0.4561 | -0.9591 |
| **2-4 m/s** | 0.2169 | 9.2616 | 13.1704 | 10.4903 | -0.1058 | -0.6776 | 0.4561 | -0.9591 |
| **4-6 m/s** | 0.3045 | 0.5075 | 0.0294 | 0.1044 | 0.6885 | -0.9660 | -0.9480 | -0.8317 |
| **6-8 m/s** | 10.7961 | 0.6296 | 0.3132 | -0.1925 | -0.6335 | -0.2254 | -0.8116 | -0.7305 |
| **8-10m/s** | 12.8245 | -0.2055 | 0.0579 | 0.0215 | 0.0526 | -0.7155 | -0.6645 | -0.5385 |
| **10-12m/s** | -- | -0.5628 | 0.0579 | 0.0215 | 0.0526 | -0.7155 | -0.6645 | -0.5385 |

*Table 2.2c.* **hc**

| Rainfall Rate / Wind Speed | 2-5 mm/hr | 5-10 mm/hr | 10-20 mm/hr | 20-30 mm/hr | 30-50 mm/hr | 50-70 mm/hr | 70-100 mm/hr | 100-200 mm/hr |
|---|---|---|---|---|---|---|---|---|
| **0-2 m/s** | 0.0454 | 0.0445 | 0.3923 | 0.0859 | 0.0413 | 0.0154 | 0.4321 | 0.0001 |
| **2-4 m/s** | 0.0605 | 0.0736 | 0.3923 | 0.0859 | 0.0413 | 0.0154 | 0.4321 | 0.0001 |
| **4-6 m/s** | 0.0852 | 0.1319 | 0.0824 | 0.1617 | 0.4083 | 0.0024 | 0.0010 | 0.0010 |
| **6-8 m/s** | 0.1385 | 0.2774 | 0.3745 | 0.4374 | 0.0701 | 1.3341 | 0.0041 | 1.9518 |
| **8-10m/s** | 0.4586 | 0.9185 | 0.3838 | 0.5333 | 0.7530 | 0.0190 | 0.0075 | 0.2759 |
| **10-12m/s** | -- | 1.7343 | 0.3838 | 0.5333 | 0.7530 | 0.0190 | 0.0075 | 0.2759 |

*Table 2.2d.* **lslope**

| Rainfall Rate / Wind Speed | 2-5 mm/hr | 5-10 mm/hr | 10-20 mm/hr | 20-30 mm/hr | 30-50 mm/hr | 50-70 mm/hr | 70-100 mm/hr | 100-200 mm/hr |
|---|---|---|---|---|---|---|---|---|
| **0-2 m/s** | 0.2711 | 0.2379 | 0.3681 | 0.2192 | 0.3897 | 0.8067 | 0.5762 | 1.5061 |
| **2-4 m/s** | 0.3741 | 0.2437 | 0.3681 | 0.2192 | 0.3897 | 0.8067 | 0.5762 | 1.5061 |
| **4-6 m/s** | 0.3535 | 0.3324 | 0.3881 | 0.4669 | 0.4840 | 1.3101 | 1.4103 | 1.4390 |
| **6-8 m/s** | 0.2900 | 0.3923 | 0.5055 | 0.8256 | 1.1144 | 1.1233 | 1.3980 | 1.5609 |
| **8-10m/s** | 0.4673 | 0.7730 | 0.6331 | 0.8359 | 0.9257 | 1.3169 | 1.1899 | 1.3694 |
| **10-12m/s** | -- | 0.9563 | 0.6331 | 0.8359 | 0.9257 | 1.3169 | 1.1899 | 1.3694 |

*Table 2.2 (Continued)*

*Table 2.2e.* **hslope**

| Rainfall Rate / Wind Speed | 2-5 mm/hr | 5-10 mm/hr | 10-20 mm/hr | 20-30 mm/hr | 30-50 mm/hr | 50-70 mm/hr | 70-100 mm/hr | 100-200 mm/hr |
|---|---|---|---|---|---|---|---|---|
| **0-2 m/s** | -5.2642 | -3.8849 | -1.0219 | -1.6682 | -2.1001 | -2.6527 | -1.0359 | -9.3603 |
| **2-4 m/s** | -4.0761 | -2.8379 | -1.0219 | -1.6682 | -2.1001 | -2.6527 | -1.0359 | -9.3603 |
| **4-6 m/s** | -3.1740 | -1.7214 | -1.5357 | -1.2627 | -1.0480 | -5.2171 | -6.6678 | -6.4785 |
| **6-8 m/s** | -2.4861 | -1.1529 | -0.9296 | -0.7487 | -1.4518 | -1.4518 | -4.5984 | -0.1006 |
| **8-10m/s** | -1.5047 | -0.4345 | -0.8350 | -0.8713 | -0.8194 | -2.8035 | -3.8332 | -0.4957 |
| **10-12m/s** | -- | -0.1646 | -0.8350 | -0.8713 | -0.8194 | -2.8035 | -3.8332 | -0.4957 |

***Summation***

Finally, the wind-only and rain generated sound spectra are combined using power summation method.

$$SPL_{w,r} = 10\log_{10}\left(10^{(SPLwind/10)} + 10^{(SPLrain/10)}\right) \tag{2.10}$$

where $SPL_{w,r}$ is the spectrum for wind and rain combined, $SPL_{wind}$ is the wind-only spectrum, and $SPL_{rain}$ is the rain spectrum. Note that a 28 dB relative 1 $\mu Pa^2/Hz$ laminate background noise is added to the wind-only spectrum when the wind speed is smaller then 2 m/s. This is due to the ARGs sampling dynamic limit and ocean background noise when neither wind nor rain present. The Eqn 2.5-2.7 for the frequencies 1-10kHz are continuous, but that the Eqn 2.8-2.9 are discrete. In order to match the predicted sound levels at 10 kHz, discrete equivalent rainfall rates are used. The equivalent rainfall rate for each discrete rainfall rate bin is estimated by equation 1.17 for the frequency band 1-10 kHz (Table 2.3). The flowchart of the model is given in figure 2.13.

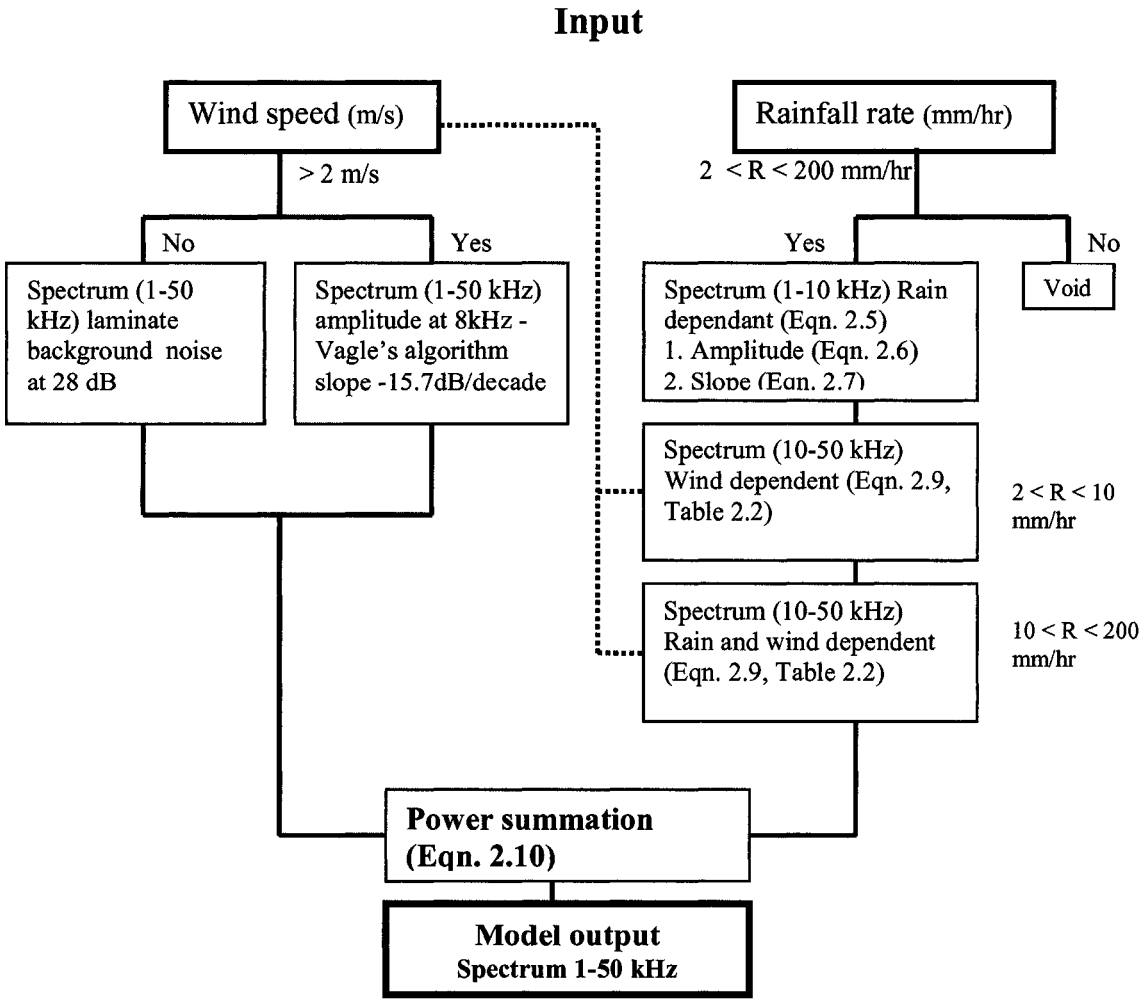


*Figure 2.13 The flowchart of ambient sound model*

*Table 2.3 The equivalent rainfall rate for each discrete data bin.*

| Rainfall rate bin (mm/hr) | 2-5 | 5-10 | 10-20 | 20-30 | 30-50 | 50-70 | 70-100 | 100-200 |
|---|---|---|---|---|---|---|---|---|
| Equivalent rainfall rate (mm/hr) | 3.096 | 7.210 | 13.480 | 24.259 | 38.801 | 59.560 | 79.344 | 126.086 |

## 2.4 Comparison with observations

A section of data during the summer rainy season from year 2000 at 0°, 165° E is used for the modeling result comparison. The input data for the model are acquired from co-located R. M. Young anemometer and rain gauges. A subset of the original 1-min sampling interval of R.M. Young rainfall data is used after obvious errors (negative values and siphoning events) are removed. The wind speeds were recorded using surface anemometer with 10-min sampling interval and interpolated into 1-min interval for model input. The acoustic data were collected using ARG at the depth of 50 meter with 1-min sampling interval during the rain and 9-min during the no-rain periods. Figure 2.14 shows three and a half hours interval before and after a mesoscale convective system (MCS) with maximum rainfall rate reaches 150 mm/hr. There is no rainfall data available from R. M. Young rain gauge at 12:40 (Fig 2.14, patched area). The new ambient sound model (Fig. 2.14, panel 3) mimics the observed sound field (Fig. 2.14, panel 2), and is an improvement of a previous model (APL-UW 9407, 1994). The previous APL-UW 9407 model does not estimate the sound generated by large raindrops well in the frequencies 1-10 kHz which perhaps due to limited rainfall observation data were available when the APL-UW9407 model was constructed (Fig. 2.14, panel 4). Figure 2.15 is a nine-hour interval before and after tropical rain storm with short and intense rainfalls during the storm. At 10:30, there is a low frequency noise in the acoustic record (Fig. 2.15, panel 2). And at 13:00, there is an unidentified high frequency noise. By comparing the model results with observations, the time and frequency of such non-geophysical sources can be extracted.

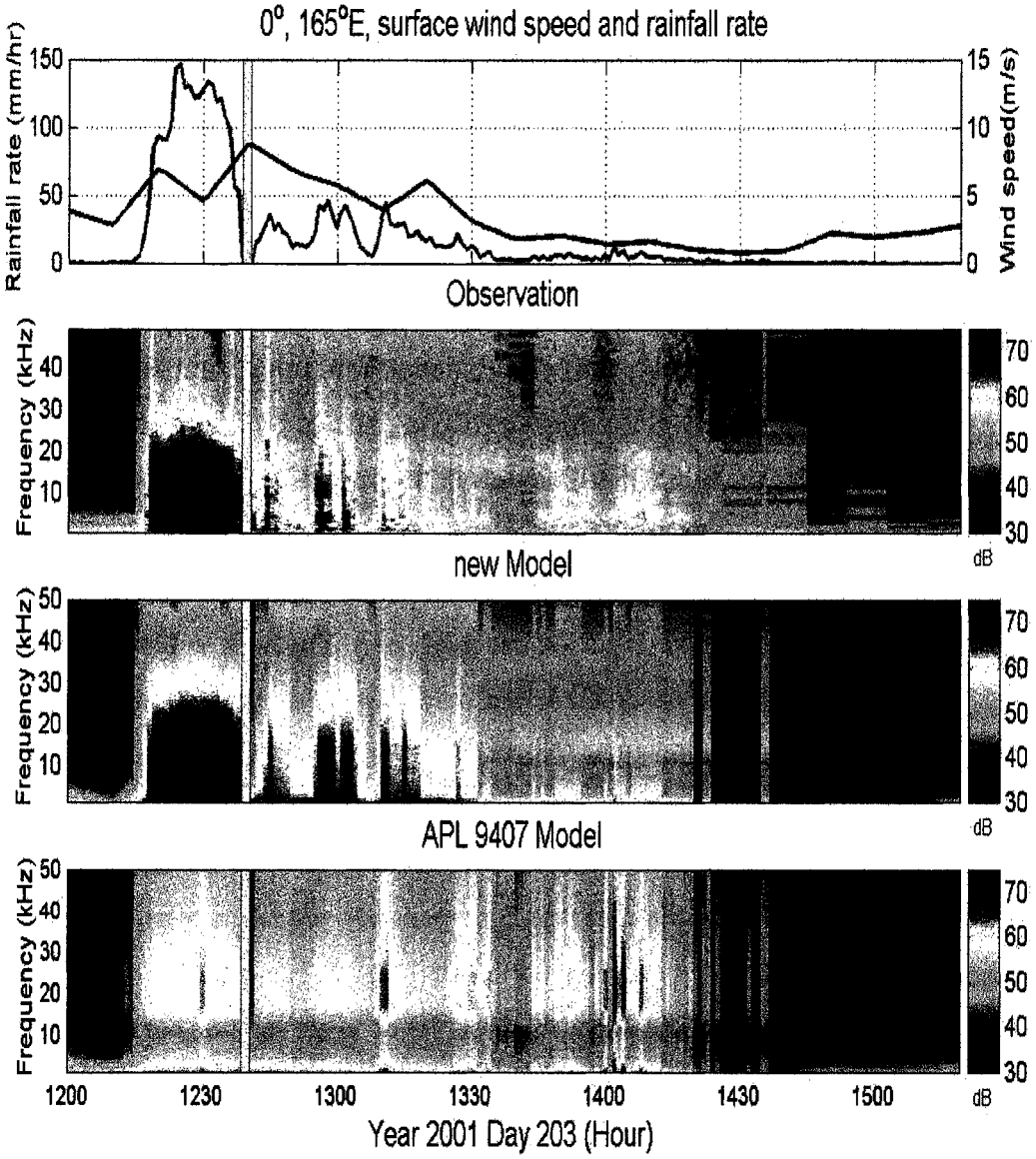


*Figure 2.14 Model results vs. observation at 0 º, 165 ºE in Year 2000 Day 203. Top panel: The input wind speeds and rainfall rate data from surface instruments. Second panel: The observed sound filed using ARG. Third panel: The new ambient sound model result. Bottom panel: The model result form APL-UW 9407. The grey patched area is the time when there was no surface rainfall rate data available.*

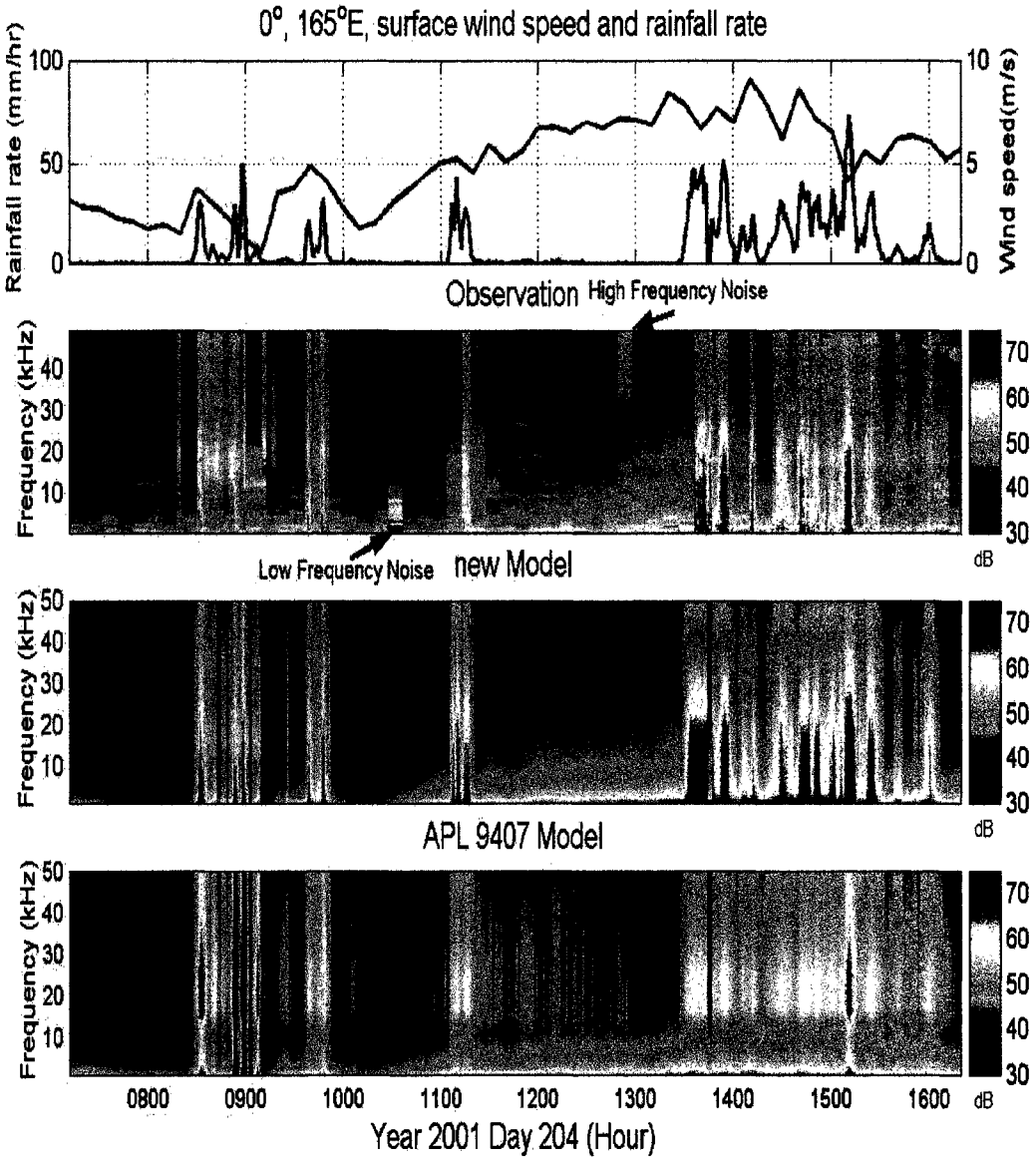


*Figure 2.15 Model results vs. observation at 0 º, 165 ºE in Year 2000 Day 204. Top panel: The input wind speeds and rainfall rate data from surface instruments. Second panel: The observed sound filed using ARG. Third panel: The new ambient sound model result. Bottom panel: The model result form APL-UW 9407.*

**2.5 Discussion and summary**

This empirical ocean ambient sound model is a continuous function for frequencies 1-10 kHz and a discrete function for frequencies 10-50 kHz, and describes acoustic spectrum of rainfall and wind with temporal resolution of one minute or less depending on the input data. There are also some limitations: 1) The algorithms are limited to the wind speed no greater than 14 m/s and rainfall rate smaller than 200 mm/hr. However this should cover most the natural variability of wind and rain. 2) For the wind-only sound prediction, the wind speed below 2 m/s does not produce wave breaking. Sound levels are low under such conditions and so, of course, no correlation with the ambient sound is expected. 3) The sound generated by the rainfall rates below 2 mm/hr are often contaminated by the wind. The probability of rainfall detection is only about 30 % (chapter 1), and thus sound predictions for rainfall rate less than 2 mm/hr are not modeled. 4) The sound levels at transition frequencies (1-2 kHz and 8-10 kHz) may not be well estimated, since there is no clear understanding of the interaction between different sound production mechanisms. 5) A 28 dB re $1\mu Pa^2/Hz$ background noise is added. This is due to ARG's dynamic range limitation and/or the ocean background noise.

Physical processes for five components of the geophysically generated sound field are empirically modeled. This allows the prediction of ocean ambient sound from 1 to 50 kHz using two universal parameters, wind speed and rainfall rate. This provides a baseline of ocean noise levels for acoustic related research, and is also an improvement of previous model APL-UW 9407.

# Chapter 3: The sound of EPIC and the epic of sound

## 3.1 The acoustic aspect of rainfall and wind during EPIC 2001

East Pacific Investigation of Climate Processes (EPIC) is a five year process study to improve the description and understanding of the Pacific cold-tongue/ITCZ complex and the stratus deck region of the Southeastern and Eastern Pacific Ocean. The rainfall climatology of the Eastern Tropical Pacific Ocean is dominated by the ITCZ. The narrow ITCZ is marked by heavy and persistent rainfall. The positions and intensities of the ITCZs are highly sensitive to the underlying sea-surface temperature distribution (Weller et al., 1999). During the EPIC 2001, ARGs were deployed at 10°N and 12°N, 95°W. Rain and wind are identified through the acoustic discrimination process (Appendix B). About 10,000 minutes of rainfall and 70,000 rain free data points (9-min interval) are identified in these two locations. This chapter describes the acoustic analysis of the rainfall and the basic rainfall climatology. A comparison to similar rainfall analysis from two different climatology regions in the Western Tropical Pacific Ocean and Southeastern Pacific are also presented. The percentages of time of overall acoustic signals and noise in these four locations are given in Table 3.1.

*Table 3.1 The percentage of time of overall acoustic signals and noise*

| | **10°N, 95°W** | **12°N, 95°W** | **0, 165°E** | **20°S, 85°W** |
|---|---|---|---|---|
| **Wind** | 64.70 % | 71.40 % | 72.20 % | 79.25 % |
| **Rain** | 1.10 % | 0.75 % | 0.37 % | 0.02 % |
| **Drizzle** | 0.40 % | 0.25 % | 0.23 % | 0 % |
| **Noise** | 33.80 % | 27.60 % | 27.20 % | 20.73% |

The acoustic wind speeds and rainfall rates are shown in figure 3.1 - 3.4 for 10°N, 95°W; 12°N, 95°W; 0, 165°E; and 20°S, 85°W respectively. The acoustic data have the sampling intervals 9-minute for wind, 3-minute for drizzle, and 1-minute for rain. Each panel on the figure 3.1 - 3.4 represents one month of record, and only the rainy months are shown. The R. M. Young anemometer wind speeds are also shown for the

intercomparison on the figure 3.1-3.3. The ARGs do not give wind speed estimates during the rainfall, since the rain generated sound is the dominant sound source when it is present. Although it is possible to estimate the wind speeds during the drizzle using the peak signal at 15 kHz or during the extreme rainfall using the sound suppressing levels due to the bubble clouds (see, chapter 2 for details), no attempt is made here to estimate wind speed during rain, drizzle or otherwise noisy conditions. The clusters of rainfall from EPIC seem to be separated at about 4-6 days interval (Fig. 3.1 & 3.2), yet the clusters of rainfall from 0, 165°E are separated by about 8-12 days (Fig. 3.3), twice as long as in the Eastern Pacific. At 20°S, 95°W, rainfall rarely occurs; the annual accumulation is only about 30mm. The rainfall climatology in these regions will be further analyzed.

The surface wind speeds and rainfall rates are calculated using the equation 1.12 and 1.17 respectively. The acoustic wind speeds are smoothed by taking a 3 data-point (27 minutes) running-mean. The correlation coefficients of acoustic wind and R.M. Young anemometer are shown in table 3.2. Different time–average intervals are considered, and a comparison using all data points and only data when the wind speeds is above 2 m/s. The correlation for the wind speeds 2 m/s above is expected to be slightly higher than the one calculated from all data points because low winds do not generate breaking waves, and thus there is no acoustic signal. Table 3.2 indicates that a 30-minute to hourly average of acoustic wind speeds is sufficient to have a comparable result to and excellent agreement with surface anemometer data. Longer time-average intervals improve the correlations, but not significantly. The correlation coefficients at 10°N are higher than 12°N. The higher amounts of rainfall and larger percentage of local mooring noises can contribute to this result. The scatter plots for time-average intervals 3-hour, 6-hour, 12-hour and daily at 12°N, 95°W are shown in figure 3.5. The acoustic wind speeds do not have any point smaller than 2.5 m/s, which is due to the algorithm limitation (Eqn. 1.12). The annual mean wind speed is 5.2 m/s and the maximum wind speed is about 14 m/s for this year-long acoustic wind record.

*Table 3.2 Correlation coefficients of acoustic wind speed estimates and surface anemometer wind speeds*

| Time-average interval | 10°N, 95°W | | 12°N, 95°W | |
|---|---|---|---|---|
| | all | > 2m/s | all | > 2 m/s |
| **10 minutes** | 0.8353 | 0.8411 | 0.9195 | 0.9210 |
| **hourly** | 0.8712 | 0.8840 | 0.9403 | 0.9428 |
| **3 hours** | 0.8937 | 0.9089 | 0.9506 | 0.9531 |
| **6 hours** | 0.9021 | 0.9146 | 0.9546 | 0.9530 |
| **12 hours** | 0.9058 | 0.9144 | 0.9599 | 0.9584 |
| **daily** | 0.9030 | 0.9142 | 0.9621 | 0.9593 |

For the rainfall, this part of the ocean has a distinctive wet and dry pattern each associated with the seasonal movement of ITCZ. The rainy season is from May to roughly the end of November (see chapter 1, Fig. 1.13). The resolution of the acoustic rainfall rate measurement is one minute, with the maximum rainfall rate 374 mm/hr recorded at the 10°N, 95°W, but for only one minute. The maximum 10-min rainfall rate from the RMY rain gauge was 83 mm/hr. This difference is expected as the acoustic rainfall measurement is an instantaneous measurement where as the RMY is an accumulation gauge, necessarily smoothing extreme values. The monthly rainfall accumulation is shown in figure 3.6. For the 10°N, 95°W, the month of September in 2001 has the rainfall accumulation 590 mm, which accounts for one third of annual precipitation for 2001. Accumulation of two extreme rainy days during September 2001 accounted for one third of monthly accumulation on September. This shows the episodic character of the rainfall climatology in this region. At 12°N, 95°W, the rainfalls are more evenly distributed throughout the wet season with monthly accumulations ranging from 150 mm to 250 mm. Histograms of acoustic rainfall rates versus the accumulations with the bin-width 2 mm/hr are shown in figure 3.7. The rainfall rates at 10 mm/hr account for most of the rainfall at these locations. This figure may be biased because the acoustic detection of lighter rainfall rates (< 2 mm/hr) is limited.

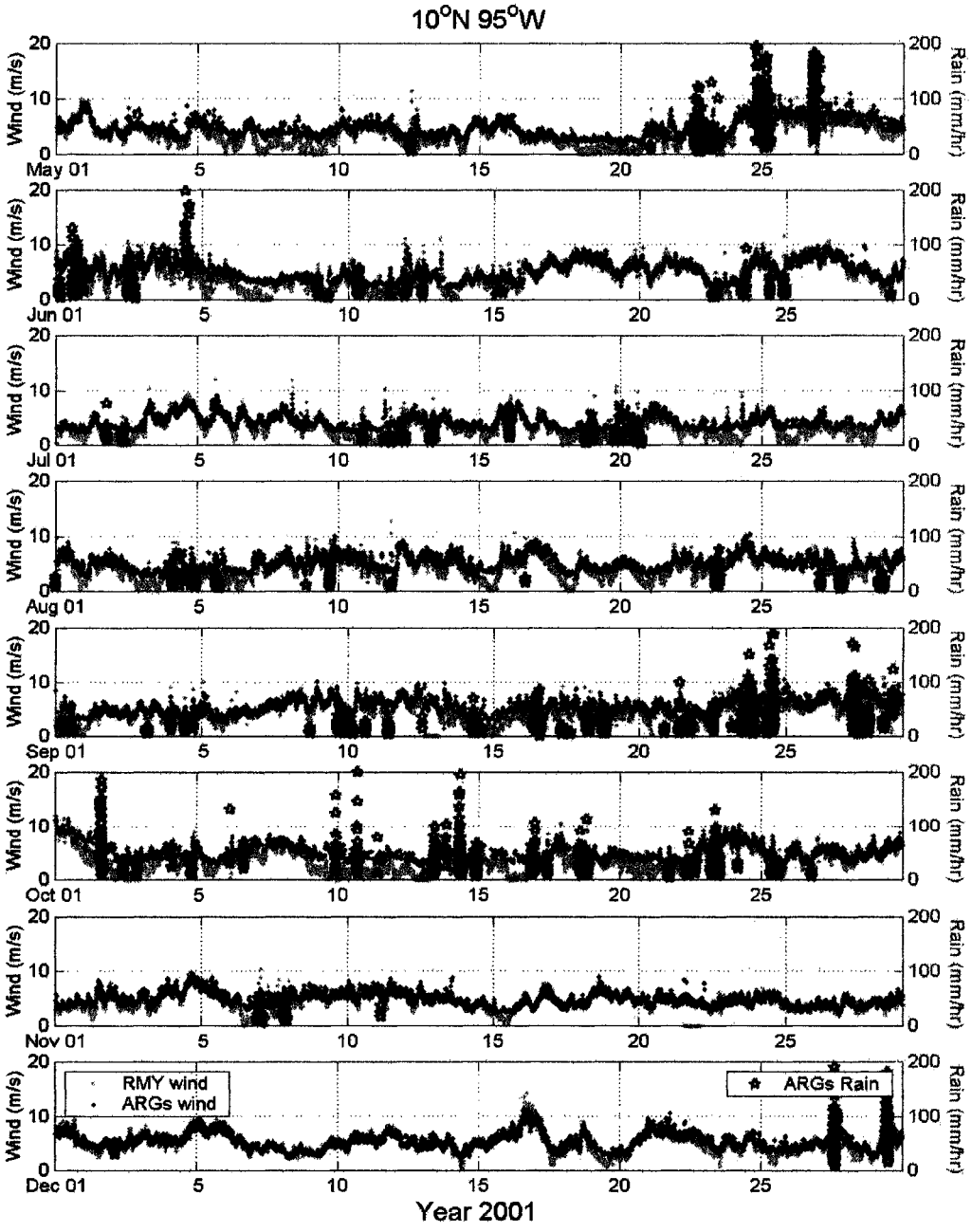


*Figure 3.1 The acoustic rainfall and wind estimates at 10°N, 95°W from May to December, 2001.*

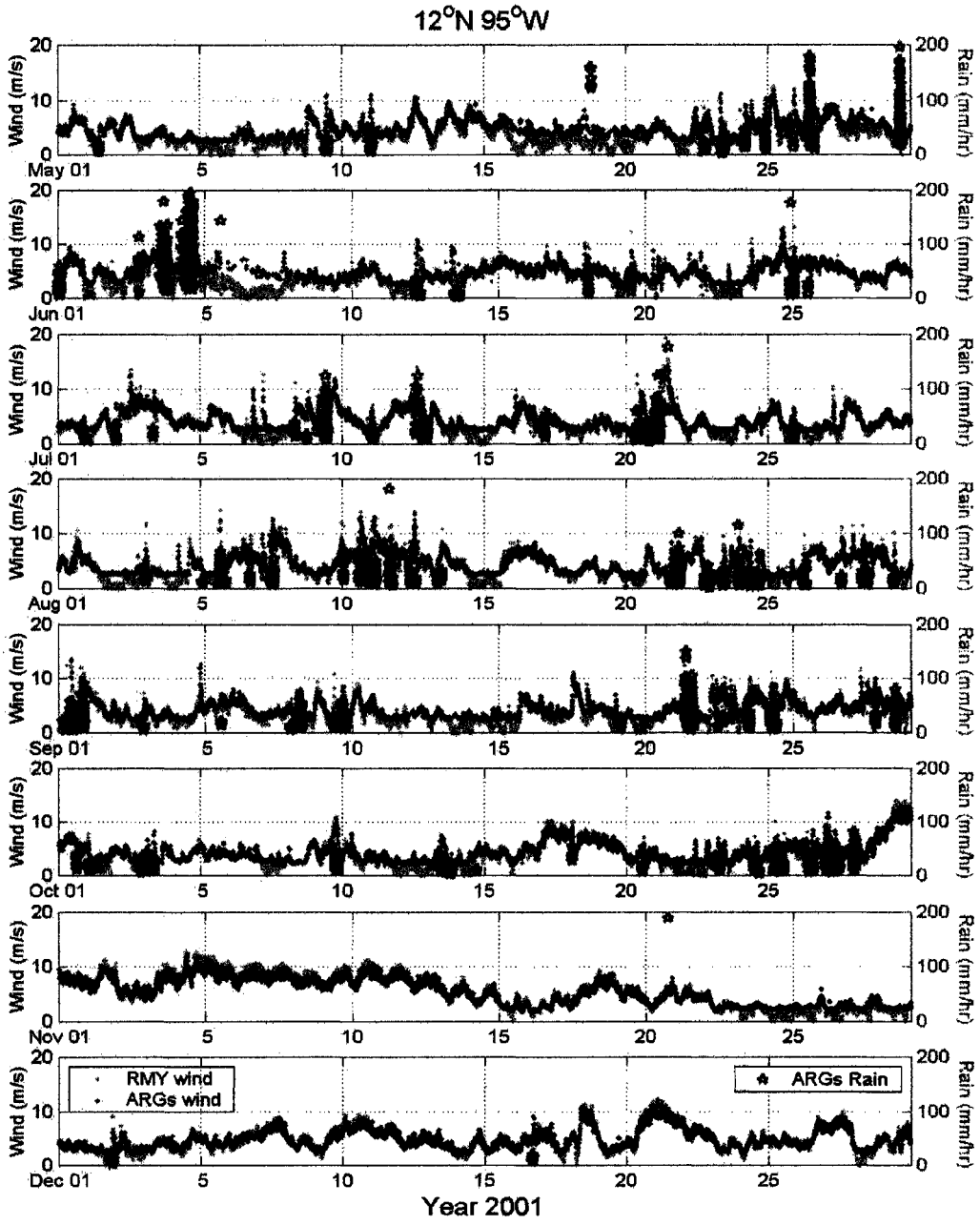


*Figure 3.2 The acoustic rainfall and wind estimates at 12°N, 95°W from May to December, 2001.*

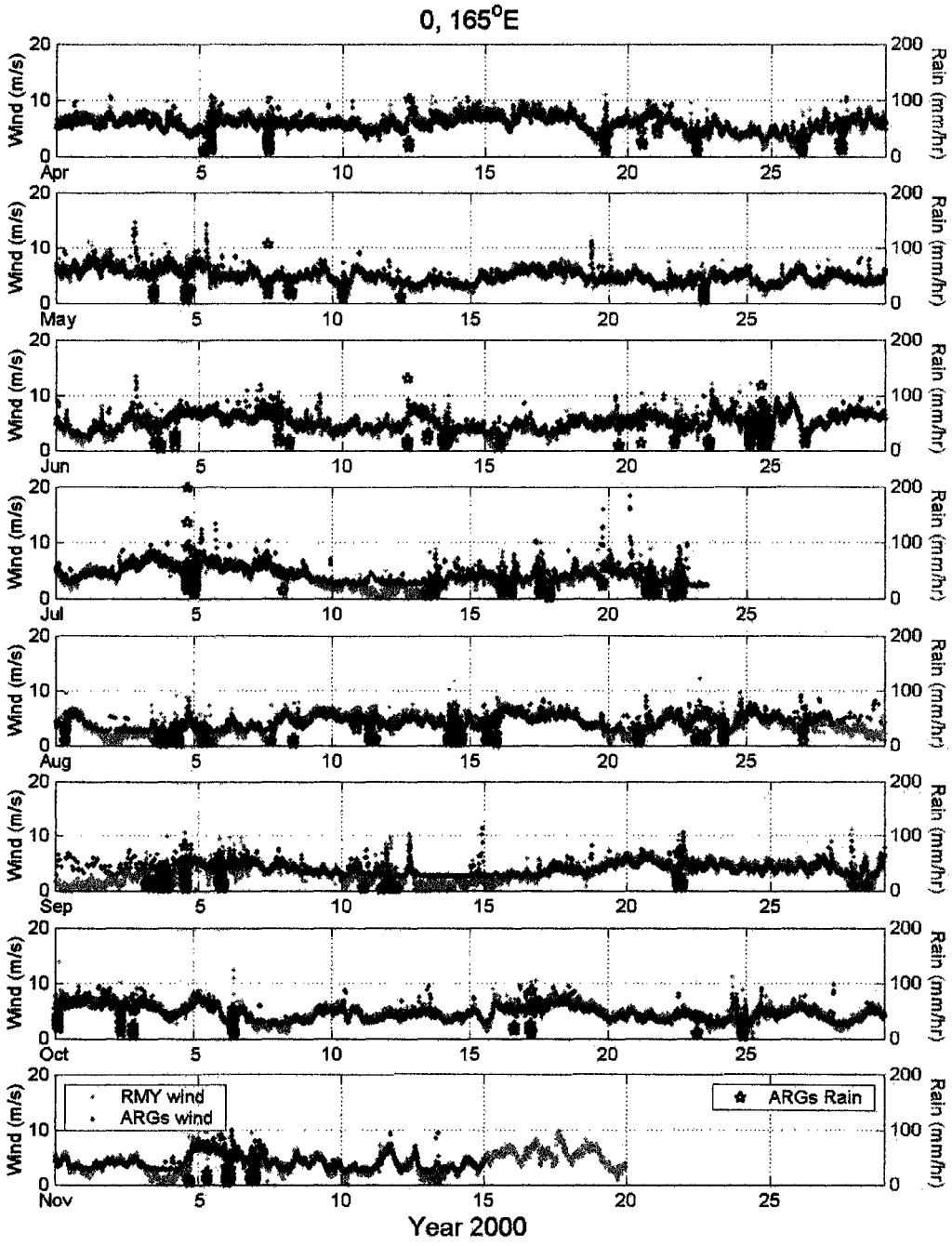


*Figure 3.3 The acoustic rainfall and wind estimates at 0, 165°E from April to November, 2000.*

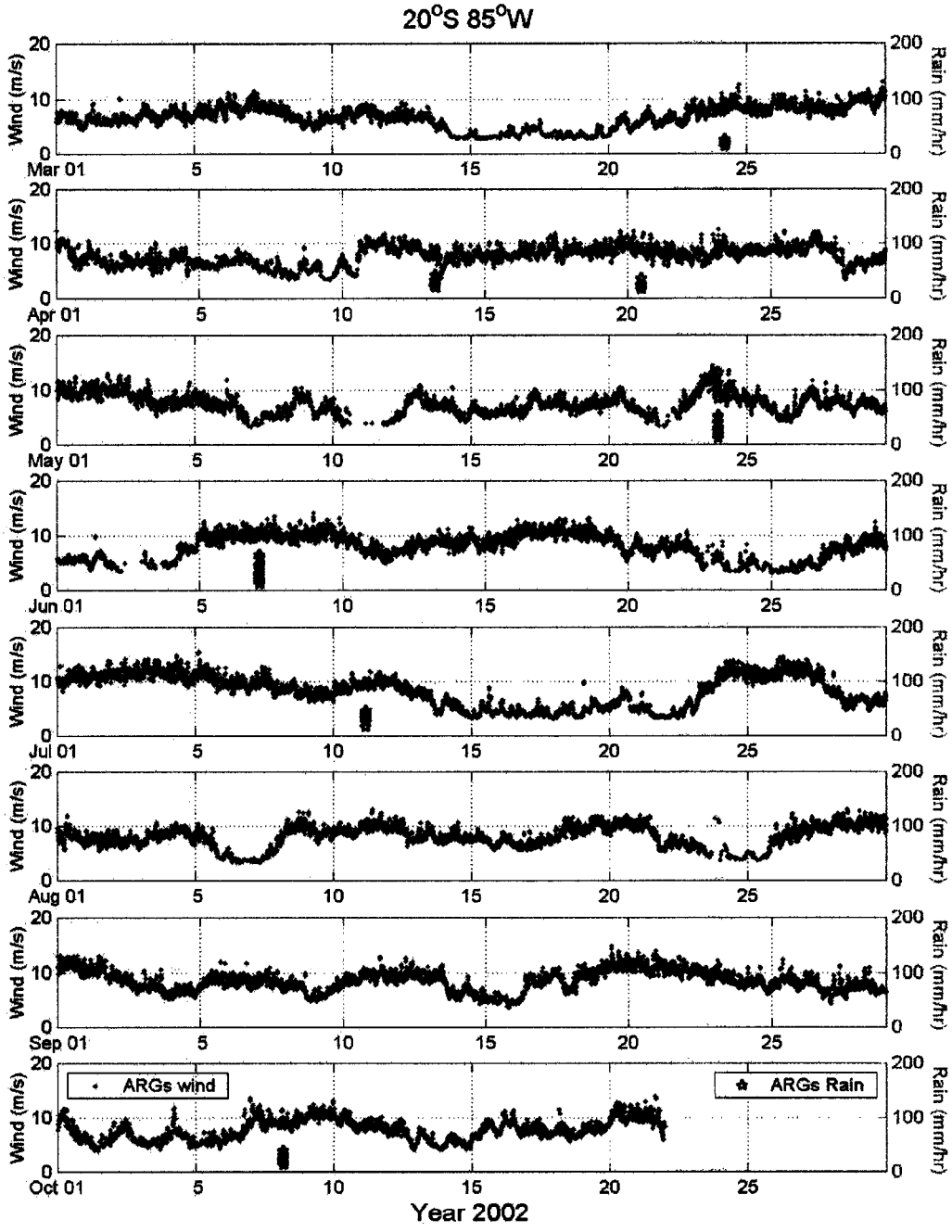


*Figure 3.4 The acoustic rainfall and wind estimates at 20°S, 95°W from March to October, 2002.*

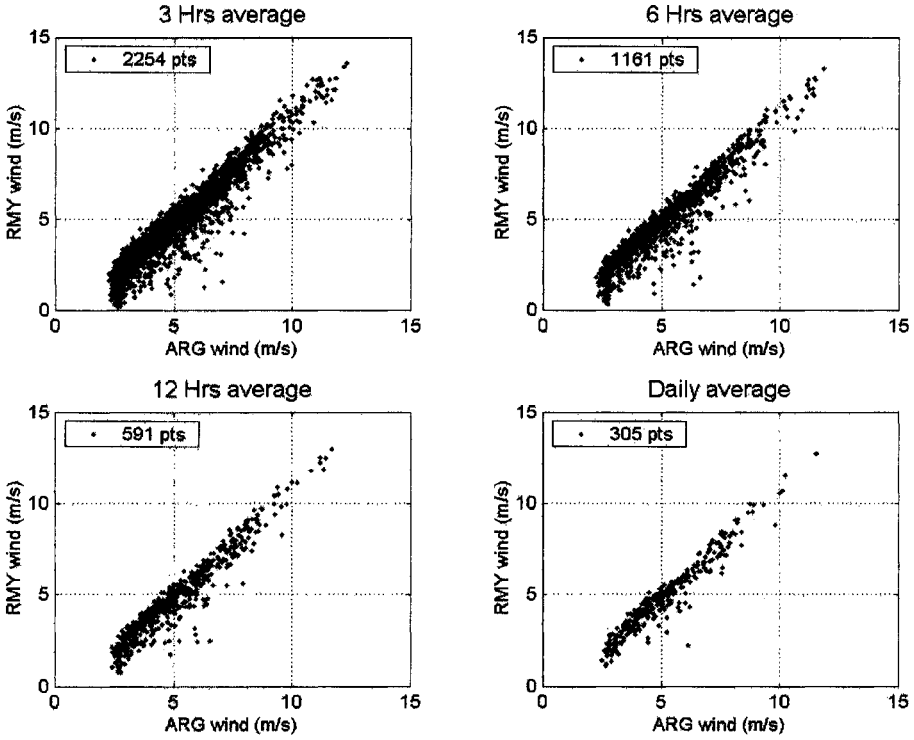


*Figure 3.5 The acoustic rainfall estimate versus R.M. Young anemometer in different time-averaging interval for the 12°N, 95°W. The numbers in the legend box represent how many data points are in each scatter plot.*

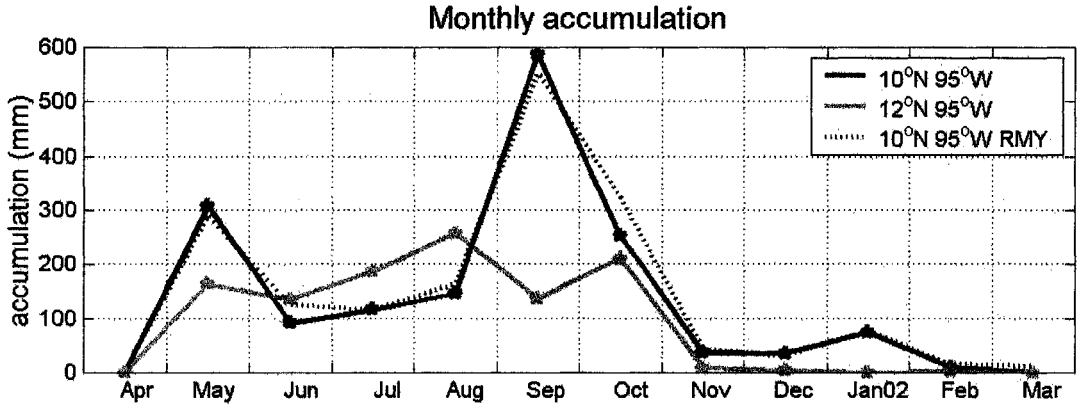


*Figure 3.6 The monthly rainfall accumulation at the 10°N, 95°W and 12°N, 95°W. The RMY accumulation is shown for the 10°N, but not at the 12°N due to the RMY failure during the deployment.*

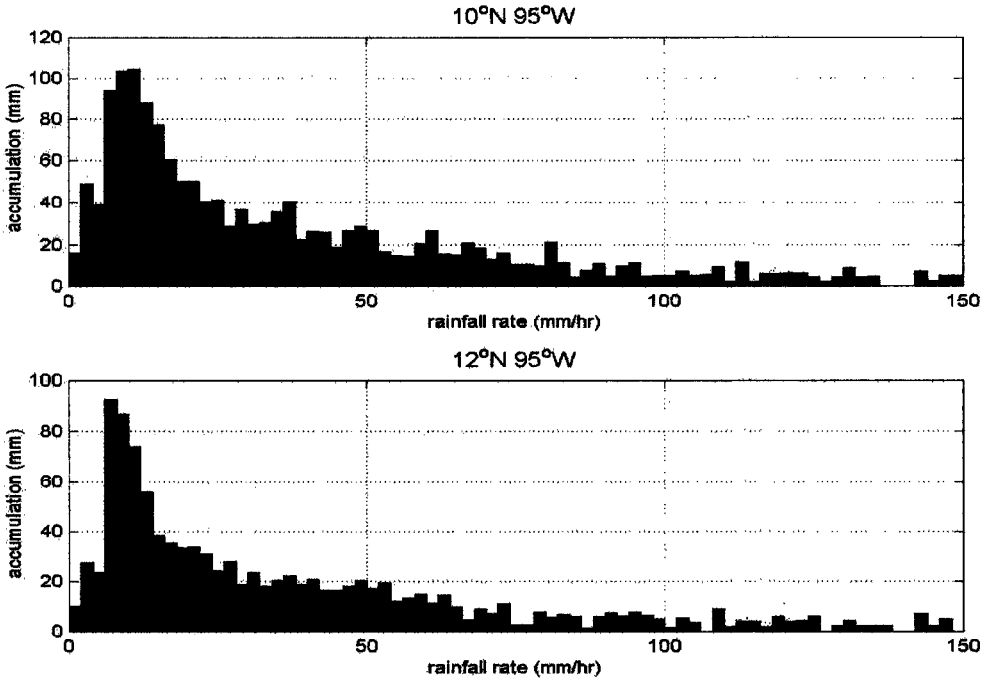


*Figure 3.7 The accumulations versus the rainfall rates for 10°N, 95°W and 12°N, 95°W.*

### 3.2 Rainfall events analysis

Ideally one would like to be able to define a "rain event", so that a "typical" rain event for a region can be described, and so that the influence of a "typical" rain event on the underlying ocean can be described. It is apparent from figure 3.1-3.4 that rain events occur in clusters separated by several days, weeks or even months and that within these clusters, individual events occur, separated by minutes, hours or days. In fact, rainfall is intermittent even within an organized atmospheric system. This means that defining an event is difficult. The acoustic data provides a very high temporal resolution of rainfall detection. We can use separation of rainfall detection to try to define what will be called separate event. Take the temporal separation of 20 minutes as an example. A "rainfall event" will be defined as a group of rainfall detections with time intervals in between data points that are all smaller than 20 minutes. In other words, there is no "new" event if the next rainfall detection is less than 20 minutes away. The schematic diagram of rainfall

event definition is given in the figure 3.8. Given this definition, there are 216 events at 10°N, 95°W, and 173 events at 12°N, 95°W. The numbers of rainfall events with correspondent separations are shown in table 3.3. Three event quantities are defined as: the "event accumulation" (EACC) is the rainfall accumulated during the event; the "event duration" (EDU) is the time from the beginning to the end of the event; and the "actual rain time" (ART) is the time that rain is actually falling during the event. The averages of these three quantities are given in table 3.3. As the event separation time increases, the events number decreases, but the EACC, EDU and ART increases. Figure 3.9 shows the scatter plot of EDU versus ART for separation cases 10, 15, and 20 min. The average EDU and average ART are roughly the same when the event separation is smaller than 20 min. However, the average EDU begins to become larger than average ART when the separation time is greater than 20 min and continues to grow as the separation time increases. When the ratio of EDU to ART becomes large, it is an indication that there is a gap of non-rain in the event, suggesting that two separate events have been combined together. A separation time of 20 minutes for the EPIC region, or 20-30 for the western Pacific site is chosen (ratio of EDU/ART $\approx$ 1.10) as this separation time subjectively partitions the data into coherent "event". It is apparent that the EACC and ART has a fixed ratio even when the separation time is different. Figure 3.10 is the scatter plot of EACC versus ART using the separation time 10, 15, 20, 30, 60, 120, and 240 minutes at 10°N, 95°W. The regression is given by

$$ART = (a + EACC) \times b \tag{3.1}$$

where $a$ is the intercept, $b$ is the slope, the ART is in minutes, and EACC is in mm. The $a$ and $b$ for three different locations are given in table 3.4. This indicates that the EACC is about one quarter of ART regardless the event separation time, and indicates a mean rainfall rate during the time when it is actually raining, ~15mm/hr.

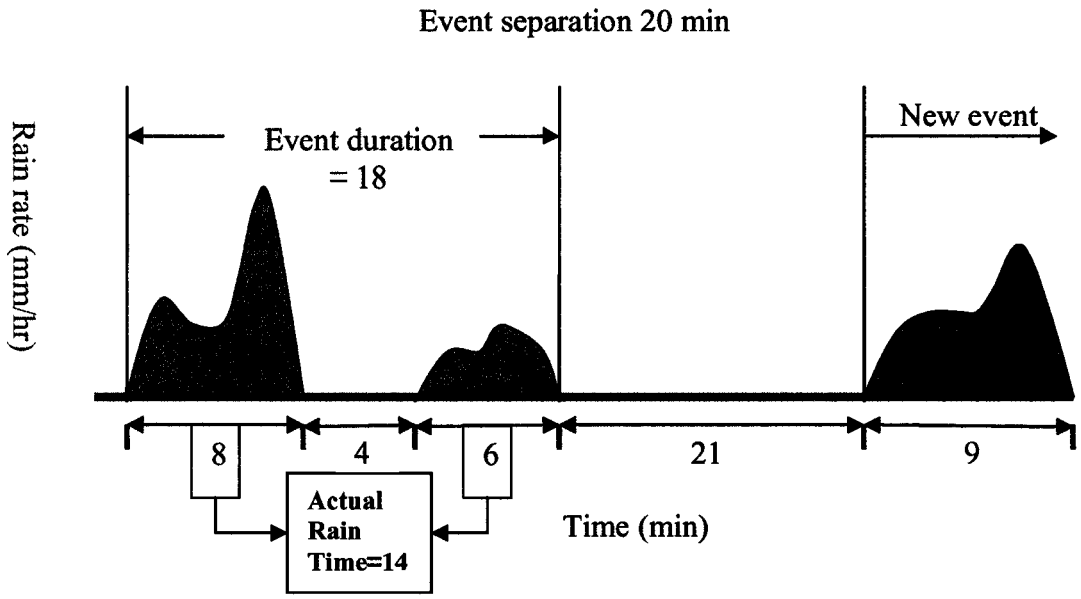


*Figure 3.8 The rainfall event definition for the event separation time 20 min.*

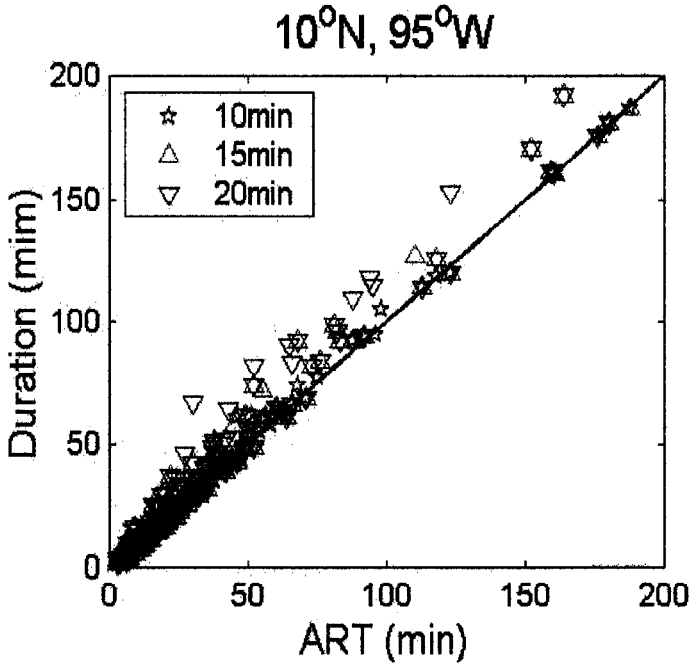


*Figure 3.9 The actual rain time versus duration for event separation cases 10, 15, and 20 min.*

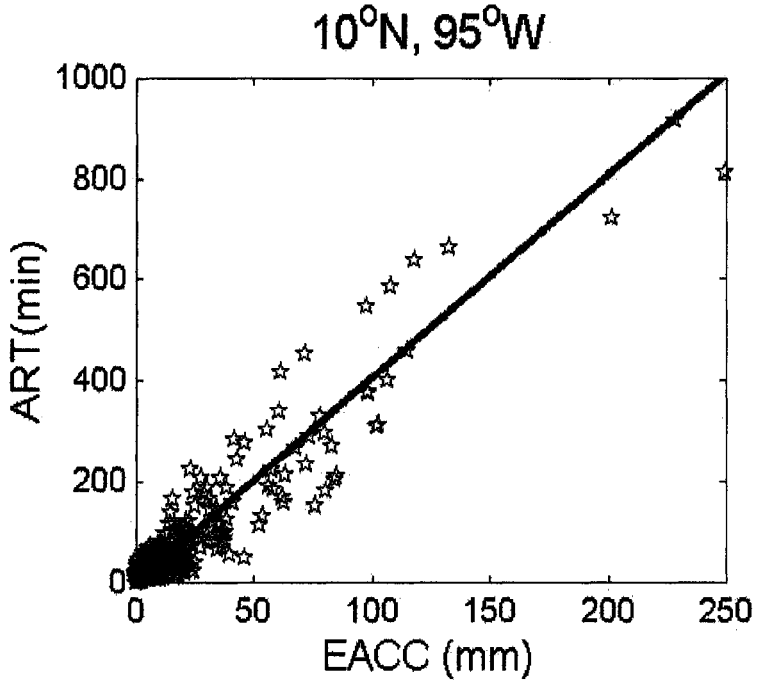


*Figure 3.10 The event accumulation versus actual rain time for event separation (10, 15, 20, 30, 60, 120, and 240 minutes)*

*Table 3.3 Rainfall events at 10°N, 95°W, 12°N, 95°W, and 0, 165°E. The 20- min separation time is selected for further analysis.*

| Event separation (minutes) | Rain events at 10°N, 95°W | | | | Rain events at 12°N, 95°W | | | | Rain events at 0, 165°E | | | |
|---|---|---|---|---|---|---|---|---|---|---|---|---|
| | Event # | average accumulation (mm) | average duration (min) | average actual rain time (min) | Event # | average accumulation (mm) | average duration (min) | average actual rain time (min) | Event # | average accumulation (mm) | average duration (min) | average actual rain time (min) |
| 10 min | 244 | 6.9 | 28.4 | 28.1 | 210 | 5.4 | 23.0 | 22.5 | 150 | 4.3 | 17.6 | 16.6 |
| 15 min | 222 | 7.6 | 32.6 | 30.9 | 183 | 6.2 | 28.4 | 25.8 | 146 | 4.5 | 18.1 | 17.4 |
| 20 min | 216 | 8.0 | 35.9 | 32.8 | 173 | 6.6 | 31.5 | 27.4 | 141 | 4.6 | 18.7 | 18.6 |
| 30 min | 188 | 9.0 | 42.7 | 36.5 | 162 | 6.9 | 34.9 | 29.1 | 130 | 5.0 | 22.6 | 20 |
| 60 min | 164 | 10.3 | 56.2 | 42 | 139 | 8.2 | 49.3 | 34.5 | 122 | 5.3 | 27.1 | 21.7 |
| 120 min | 143 | 11.8 | 76.5 | 48 | 118 | 9.5 | 70.7 | 40 | 108 | 6.0 | 41.18 | 24.5 |
| 240 min | 123 | 13.8 | 115.6 | 55.8 | 97 | 11.6 | 121.8 | 48.7 | 94 | 6.9 | 74.8 | 28.1 |

*Table 3.4 The intercepts and slopes for equation 3.1.*

| location | a ( intercept) | b (slope) |
|---|---|---|
| 10°N, 95°W | 0.3 | 4.0 |
| 12°N, 95°W | -2.2 | 4.4 |
| 0, 165°E | 0.8 | 3.9 |

We can now generate statistics for rain events. Consider the case of 20-minute separation, the average duration is about 33 minutes and the average accumulation is 7 mm in the EPIC region. In contrast, at 0, 165°E these numbers are about 19 min and 4.6 mm (Table 3.3). In other words, the average event in the EPIC region is bigger-longer with higher accumulation than in the western Pacific. The histograms of events versus durations (bin-width 3 minute) and accumulations (bin-width 3mm) are shown in figure 3.11 and 3.12. The mode of the distribution is at 11 minutes, but with important long-duration outliers. The largest event at 10°N has 80 mm of rainfall and 58 mm of rainfall at 12°N. The longest event duration is about 4 hours for 10°N and 3 hours for 12°N. The mode of the accumulation histogram is at the smallest event accumulation bin (0-3 mm) but one half of the annual precipitation at 10°N, 95°W and 12°N, 95°W comes from the events with accumulations larger than 15 mm. At 0°, 165°E, large events only account for about one third of the total rain. This means that the rainfall climatology includes longer rainfall events in the Eastern Tropical Pacific Ocean. Yet the mean rainfall rate during rain is the same, roughly 15 mm/hr (Table 3.4).

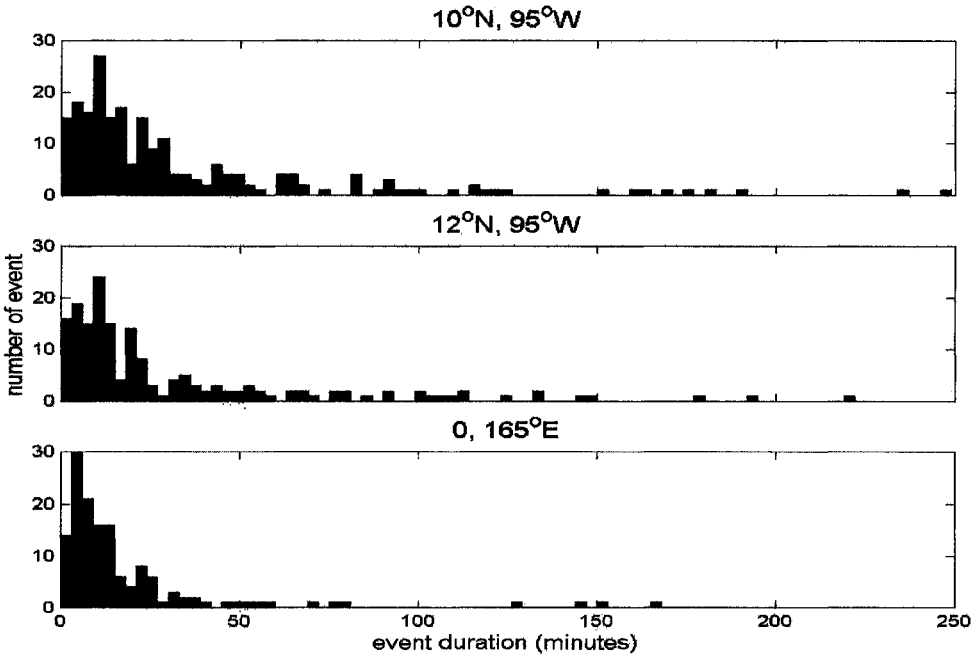


*Figure 3.11 Histogram of rainfall duration with bin-width 3 mm/hr and event separation 20 min.*

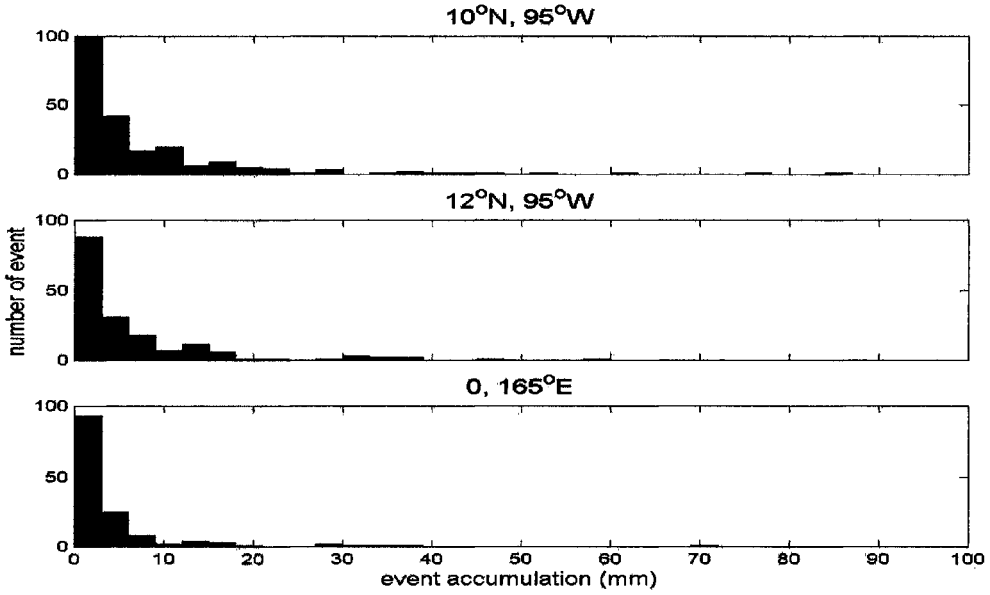


*Figure 3.12 Histogram of rainfall event accumulation with bin-width 3 mm and event separation 20 min.*

### 3.3 Detection of rain events using air-sea temperature difference

Because detection and measurement of rainfall at sea is difficult, other methodologies for identifying rain events have been pursued. One of these is to use the air-sea temperature difference change that occurs as the rainfall begins. Yuter et al. 2003 attempted to detect drizzle by comparing the time series of actual drizzle area fraction from a C-band radar and air-sea temperature difference [$\Delta T$ = sea surface temperature (SST) - air temperature (AT)]. Figure 3.13 shows the acoustic rainfall rates and air-sea temperature differences for a 20-day period at 12°N, 95°W. This figure suggests that the rainfall events are positively associated with $\Delta T$, and demonstrates that there is a cooling of the near-surface atmosphere (AT) by precipitation. The year-long record from 12°N, 95°W shows that the mean SST is 28.11°C with standard deviation 2.0, and the mean AT is 26.68°C with standard deviation 5.9. The correlation of SST and $\Delta T$ is 0.03; while for AT and $\Delta T$ it is 0.97. This means that the air-sea temperature differences are caused mainly by the fluctuations of AT.

To assess the potential of rainfall detection using the $\Delta T$ thresholds, the acoustic rainfall events (20-min separation as defined in chapter 3.2) are compared with observed $\Delta T$ from the moorings which interpolated into 20-min intervals. Different $\Delta T$ thresholds are tested for the data from 10°N, 95°W and 12°N, 95°W. The $\Delta T$ from 10 minutes prior to the rainfall event and 10 minutes after the rainfall event are examined for two quantities, average $\Delta T$ and maximum $\Delta T$. This ensures that a $\Delta T$ can be retrieved even in the shortest rainfall event. Three events from 12°N, 95°W with failed SST records are disqualified. The analysis uses the acoustic rainfall data as ground truth. If the $\Delta T$ (maximum or average) in a rainfall event is higher than the given threshold, this event will be defined as "detected". If a $\Delta T$ sample is higher than the threshold but without an associated rainfall event, the sample will be defined as "false alarm". The results are given in table 3.5. At the 12°N, 95°W, the probabilities of detection are 90 % (average $\Delta T$) and 93.5 % (maximum $\Delta T$), and the false alarm rate is 17.4 % for the threshold setting at 0.8°C. At 10°N, 95°W, the probabilities of detection are 90.2 % (average $\Delta T$)

and 93.5 % (maximum $\Delta T$), and the false alarm rate is 13.3% for the threshold setting at 1.2°C. These results are similar to the study of Yuter et al. (2003), but the thresholds are lower. Yuter et al. reported that the probability of detection and false alarm rate, for the $\Delta T$ threshold at 1.8°C, are 90% and 15% respectively. However they studied the heavy drizzle in the stratocumulus regions (18°S, 85°W) where the drizzle is prevalent; and compared every $\Delta T$ within the event, not the average or maximum $\Delta T$. Thus, the differences between these two results should be expected.

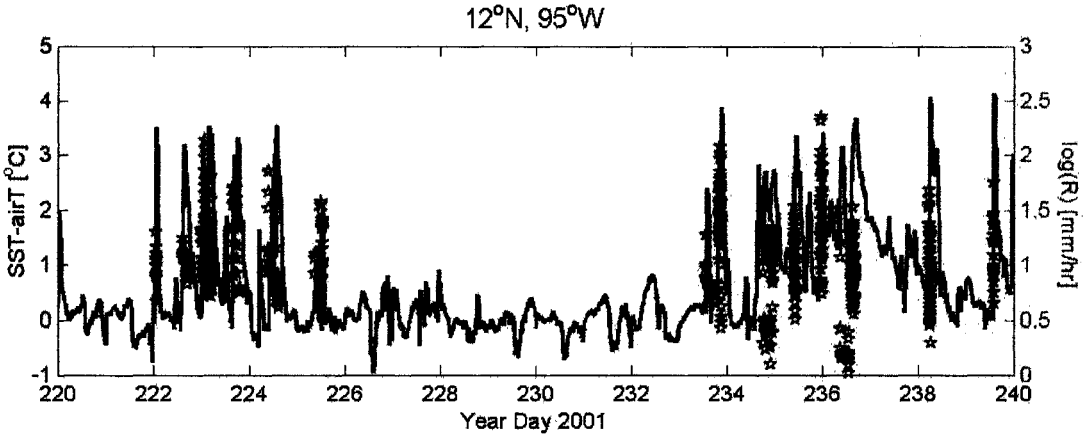


*Figure 3.13 Air-sea temperature differences and 1-min acoustic rainfall rates. The air temperature measurements are acquired every 10-min from the mooring's resistance temperature recorder (Pt-100) with resolution 0.01°C and accuracy ± 0.2°C at 3 meter above the sear surface. The SSTs are acquired from temperature sensor every 10-min with resolution 0.001°C and accuracy ±0.003°C at 1 m deep.*

A low false alarm rate is desired for rainfall detection given the intermittence of naturally occurring rainfall. Comparing the detection analysis of ARG and RMY given in chapter 1 (Fig. 1.10), the false alarm rate smaller than 0.5 % is desirable to make the instrument reliable for year-long rainfall detection at sea. As the temperature threshold setting increases, the false alarm rate decreases, but the probability of detection becomes lower as well (Table 3.5). For the false alarm rate smaller than 1% (threshold 3.5°C), the probability of detection will be reduced to 20-30 %. This is much too low to measure rainfall properly. Thus, as a single indicator, the air-sea temperature difference should not

be used as a rainfall detector, but it is still an important reference for the occurrences of rainfall, especially for the large accumulation events. Note that with a detection threshold of 3.5°C, the probability of detection is 40.7 % using maximum $\Delta T$, yet accumulation in these detections is 68 % of total accumulation.

*Table 3.5 The probabilities of rainfall detection and false alarm rates using air-sea temperature difference.*

| **temperature threshold (°C)** | **10°N, 95°W** | | | | | |
|---|---|---|---|---|---|---|
| | 216 rain events | | | | 27708 no rain $\Delta T$ samples | |
| | average ($\Delta T$) events detected | % | max($\Delta T$) events detected | % | false alarms | % |
| 0.8 | 203 | 94 | 209 | 96.7 | 6505 | 23.5 |
| 1 | 199 | 92.1 | 204 | 94.4 | 4904 | 17.7 |
| 1.2 | 195 | 90.2 | 202 | 93.5 | 3686 | 13.3 |
| 1.5 | 174 | 80.5 | 192 | 88.8 | 2430 | 8.7 |
| 2 | 155 | 71.8 | 178 | 82.4 | 1117 | 4.0 |
| 2.5 | 123 | 56.9 | 147 | 68.0 | 538 | 1.9 |
| 3 | 85 | 39.3 | 122 | 56.4 | 275 | .99 |
| 3.5 | 53 | 24.5 | 88 | 40.7 | 127 | .46 |
| **temperature threshold (°C)** | **12°N, 95°W** | | | | | |
| | 170 rain events | | | | 26983 no rain $\Delta T$ samples | |
| | average ($\Delta T$) events detected | % | max ($\Delta T$) events detected | % | false alarms | % |
| 0.8 | 153 | 90 | 159 | 93.5 | 4698 | 17.4 |
| 1 | 148 | 87 | 157 | 92.3 | 3274 | 12.3 |
| 1.2 | 144 | 84.7 | 152 | 89.4 | 2339 | 8.6 |
| 1.5 | 136 | 80.5 | 150 | 88.2 | 1532 | 5.6 |
| 2 | 119 | 70 | 137 | 80.5 | 791 | 2.9 |
| 2.5 | 85 | 50 | 117 | 68.8 | 395 | 1.4 |
| 3 | 49 | 28.8 | 80 | 47 | 165 | 0.61 |
| 3.5 | 23 | 13.5 | 51 | 30 | 70 | 0.26 |

### 3.4 Acoustic classification of rainfall types

Measuring the drop size distribution (DSD) within a naturally occurring rain allows different measures of the rain, such as liquid water content, optical cross-section, rainfall-rate or radar reflectivity, to be calculated. Furthermore, different rainfall types can often be identified by changes in DSD (Atlas et al. 1999). Nystuen (1996; 2001) demonstrates that the DSD can be measured acoustically, and Nystuen and Amitai (2003) show that acoustic rainfall classification is possible. This is possible because different sound generating mechanisms are present for different raindrop sizes, producing unique sound signals for the different raindrops sizes (Fig. 3.14).

Nystuen (1996, 2001) describes the inversion in detail. Briefly, the sound intensity, $I_o$, at the surface is related to the DSD in the rain by:

$$I_0(f)=\int A(D,f)V_T(D)N(D)dD \tag{3.2}$$

where $f$ is frequency, $A(D,f)$ is the transfer function describing the radiated sound as a function of frequency for a given drop size, $D$, $V_T$ is the terminal velocity of the drop and $N(D)$ is the drop size distribution (DSD) in the rain. In a measurement situation, this equation is discrete and given by:

$$I_0(f)=A(D,f)\cdot DRD(D) \tag{3.3}$$

where DRD is the drop rate density, $DRD = V_T \bullet N(D)$. If the inversion matrix, **A**, is known, then, using singular value decomposition, equation 3.3 can be inverted to make a measurement of the drop size distribution in the rain.

$$A=\mathbf{U}\Lambda\mathbf{V}^T$$

$$DRD = \mathbf{V}\left[\Lambda^{-1}\left(\mathbf{U}^{T}\mathbf{I}_{0}\right)\right] \tag{3.4}$$

The transfer function *A(D,f)* has been determined by empirical decomposition of field observations, and is shown in figure 3.14. The acoustic drop size categories and equivalent drop size for each acoustic inverted category are shown in table 3.6.

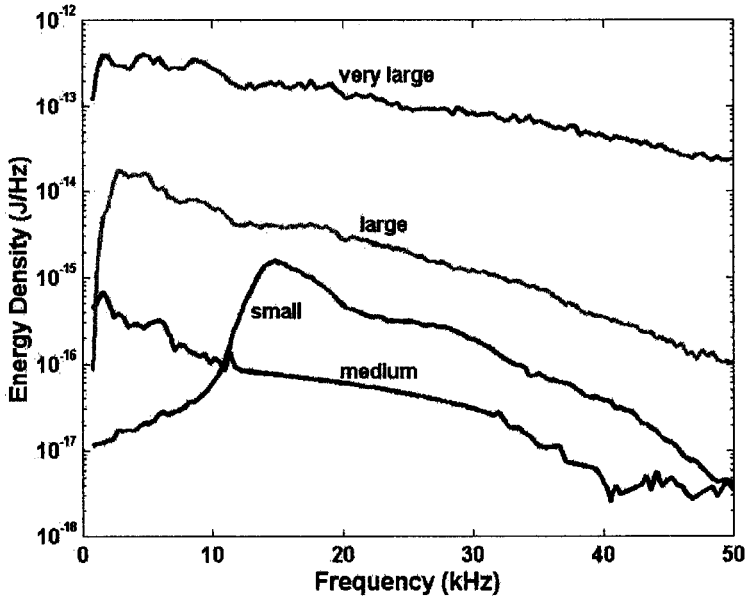


*Figure 3.14 Radiated acoustic energy densities for very large, large, medium and small raindrop sizes. Note the spectral peaks associated with different raindrop sizes. These peaks are due to the each drop size produces sound underwater with unique spectral features that can be used to acoustically identify the present of that drop size within the rain. This is the result from a brackish pond in Miami, FL. (Nystuen 1996, 2001).*

*Table 3.6 the acoustic drops size categories and equivalent drop size.*

| | small | medium | large | very large |
|---|---|---|---|---|
| Acoustic drop sizes (mm) | 0.72-1.23 | 1.23-2.08 | 2.08-3.5 | 3.5 and up |
| Equivalent drop size (mm) | 0.95 | 1.6 | 2.8 | 4.5 |

The acoustic inversion for DSD is demonstrated by Nystuen (2001), but that work was based on field data collected in a shallow brackish pond. Applying the same inversion algorithm to open ocean data required some adjustment. Ideally a new

transform function $A(D,f)$ should be determined. However, the inversion matrix for the open ocean is very difficult to acquire, since the direct measurement of DSD is almost impossible. Thus the inversion matrix **A** computed from the field data of the Florida experiment is used, but it is expected that bottom reverberation in shallow water will produce an overall sound level increase. Furthermore, the average energy spectral densities from large drops are 3 to 4 dB less in salt water than in fresh water, due to a lower initial acoustic pressure of the bubble formed in salt water (Medwin et al, 1992). Therefore, a correction factor is needed to offset these increased sound levels before applying the inversion matrix **A** to the open ocean data. The correction factor is assumed to be frequency independent.

$$I_o = 10^{(SPL_o + SPL_{corr})/10} \tag{3.5}$$

where $SPL_o$ is the original sound pressure level observed from the open ocean, and the $SPL_{corr}$ is the correction factor. The correction factor is determined by matching the total accumulation of rainfall over a long-term deployment period (~1 year) using the inversion with the total accumulation using equation 1.17 at each location. Figure 3.15 is an example from 0°, 165°E in 2000. The $SPL_{corr}$ is 9 dB at this location. The DSD is inverted using equation 3.4 (Fig. 3.15, second panel). The rainfall rates are calculated using both single frequency conversion and full inversion (Fig. 3.15, third panel). The rainfall types are acoustically classified using the criteria described in the Nystuen and Amitai, 2003. The convective rains start at the beginning of the heavy downpour which have maximum rainfall rate at about 200 mm/hr and followed by stratiform rain lasting about 2 hours. From the DSD data it is possible to calculate a variety of the rainfall products, including accumulation, equivalent reflectivity [the radar measurement (Z)] and rainfall rate (R).

Rainfall shows not only an intermittence in time, but also a patchiness in space. This makes rainfall one of most difficult natural variables to measure. In addition to the ancillary data from the mooring itself, the R.V. Ronald H. Brown (RHB) was positioned near 10°N 95°W from September 12 to October 1, 2001, and its ship-borne radar data are

available. Radar provides great spatial coverage (240 x 240 km) with 10 minutes interval in 1x1 km resolution, and it provides rainfall classification information. Figure 3.16 shows the patchiness of the rainfall spatially. Small convective cells are imbedded within a more stratiform rainfall.

On the other hand, ARGs have excellent temporal resolution (< 1 minute) with a spatial of roughly 200 m x 200 m. The original sound field is inverted using equation 3.4 to obtain the DSD with the $SPL_{corr}$ at 10 dB. This particular event was a major rainfall event lasting about four hours and consisted of a convective cell with a series of pulses of heavy rainfall lasting from 1015 to 1215, followed by a long stratiform interval starting at 1240. For comparison, 10-min RMY rain gauge (accumulation gauge) and the 10-min radar measurement (RHB) are converted to rainfall rate (Fig. 3.17). The difference in temporal resolution is very apparent, with the RMY accumulations lagging the acoustic measurement as is expected of a comparison of "instantaneous" measurements versus an accumulation-type instrument. The radar measurements from the RHB are quite low relative to the acoustic measurements, and the ultimate RMY accumulations (Fig. 3.17). This might be due to poor temporal sampling of the strong, but brief rain cells, but probably the relation used to estimate rainfall rate, R, from reflectivity, Z, (Z-R relationship) may need some adjustment.

The two acoustic estimates of rainfall diverge as the rain changes from convective to stratiform. This is because equation 1.17 implicitly assumes a DSD shape typical of convective rainfall. Stratiform rainfall has relatively fewer small and medium sized raindrops, and thus equation 1.17 overestimates stratiform rainfall rates. However, if the full inversion for DSD is used, then the agreement with the RMY rain gauge improves, and is probably correct. This results suggests that the full DSD acoustic inversion for rainfall rate should be used when mixed stratiform / convection rainfall systems are being measured acoustically, and may explain some of the discrepancies observed when comparing the single frequency inversion (Eqn. 1.17) with R. M. Young rain gauge accumulations (Fig. 1.12).

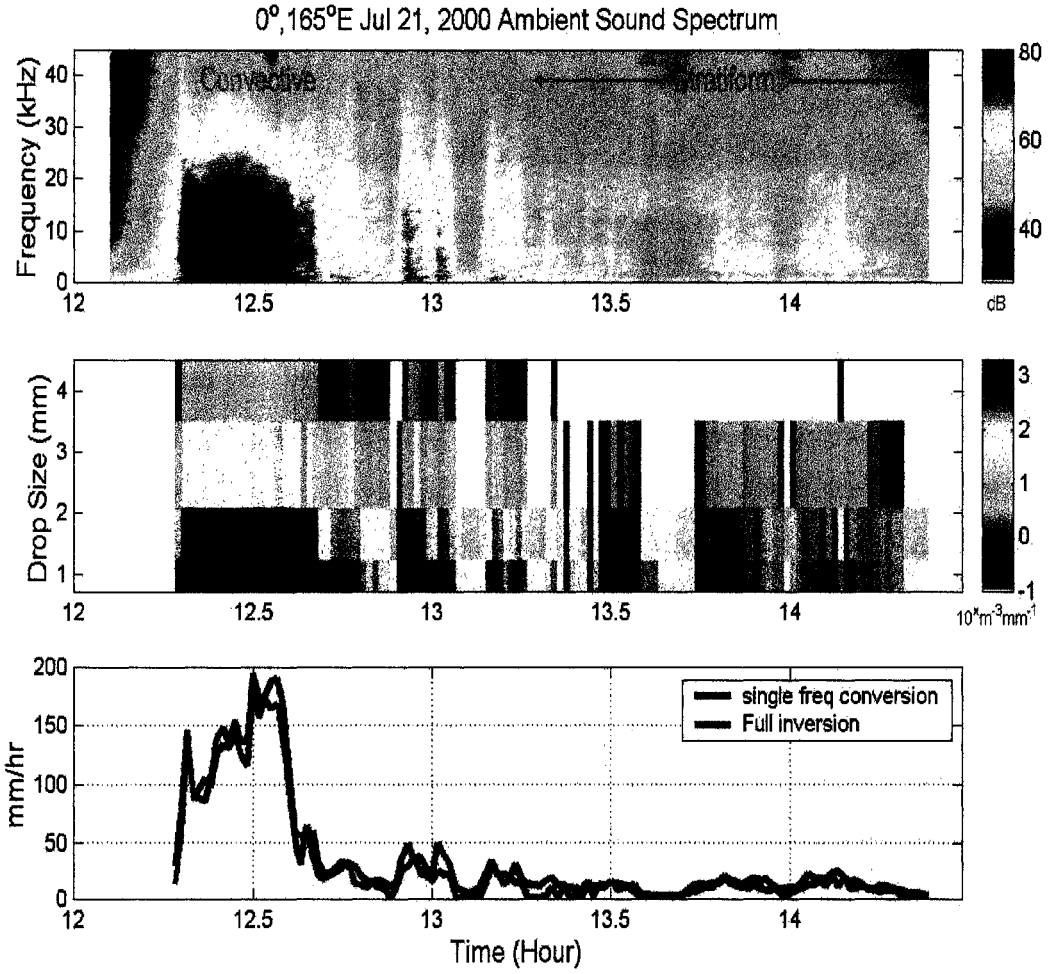


*Figure 3.15 The ocean ambient sound from 0, 165°E. The convective rain produces strong sound signals from 1 to 35 kHz. The stratiform rain (drizzle) has a peak signal at 15 kHz.*

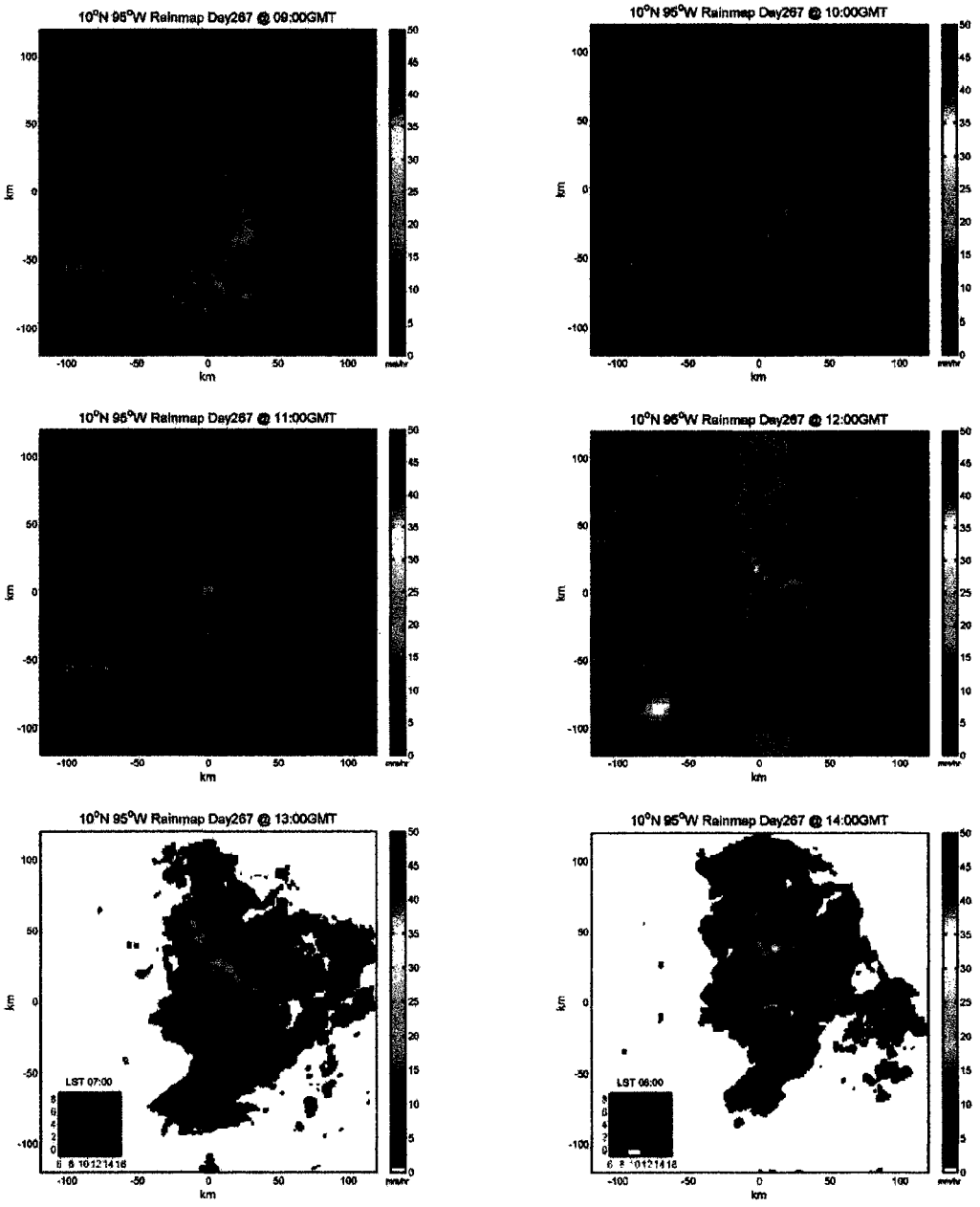


*Figure 3.16 Rainmaps from RHB precipitation radar centered at 10°N, 95°W in 2001. The subplot in each panel at left-bottom corner is the zoom in of the red square in the middle (10 x 10 km). The red star is position of the mooring at the moment. The R.V. Ronald H. Brown was positioned near by the 10°N, 95°W mooring. The black and white backgrounds represent the contrast of day and night.*

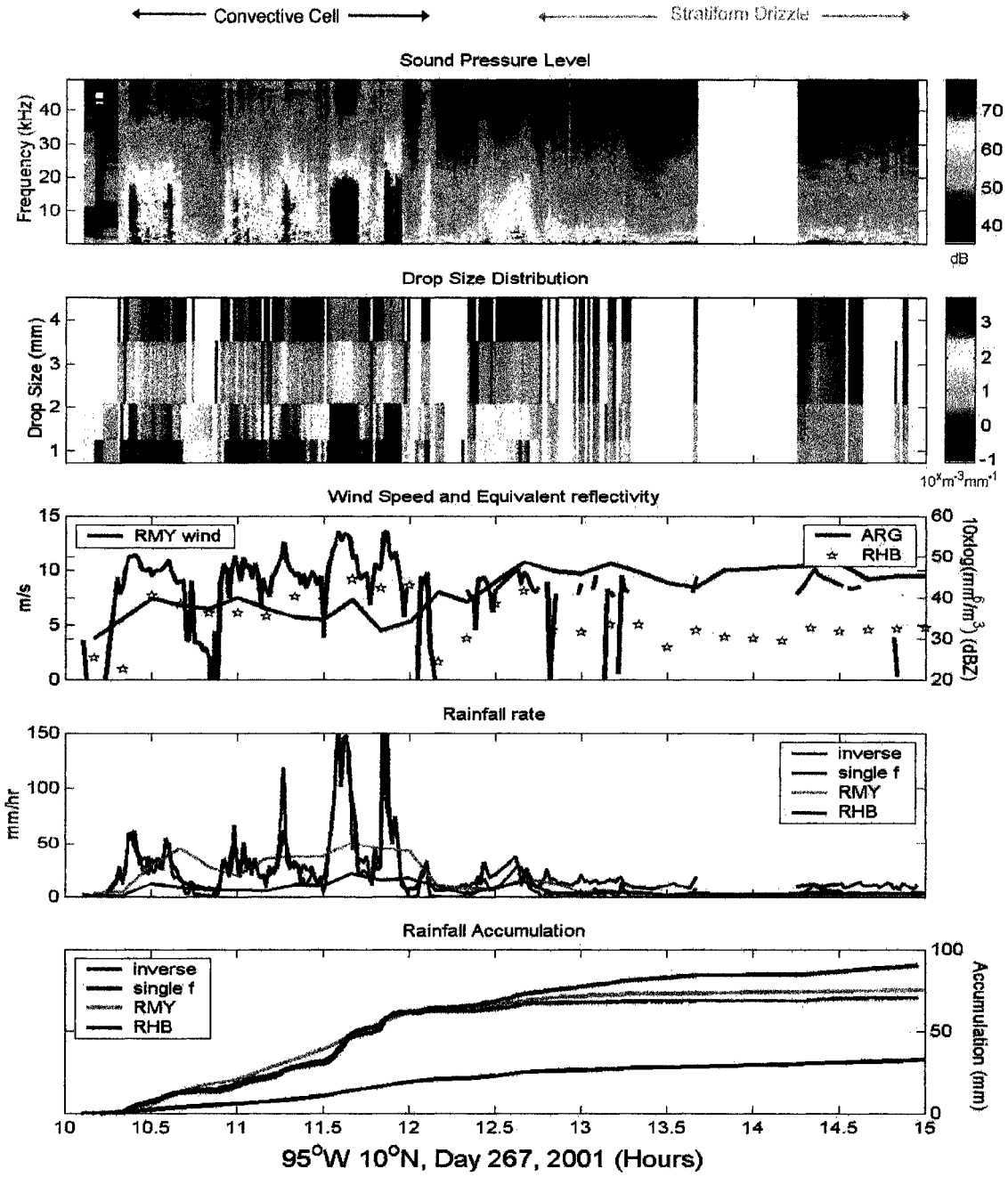


*Figure 3.17 A heavy rainfall event on the year day 267 (Sep 24th), 2001. The sound field is shown along with the acoustic inversion for DSD. Acoustic rainfall products [accumulation, rainfall rate, reflectivity (dBZ)] are compared to shipboard radar (RHB) and buoy-mounted instruments (R.M.Y anemometer and rain gauge). Both the single frequency (single f) and multi-frequency (inverse) acoustic rainfall rate algorithms are shown.*

### 3.5 Ocean surface salinity responses due to the rainfall during EPIC 2001

Rains deposit pools of fresh water locally on the ocean resulting in a stratified surface layer. The buoyant fresh water on the surface inhibits downward surface mixing. Lateral-spreading and vertical mixing slowly dissipates the fresh puddles while advection moves it around. Because the ocean mixed layer responds to the surface-generated turbulence through wind and buoyancy forced processes, the surface mixed layer can often be modeled successfully using one-dimensional physics (Cronin and Sprintall, 2001). In this section, the fresh water penetration to the ocean due to the rainfall will be examined using the acoustic rainfall data and ancillary data from the TAO mooring at 10°N, 95°W.

Figure 3.18 shows the mean salinity structure at 10°N, 95°W from April 25 to September 25, 2001. This shows a relatively well mixed fresh water layer in the top 20 m. The monthly mean salinity structure and ± 1 standard deviation are shown in figure 3.19. This figure shows the mean freshening of the upper 10 m during the rainy season, and indicates that the standard deviation of the salinity in this layer increases once the rainy season commences in mid-May. Generally the top 10m is well mixed, but individual rain events inject fresh water plumes that can be detected as they mix downward. These features are shown in figure 3.19 by plotting individual salinity data 1-5 hours after individual events are recorded at 1m, 5-10 hours at 5m and 10-20 hours at 10m. The fresh water plumes appear as fresh water outliers on the salinity distributions prominent in May, July, and September when large accumulation events occurred (Fig. 3.1).

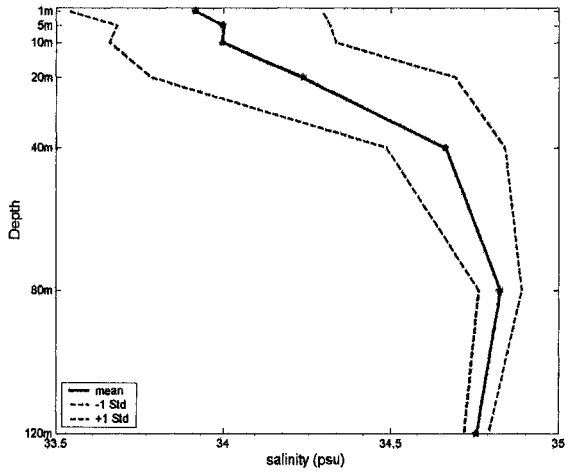


*Figure 3.18 The mean salinity structure at 10°N, 95°W from April 25 to September 25, 2001. The mean salinity and ±1 standard deviation are shown for each depth.*

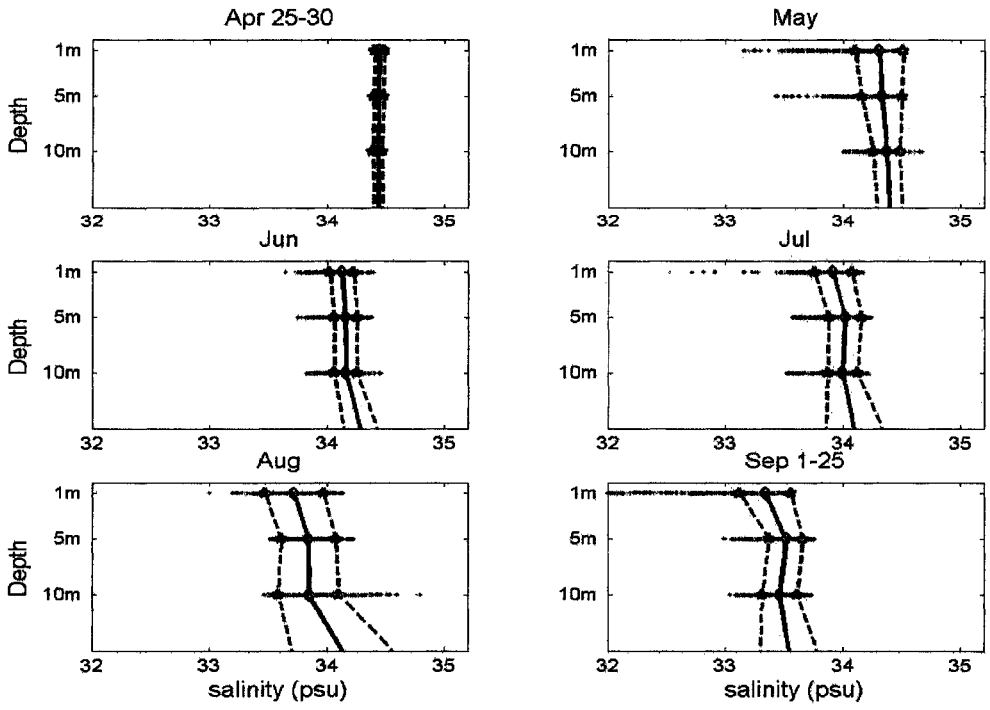


*Figure 3.19 The monthly mean salinity and ± 1 standard deviation. Salinity data for individual events 1 hour after rain started to 5 hours after rain stop at 1m, 5-10 hours after the rain event at 5m, and 10-20 hours after the rain event at 10m are shown.*

Three individual events with heavy rainfall on days 261, 264, and 267 are shown in more detail in figure 3.20. The first event on day 261 is an afternoon rainfall event lasting about 2 hours with an accumulation 30mm, a relatively low mean wind speed of 3.8 m/s and a maximum wind gust of 6.7 m/s. The second event on day 264 is a nighttime rainfall with two squalls of rain combining 50mm of rain. The mean wind speed and wind gust are also relatively low. The third event is a pre-dawn rainfall event with more than 100 mm accumulation and high mean wind speed and wind gust, 8.7 m/s and 10.2 m/s, respectively. The sub-surface salinity, temperature, and salinity data at 1, 5, and 10 m are given in the second, third, and fourth panel. The rain plumes are relatively fresh and cool. The incoming shortwave and outgoing long-wave radiation is shown on the fifth panel. The rainfall data from the ARG and RMY rain gauges are given in the panel 6. The acoustic rainfall rate is given in 1 min interval, and the RMY is given in 10 min. Thus the acoustic rainfall shows larger rain rate than the RMY. The wind speeds are given in the last panel with both acoustic and surface anemometer data shown.

The freshwater penetration rate are calculated using the lagged correlation between acoustic rainfall rate and subsurface salinity data at each depth (Fig. 3.21-3.23). The first event (Fig. 3.21) has an accumulation about 30 mm. The lagged correlation indicates that the fresh water takes 4 hours to mix down to the 1m deep, 12 hours to 5 m, and 22 hours to 10m. The penetration rates are subjectively calculated by inspecting the dipping feature of salinity records at each depth. The penetration rate in this event is 25 cm/hr to a depth of 1m, and 38 -43 cm/hr to penetrate from 1 to 10m. For the second event, two squalls of rain are present (Fig. 3.22). The combined rainfall squalls make the determination of fresh water penetration difficult to interpret. However, high correlations still can be seen. The highest correlation at 1m, 5m, and 10m are after 6, 7, and 14 hour lags, respectively. The salinity record at top 1 m shows several large correlations with acoustic rainfall, thus the penetration rate is not calculated. The penetration rate from 1 to 10m is about 84-100 cm/hr. Note that at 20 hours after the event the fresh water salinity feature suddenly disappears at all 3 depths. This suggests that lateral advection of the fresh water puddle from this event away from mooring has occurred. The third event has

a heavy downpour with maximum rainfall rate of 155 mm/hr (Fig. 3.23). The lagged correlations show quick mixing down to 5 m just 1 hour after the peak of rainfall, and down to 10 m after 3 hours. And there is even suggestion of penetration to 20m. The penetration rate is 125 cm/hr at 1m, 180 cm/hr at 5m, and 335 cm/hr at 10m.

The minimum fresh water required for the observed salinity change can be estimated by assuming the water layers are well mixed at the maximum salinity dips.

$$Accum \geq \frac{\Delta S}{S_o} \times D \tag{3.6}$$

where *Accum* is the fresh water accumulation requirement for the salinity anomaly, $\Delta S$ is the maximum salinity anomaly during the rainfall event, $S_o$ is the salinity prior to the rain started, and $D$ is the depth of the observation. This assumes that all of the fresh water is between the surface and the depth of the measurement and that there is no lateral advection or diffusion of the fresh water. The *Accum* estimates are given in table 3.7 for event 1 and 3. The maximum salinity anomaly observed at 1m for the first event needs 60 mm, which is twice the event accumulation, but at 5 and 10m depths the fresh water input requirement matches the observations. This suggests slow, steady mixing of the rainfall downward. In contrast, during the third event the freshwater needed for the salinity anomaly observed at 1 m is 45 mm which is about half of the event accumulation. However, at 5 and 10m, the required fresh water input matches the measurements. This suggests quick mixing to depths greater than 1 meter, which given the high winds that are present, is a reasonable conclusion.

There are about 216 events during the rainy season (using 20 min separation) at 10°, 95°W in year 2001. The overall rainfall and salinity correlations are given in the figure 3.24. The correlation reaches its maximum at 4 hours lag at 1m, 8 hour lag at 5 m, and 20 hours lag at 10m. By applying the preceding analysis to all the events, general picture of how fast the fresh rain water penetrates into the ocean is observed. The

penetration rate is about 25-200 cm/hour to 1 m depth, and 65cm/hour to 5 and 10 m depths. The correlation at 20 m depth does not appear to be correlated with individual rainfall. These results are summarized in table 3.7. In summary, these rain events produce fresh water that stay on the surface for couple hours after the rain stops. The fresh water is mixed downward at a rate of 65 mm/hr, but can be as high at 300 cm/hr during high wind conditions. Generally, there is no evidence of fresh water penetration from individual events at 20m, but a very large fresh water event with high winds and rapid mixing can occasionally be detected at 20m (Fig. 3.23). Wind appears to be the primary driving force for the rate of penetration of vertical mixing of fresh water to at least 10m depth.

*Table 3.7 Three heavy rainfall events at 10°N, 95°W*

| | All events | Event 1 Day 261 | Event 2 Day 264 | Event 3 Day 267 |
|---|---|---|---|---|
| Time (year day) | 115 - 269 | 261.7 – 262.7 | 264.2 – 265.2 | 267.2 – 268.2 |
| Rainfall type | --- | afternoon | nighttime | pre-dawn |
| Maximum rain rate | 373 | 68.8 | 81.2 | 155.6 |
| Mean wind speed (m/s) | 4.7 | 3.81 | 3.4 | 6.27 |
| Maximum wind gust (m/s) | --- | 6.3 | 8.8 | 10.7 |
| Rainfall accumulation (mm) | 1691 | 31.2 | 50.3 | 102.8 |
| Penetration rate 0-1m | 25-100 cm/hr | 25 cm/hr | --- | 125 cm/hr |
| Penetration rate 1-5m | 65 cm/hr | 38 cm/hr | 84 cm/hr | 180 cm/hr |
| Penetration rate 5-10m | 65 cm/hr | 43 cm/hr | 100 cm/hr | 335 cm/hr |
| Minimum fresh water estimates 0-1m | --- | > 60 mm | --- | > 45 mm |
| Minimum fresh water estimates 1-5m | --- | > 30 mm | --- | > 75 mm |
| Minimum fresh water estimates 5-10m | --- | > 30 mm | --- | > 120 mm |

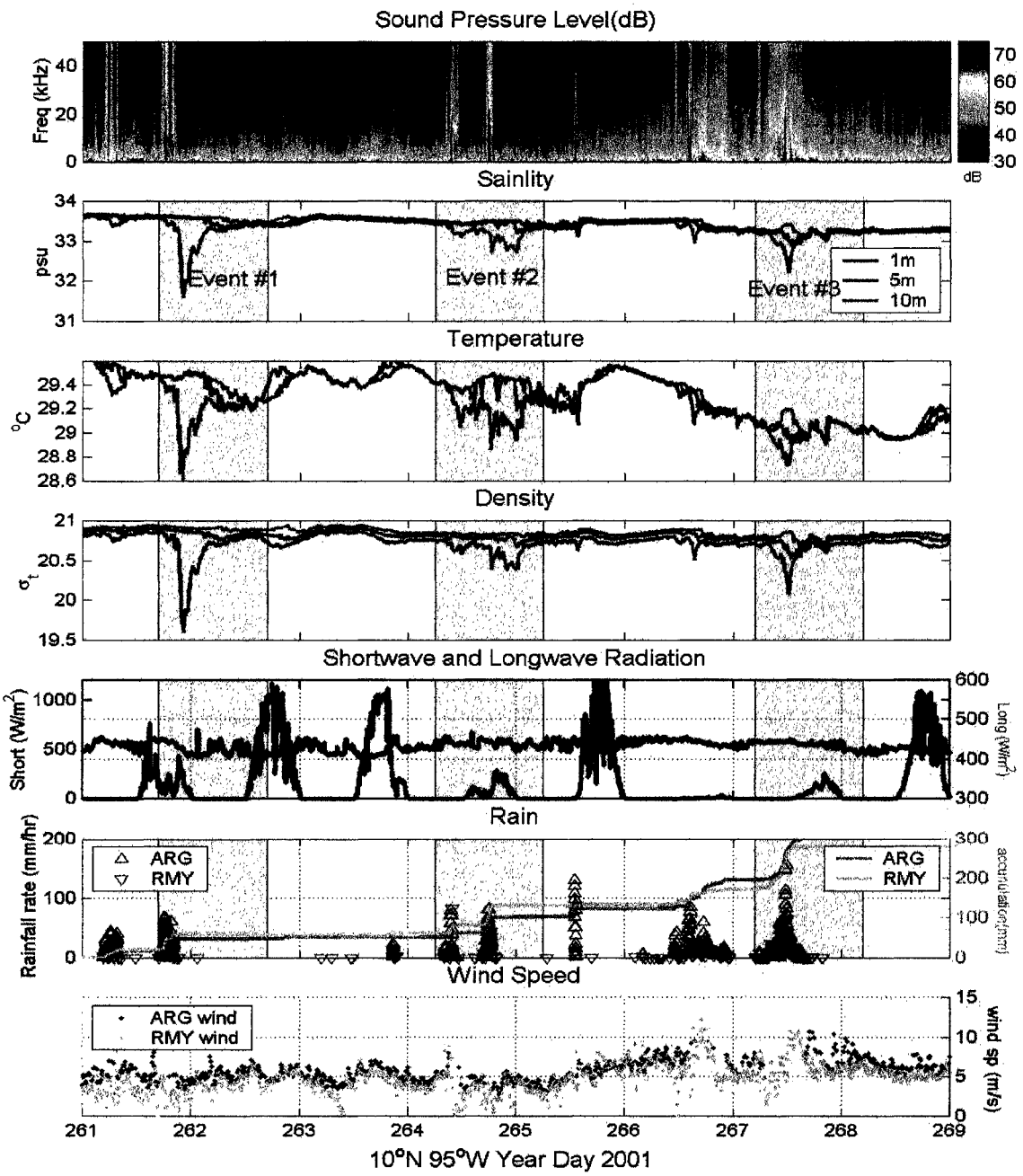


*Figure 3.20 Three heavy rainfall events at late September, 2001 at 10°N, 95°W. The first panel shows the acoustic ambient sound level. Second panel shows the salinity. Third panel shows temperature. Fourth panel shows density derived from salinity and temperature. Fifth panel shows the incoming shortwave radiation and net outgoing longwave radiation. Sixth panel shows 1-min acoustic rainfall and 10-min RMY rainfall. Seventh panel shows the wind speeds from both acoustic and surface anemometer.*

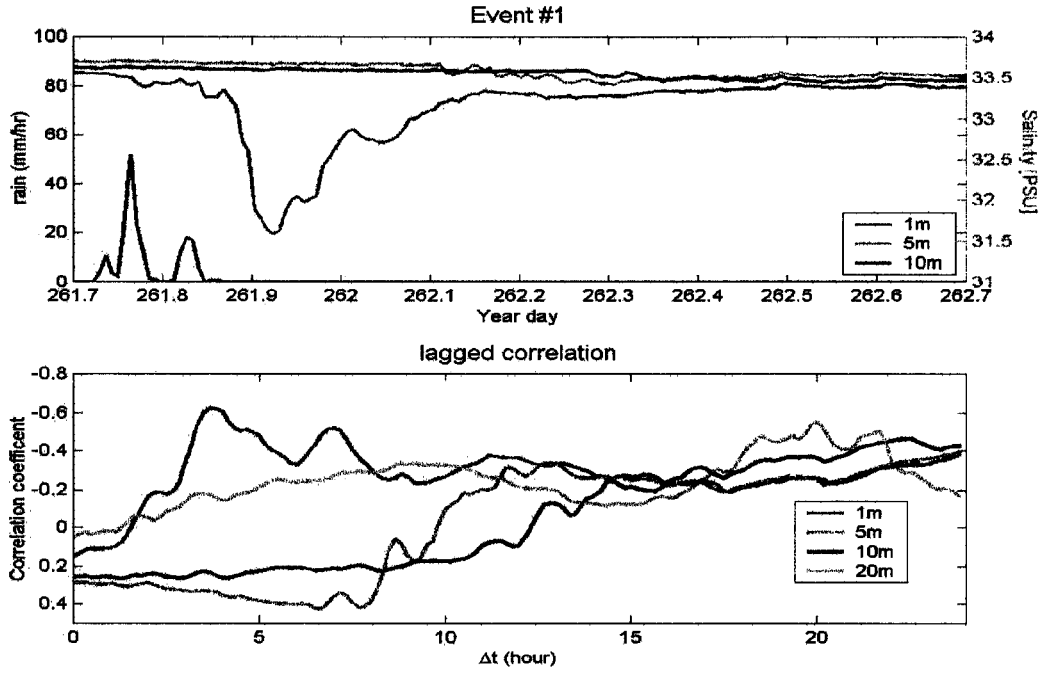


*Figure 3.21 The correlations of a day-time rainfall and salinity at Day 261.*

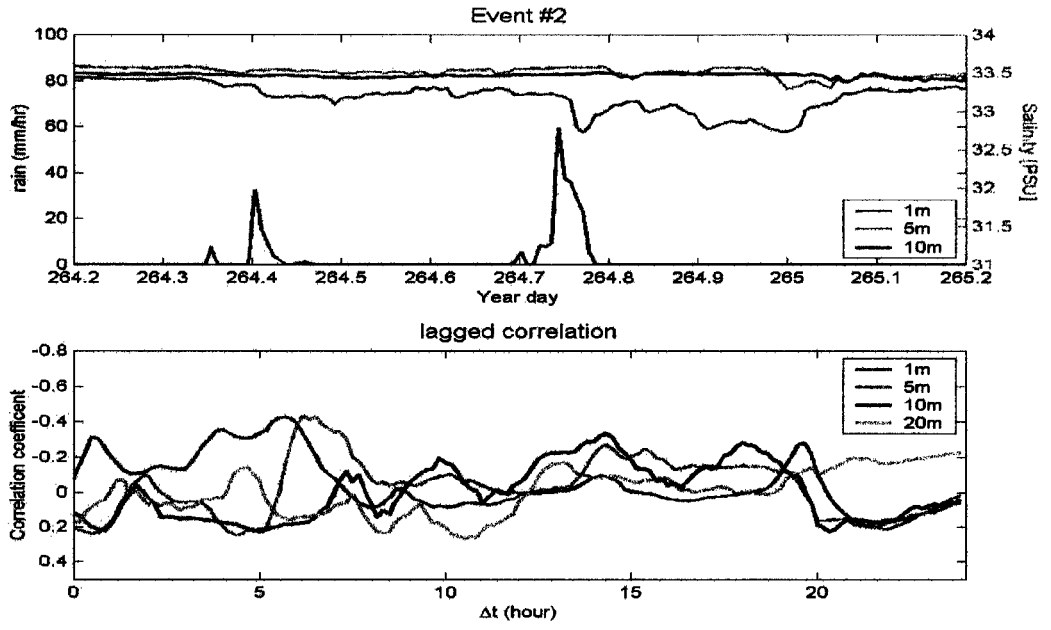


*Figure 3.22 The correlations of a night-time rainfall and salinity at Day 264.*

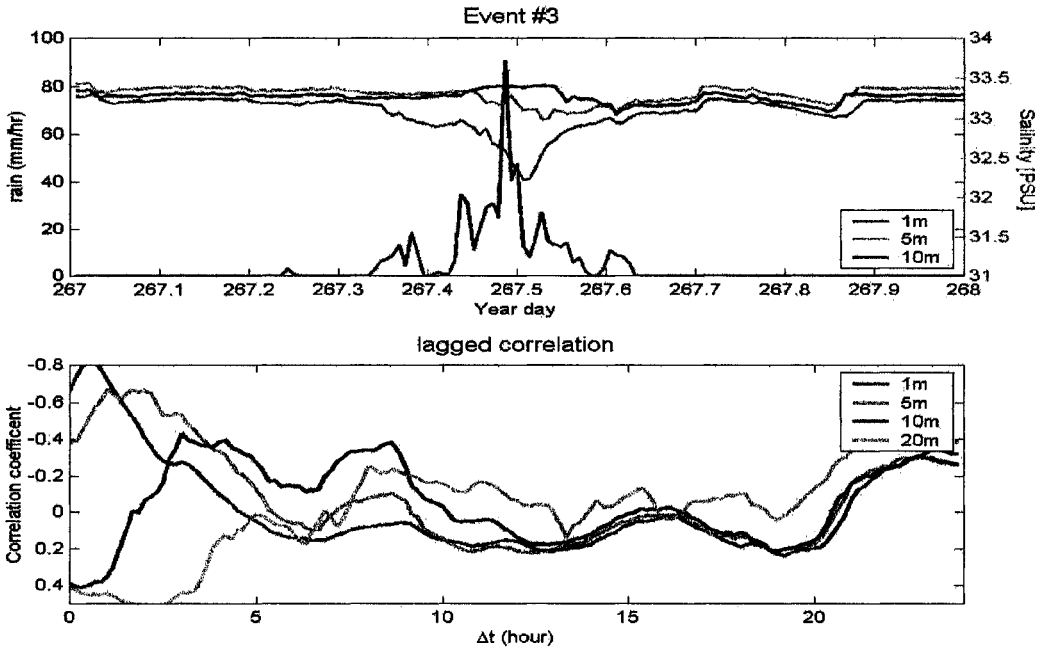


*Figure 3.23 The correlations of a pre-dawn rainfall and salinity at Day 267.*

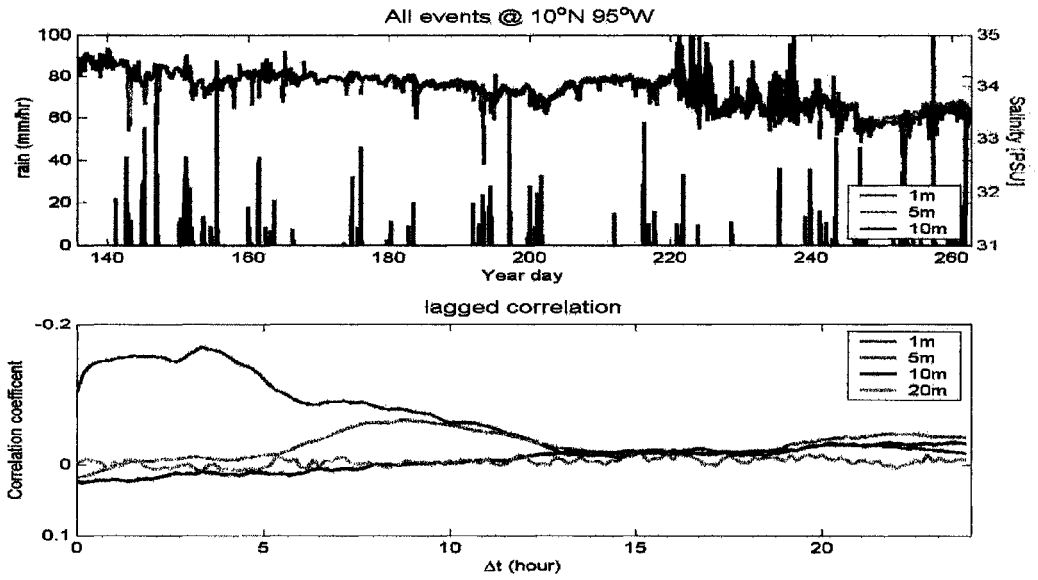


*Figure 3.24 The overall correlations of rainfall and salinity.*

## Chapter 4: Summary and conclusions

The rainfall measurement over the ocean using ambient sound relies on the accuracy of sound pressure level measurement. A calibration method is demonstrated by using the expected sound signal from the wind. Using months of co-located wind speed data, the sensitivity bias and instrument noise for each ARG are derived, providing a frequency-dependent sensitivity correction. After applying this sensitivity correction, an empirical rainfall conversion algorithm based on the sound levels of a single frequency (5 kHz) is proposed and tested on year long deployments at 10°N, 95°W and 12°N, 95°W in 2001. The results show the excellent agreement between ARGs and R. M. Young rain gauges at the time scale of rainfall events and longer. At shorter time scales, the sampling differences between satellite and both in situ instruments (ARG and RMY) prevent agreement. However, at monthly to seasonal time scales there is also good agreement between TRMM satellite data and the ARGs.

The effect of wind on the acoustic signal from rain is examined and shows that the rain signal is wind speed dependent at some frequencies, but not at all frequencies. At lower frequencies, the signal from rainfall becomes "contaminated" by the sound produced from wind-generated waves breaking. The unique spectral feature of light rain, a peak in the spectrum at 15-25 kHz is affected by wind. This spectral peak is due to the sound generated by small raindrops within the rain and is not a reliable indication of rainfall rate, but can be used to detect rainfall, even light drizzle. Above 30 kHz, the sound levels for high rainfall rates are observed to decrease as the wind speed increases. This is likely to be due to the attenuation of the rainfall signal by ambient bubbles that have been stirred down into the ocean and act as an absorption layer for an acoustic measurement made below the bubbles. The frequency band from 2 to 10 kHz is relatively invariant to wind speed and is therefore chosen as the frequency band to quantify rainfall rate.

Given wind speed and rainfall, it is possible to predict the ambient sound levels in the ocean. A physically-based empirical algorithm is constructed using ocean ambient sound collected from ITCZ and is compared with observation data from the Western Pacific warm pool. Different frequency bands are treated separately as the characteristics of sound generating by rain and wind differ within several frequency bands. The wind only generated sounds have a constant slope -15.7 dB/decade from 1 to 50 kHz. Thus the wind components of the spectra can be generated using Vagle's wind speed algorithm at 8 kHz plus a slope component. The rainfall spectra are constructed separately for the 1-10 kHz and 10-50 kHz bands. The spectra slope for rainfall-generated sound from 1 to 10 kHz linearly increases as rainfall rate increases. Thus, the rainfall spectra at 1-10 kHz can also be generated using a single frequency (5 kHz) rainfall rate algorithm (Eqn 1.17) plus a slope component. For the 10-50 kHz rain spectra, the drizzle produces a unique spectra peak at 15 kHz that is inversely proportional to the wind speed. By combining discrete bins of wind speed and rainfall rate, this part of the spectrum is modeled using a five coefficient empirical fit. Overall, with two universal input parameters, wind speed and rainfall rate, this model provides a means to predict the oceanic sound levels from 1 to 50 kHz for wind from 2 to 14 m/s and rainfall rate from 2 to 200 mm/hr.

The acoustic method is applied to data collected in the ITCZ during EPIC 2001 to describe the rainfall climatology of the region. The acoustic measurements show an intermittency in time that is consistent with spatial patchiness shown by radar. Combining the rainfall detections into events is useful for rainfall climatology studies. An event is defined based on the temporal characteristics of rainfall detection. This definition produces a mean event description as 35 minutes with 8 mm of rainfall accumulation for the EPIC 2001. The mode of the distribution is 11 minutes. However, the distribution contains large event outliers; events with duration greater than an hour contain 50 % of the annual accumulation. In contrast, rainfall in the Western Pacific (at 0° 165°E) has mostly smaller events (mean duration 18.6 min with 4.6 mm accumulation). Interestingly, the mean rainfall rate when it is raining is about 15 mm/hr for both locations.

An attempt to describe the penetration of fresh water into the upper ocean is undertaken. Measurements of a point location are necessarily one dimensional and can not completely describe the full situation with advection moving patchiness of salinity distribution laterally. However on the time scale of hours, penetration into the surface is observed and is documented. Rainfall anomalies are typically fresh and cool. The penetration rate is typically 25-200 cm/hr to 1 meter and 65 cm/hr to 5-10 meters. High wind appears to be the dominant factor controlling the vertical mixing rate.

The acoustic measurement of oceanic rainfall is an innovative method for detecting and quantifying oceanic rainfall. It has a large sampling area compared with traditional accumulation type rain gauges; and is deployed underwater away from the potential catastrophic environment of air-sea interface. However it is still a point measurement when one considers the size of the ocean. Thus full spatial coverage of the distribution of oceanic rainfall will require the application of satellite-based measurements. However, acoustic measurement of rainfall will provide surface truth for the satellite rainfall measurements.

**Bibliography:**

Applied Physics Laboratory, University of Washington, 1994: APL-UW High-Frequency Ocean Environmental Acoustic Models Handbook, *Applied Physics Laboratory Technical Report*, TR9407.

Atlas, D., C. Ulbrich, F. D. Marks Jr., E. Amitai, and C. R. Williams, 1999: Systematic variation of drop size and radar-rainfall relations. *J. Geophys. Res.*, **104**(D6), 6155-6169.

Black, P. G., J. R. Proni, J. C. Wilkerson, and C. E. Samsury, 1997: Oceanic rainfall detection and classification in tropical and subtropical mesoscale convective systems using underwater acoustic methods. *Mon. Wea. Rev.* **125**, 2014-2024.

Cronin, M. F., M. J. McPhaden, 1998: Upper ocean salinity balance in the western equatorial Pacific, *J. Geophys. Res.*, **103**(C12), 27567-27588, 10.1029/98JC02605.

Cronin, M. F., and J. Sprintall. 2001: Wind and buoyancy-forced upper ocean. In: J. Steele, S. Thorpe, and K. Turekian (eds.) *Encyclopedia of Ocean Sciences*, Vol. 6, 3219-3227, Academic Press, London, UK.

Fairall, C. W., E. F. Bradley, D. P. Rogers, J. B. Edson, and G. S. Young, 1996: Bulk parameterization of air-sea fluxes for Tropical Ocean-Global Atmosphere Coupled-Ocean Atmosphere Response Experiment. *J. Geophys. Res.* **101**, 3747-3764.

Farmer, D. M., and D. D. Lemon, 1984: The influence of bubbles on ambient noise in the ocean at high wind speeds, *J. Phys. Oceanogr.*, **14**, 1762-1778

Farmer, D. M., C. McNeil, and B. Johnson, 1993: Evidence for the importance of bubbles to the enhancement of air–sea gas flux, *Nature*, **361**, 620–623.

Freitag, H.P., M. O'Haleck, G. C. Thomas, and M. J. McPhaden, 2001: Calibration procedures and instrumental accuracies for ATLAS wind measurements. *NOAA. Tech. Memo. OAR PMEL*-**119**, NOAA/Pacific Marine Environmental Laboratory, Seattle, Washington, 20 pp.

Ho, D. T., C. J. Zappa, W. R. McGillis, L. F. Bliven, B. Ward, J. W. H. Dacey, P. Schlosser, and M. B. Hendricks, 2004: Influence of rain on air-sea gas exchange: Lessons from a model ocean, *J. Geophys. Res.*, ***109***, C08S18, doi:10.1029/2003JC001806.

Houze, R. A., Jr., 1989: Observed structure of mesoscale convective systems and implications for large scale heating. *Quart. J. Roy. Meteor.* Soc., **115**, 425-461.

Knudsen, V. O., R. S. Alford, and J. W. Emling, 1948: Underwater ambient noise. *J. Mar. Res.,* **7**, 410-429.

Ma, B. B., and Nystuen, J. A. 2004: Passive acoustic detection and measurement of rainfall at Sea, *J. Atmos. and Oceanic Tech.* in press.

Marshall, J. S., and W. M. Palmer 1948: The distribution of the raindrops with size, *J. Meteorol.*, ***5***, 165–166.

Medwin, H., and M. M. Beaky, 1989: Bubble sources of the Knudsen sea noise spectrum. *J. Acoust. Soc. Amer.*, **86**, 1124-1130

Medwin, H., A. Kurgan, and J. A. Nystuen, 1990: Impact and bubble sound from raindrops at normal and oblique incidence, *J. Acoust. Soc. Am.* **88**, 413-418

Medwin, H., J. A. Nystuen, P. W. Jacobus, D. E. Snyder, and L. H. Ostwald, 1992: The anatomy of underwater rain noise, *J. Acoust. Soc. Am.* **92**, 1613-1623

Medwin, H., and C.S. Clay, 1998: *Fundamentals of Acoustical Oceanography.* Academic Press, 712 pp.

McPhaden, M.J., A. J. Busalacchi, R. Cheney, J. R. Donguy, K. S. Gage, D. Halpern, M. Ji, M. Julian, G. Meyers, G. T. Mitchum, P. P. Niiler, J. Picaut, R. W. Reynolds, N. Smith, and K. Takeuchi, 1998: The Tropical Ocean-Global Atmosphere (TOGA) observing system: A decade of progress. *J. Geophys. Res,* **103**, 14,169-14,240.

Milburn, H.B., P. D. McLain and C. Meinig, 1996: ATLAS buoy - Reengineered for the next decade. *Proc. IEEE Oceans'96*, Fort Lauderdale, FL, Institute of Electrical and Electronics Engineers, 698-702.

Nystuen, J. A., 1993a: An explanation of the sound generated by light rain in the presence of wind, *Natural physical sources of underwater sound*, B. R. Kerman, Ed., Kluwer Academic Publishers, 659-668

Nystuen, J. A., C. C. McGlothin and M.S. Cook, 1993b: The underwater sound generated by heavy rainfall, *J. Acoust. Soc. Am.* **93**, 3169-3177

Nystuen, J. A., and H. Medwin, 1995: Underwater sound produced by rainfall: Secondary splashes of aerosols, *J. Acoust. Soc. Am.* **97**, 1606-1613

Nystuen, J. A., 1996: Acoustic rainfall analysis: Rainfall drop size distribution using the underwater sound field. *J. Atmos. And Oceanic Tech.*, **13**: 74-84.

Nystuen, J. A., and H. D. Selsor, 1997: Weather classification using passive acoustic drifters, *J. Atmos. Oceanic Technol.*, **14**, 656-666.

Nystuen, J. A., M. J. McPhaden, and H. P. Freitag, 2000: Surface measurements of precipitation from an ocean mooring: The Acoustic Log from the South China Sea. *J. Appl. Meteor.* **39**, 2182-2197.

Nystuen, J. A., 2001: Listening to raindrops from underwater: An acoustic disdrometer. *J. Atmos. and Oceanic Tech.* **18**, 1640-1657.

Nystuen, J. A., and E. Amitai, 2003: High temporal resolution of extreme rainfall rate variability and the acoustic classification of rainfall, *J. Geophys. Res.* **108**(D8), 8378, doi:10. 1029/2001JD001481, 2003.

Olsen, R. L., D. V. Rogers, and D. B. Hodge 1978: Arb relation in calculation of rain attenuation, *IEEE Trans. Antennas Propag.*, ***26***, 318–329.

Pumphrey, H. C., L. A. Crum, and L. Bjorno, 1989: Underwaer sound produced by individual drop impacts and rainfall. *J. Acoust. Soc. Amer.*, **85**, 1518-1526

Serra, Y., P. A. Hearn, H. P. Freitag, and M. J. McPhaden. 2001: ATLAS Self-siphoning rain gauge error estimates. *J.Atmos.and Oceanic Tech,.***18**, 1989-2002

Urick, R. J., 1983: *Principles of Underwater Sound,* third ed. McGraw-Hill, 423 pp.

Vagle, S., W. G. Large, and D. M. Farmer, 1990: An evaluation of the WOTAN technique for inferring oceanic wind from underwater sound. *J. Atmos. and Ocean. Tech.* **7**, 576-595.

Weller, B., B. Albrecht, S. Esbensen, C. Eriksen, A. Kumar, R. Mechoso, D. Raymond, D. Rogers, and D. Rudnick, 1999: A Science and Implementation Plan for EPIC: An Eastern Pacific Investigation of Climate Processes in the Coupled Ocean-Atmosphere System. *EPIC program document.*

Wenz, G. M., 1962: Acoustic ambient noise in the ocean: Spectra and sources. *J. Acoust. Soc. Amer.*, **34,** 1936-1956

Yuter, S., K. Comstock, R. Wood, and C. Bretherton, 2003: Mesoscale variability of Stratocumulus clouds and drizzle. *EPIC workshop 2003 poster, Boulder, CO*

## Appendix A

### Sensitivity bias and instrument noises correction

Absolute sound levels are required in order to apply geophysical conversion relationships such as equation 1.12 and equation 1.17. And while hydrophone manufacturers provide frequency-dependent sensitivity curves, these curves are for an isolated transducer in a free field. Once the transducer is installed in an instrument, the mounting geometry of the instrument may produce a change in the sensitivity. Furthermore, the geophysical signal for rainfall or wind (breaking waves), is assumed to be a uniformly distributed planar source (the ocean surface) rather than a point source, typically used in laboratory calibration. Consequently, the frequency-dependent sensitivity curve is calculated post-deployment using two assumptions. First, that the wind curve of Vagle et al. (1990) is universal and second, that the slope of the wind generated sound spectrum is not a function of wind speed. Ultimately these assumptions will be justified by observing that the resulting rainfall rate relation (Eqn. 1.17) is also universal. The steps in finding sensitivity curve are as follow:

#### *a. Clean the data for non-wind noise*

Data records initially identified as wind are treated separately from the rain and drizzle data. The shape of each spectrum is inspected to identify noise. Five "noise" removal schemes are applied, including "low-noise", "high-noise", "slope-problem", "steep-problem", and "contaminated". Signals not consistent with expected geophysical signals (rain, wind, and drizzle) and called "noise" for the purpose of making geophysical measurements.

**Low noise** — If $SPL_{2\text{-}4\,kHz}$ is greater than $SPL_{5kHz}$ plus 5dB, and $SPL_{2\text{-}4kHz}$ is greater than 60 dB.

**High noise** — If $SPL_{15\text{-}20kHz}$ is smaller than $SPL_{20\text{-}30kHz}$ and $SPL_{15\text{-}20\ kHz}$ is greater than 35 dB.

**Slope problem** — If $SPL_{2\text{-}4kHz}$ is smaller than $SPL_{5kHZ}$, or $SPL_{5kHz}$ is smaller than $SPL_{6\text{-}9\ kHz}$, or $SPL_{6\text{-}9\ kHz}$ is smaller than $SPL_{10\ kHz}$, or $SPL_{10kHz}$ is smaller than $SPL_{15\text{-}20\ kHz}$.

**Steep problem** — If $SPL_{5\ kHz}$ minus $SPL_{10\ kHz}$ is greater than 10 dB.

**Contaminated** — If $SPL_{20\ kHz}$ is greater than 50 dB (not wind only spectrum).

Figure A1 shows some individual examples of such noise. The non-geophysical signals could be produced by the "noise" from the mooring lines or water splashing on the buoys, or biological sources.

***b. Remove low wind data.***

There is no wind-generated signal present. This means that the acoustic signal recorded is a combination of electrical instrument noise and location-dependent background ocean noise. The wind speed is assumed to be less than 3 m/s.

***c. Identify sensitivity bias***

Use the anemometer data to find the expected sound level at 8 kHz using equation 12.

Find the mean difference between these sound levels and the observed sound levels (Fig A2). This offset at 8 kHz is defined to be the sensitivity bias. The bias for ARG "B" is +3.57 dB. The data are offset by this bias.

### *d. Identify frequency dependent instrument noise*

The shape of the wind-generated sound spectrum is independent of wind speed for wind speeds less than about 8 m/s (Vagle et al. 1990). Above 8 m/s an attenuation by trapped bubbles changes the shape of the spectrum (Farmer and Lemon, 1984) at higher frequencies, above 8 kHz. This is shown in figure A3. Using the anemometer wind speeds, the data have been partitioned into wind speed bins: 0-2 m/s. 2-4 m/s, 4-6 m/s, 6-8 m/s, 8-10 m/s, and over 10 m/s.

Small scale frequency structure is present in these spectra. This is assumed to be residual frequency-dependent instrument sensitivity. Using only the bins 2-4 m/s, 4-6 m/s and 6-8 m/s, a linear regression is applied to the averaged spectrum in each bin (Fig. A3). These lines are parallel for 500 Hz – 45 kHz supporting the assumption that the shape of wind-generated sound spectrum is independent of wind speed for this wind speed range (2-8 m/s) (Medwin and Beaky 1989, Vagle et al. 1990). The differences between the regression lines and averaged spectra are further averaged to produce the frequency-dependent instrument noise correction for each ARG (Fig. A4). This procedure could remove a true frequency-dependent structure in the wind- generated sound spectra, associated with the source mechanism (bubbles from breaking waves (Medwin and Beaky 1989). However, the source mechanism for rainfall is different (bubbles from raindrop splashes (Medwin et al. 1992; Nystuen 2001)), and should not show the same fine-scale frequency dependence as the wind. Mean rain-dependent spectra are shown in figure 15 along with mean wind-speed dependent spectra. Neither show the fine-scale frequency dependence of the sensitively correction, confirming that instrument noise has been removed by this procedure and not part of the geophysical signal. The wind speed comparison before and after the sensitivity correction of "B" ARG are shown in the figure A5. The wind speed comparison does not match well before the correction, but after the correction, the agreement is excellent. The daily wind speed comparison of "C" ARG after correction is shown in figure A6, which has very good agreement in both scattering plot and time series. The correlation coefficient and

standard deviation of ARGs converted wind speed and R.M. Young anemometer are shown on table A1.

*Table A1. The correlation coefficient and standard deviation of each data set after the sensitivity correction.*

| ARG | "K" | "B" | "C" | "D" |
|---|---|---|---|---|
| Correlation coefficient | 0.8953 | 0.8122 | 0.8717 | 0.8446 |
| Standard deviation ARGs | 1.547 m/s | 1.5655 m/s | 1.8899 m/s | 1.5908 m/s |
| Standard deviation RMY | 1.6979 m/s | 1.6979 m/s | 1.9536 m/s | 1.7687 m/s |

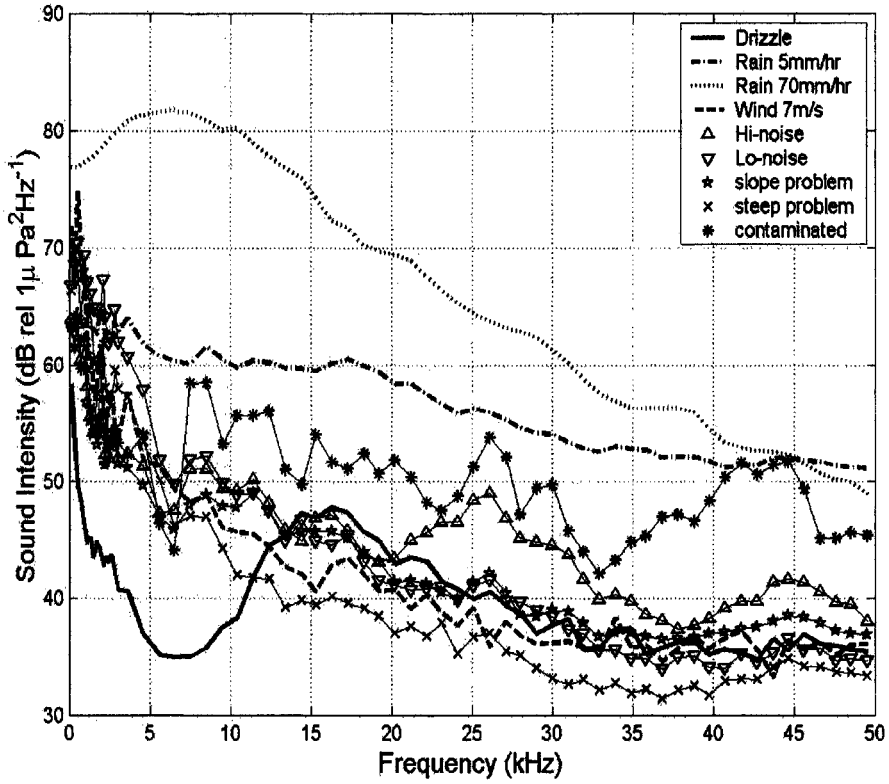


*Figure A1. The typical geophysical acoustic signals and noises. The correspondent symbols are five types of non-geophysical signals, which have been removed from sound field data .*

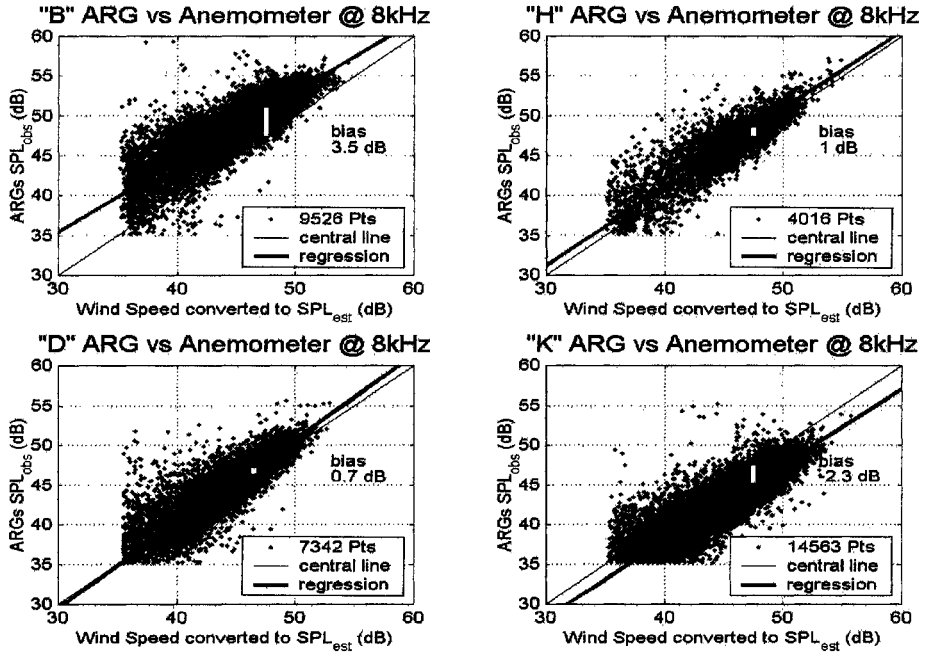


*Figure A2. The sensitivity bias corrections of different ARGs. The $SPL_{est}$ is produced by using equation 1.12, and the $SPL_{obs}$ is from ARGs' measurement at 8 kHz.*

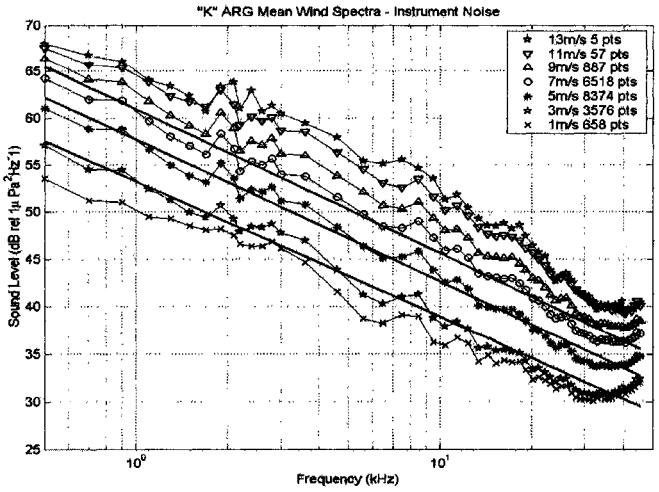


*Figure A3. Mean wind spectra in different wind speed categories. The instrument noise is acquired by applying the linear regression on the 3, 5, 7 m/s wind speed categories and averaged the difference in between regression lines ($SPL_{fit}$) and observed field data ($SPL_{obs}$).*

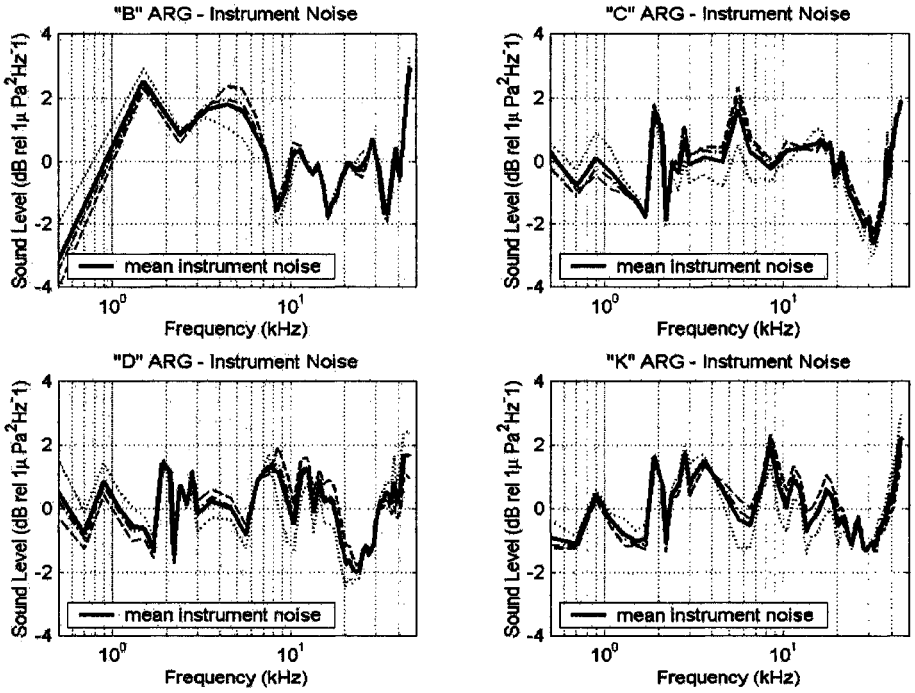


*Figure A4. The darkened lines are the mean instrument noise for each ARG, which acquired from averaging the difference in between $SPL_{obs}$ and $SPL_{fit}$ of wind speed 2-4, 4-6, and 6-8 m/s categories.*

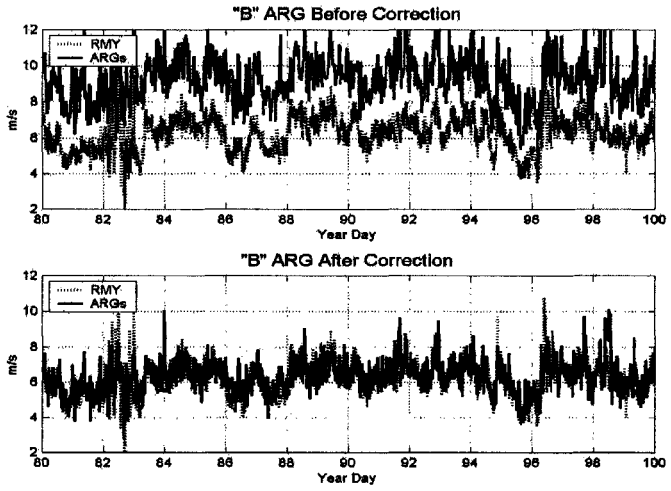


*Figure A5. Before and after sensitivity correction. The wind speed comparison in between "B" ARG and R.M. Young surface anemometer. The top panel is the time series before the sensitivity correction, and the bottom is the time series after the sensitivity correction.*

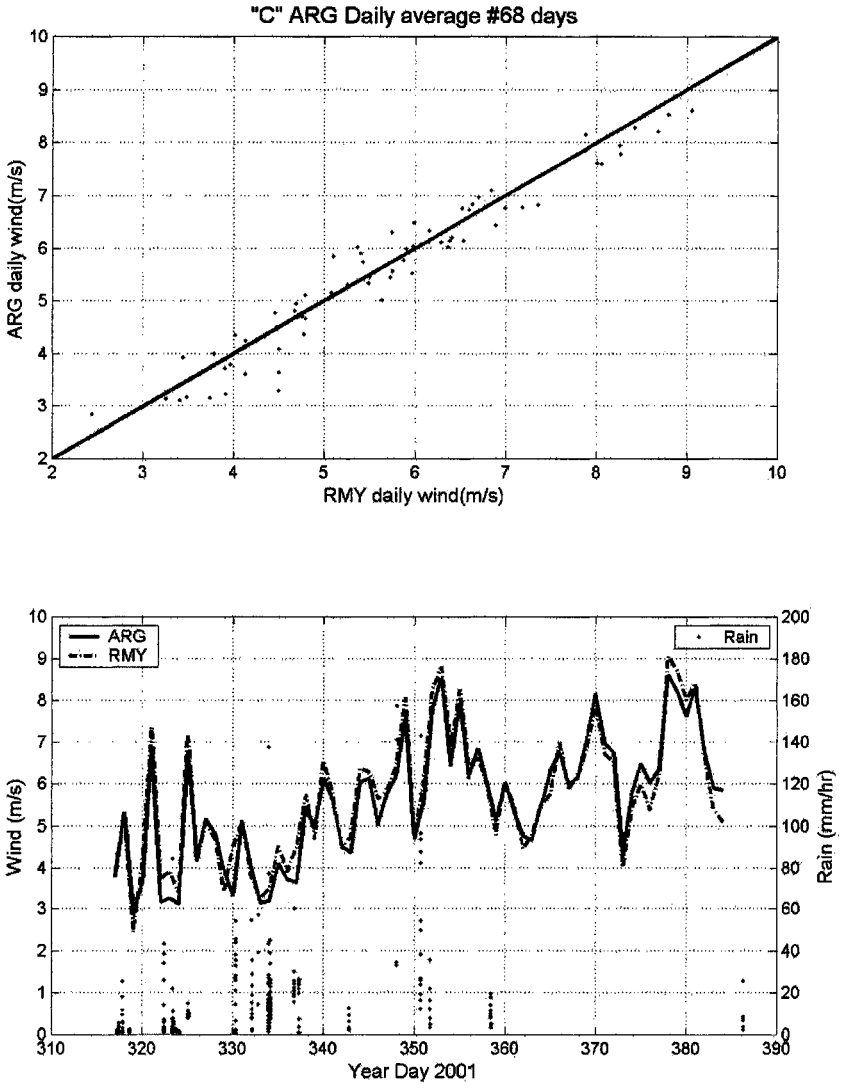


*Figure A6. The "C" ARG daily wind speed comparison after the sensitivity correction. The top panel is the scatter plot of daily wind speed for 68 days. The bottom panel is the daily time series of wind speed comparison. The ARG rainfall rate is also shown with the scale on the right hand side.*

## Appendix B

### Acoustic Discrimination Process

#### *a. Initial sorting of the acoustic data.*

Objective tests on the shape of the spectrum are used to control the time step of data collection in the ARGs. This time step is used to sort the data into three categories: wind (no-rain), drizzle, and rain. For the data considered here, the temporal resolution of wind triggered data is 8-9 minutes with one spectrum stored, drizzle is 3 or 4 minutes with 4 spectra stored, and rain is 1 min interval with 4 spectra stored. These data contains noise from non-geophysical sources. This noise must be identified and removed.

#### *b. Remove the transient sound "bangs" and average over spectra*

Data records initially identified as drizzle or rain can also contain non-geophysical noise. These records are actually recorded as 4 individual spectra separated by 5 second intervals. An assumption is made that the geophysical signal is continuous over this 20 second period. If one of the spectra is significantly louder than the others, then a "bang" is assumed to be present. Two types of "bangs" are defined as follow:

$$\Delta SPL_{5kHz} = \max(SPL_{5kHz}) - \min(SPL_{5kHz}) > 5dB \quad \textit{Low-bang present}$$

$$\Delta SPL_{25kHz} = \max(SPL_{25kHz}) - \min(SPL_{25kHz}) > 5dB \quad \textit{High-bang present}$$

If no "bangs" present, the precipitation record is assumed to be good and is the average of the initial four spectra. If only one of the spectrum has a "bang" (High or Low bangs), then the precipitation record will be the average of the remaining three spectra. If more than one spectra has a bang present, then the record is assumed to be contaminated and is removed. The examples of high and low bangs are shown in the figure B1. In these data,

bangs appear to be associated with time periods when high currents are present at the moorings. This suggests wave slapping on the mooring hull or stress noise associated with the mooring line. The exact source of this type of noise is not known.

### *c. Compare with sample spectrum*

Shape tests are applied to the precipitation generated spectra to remove spectra not consistent with the expected signal of rainfall (Nystuen, 2001). Three sample spectra; heavy (S1), medium (S2), and drizzle (S3) are used to identify the precipitation events. The observed SPL are assumed to be in the range of S1 + 10 dB and S2 −12 dB during the rain, and in the range of S2 and S3-10 dB during the drizzle. The sample spectra are shown in the figure B2.

### *d. Remove non-geophysical signals for precipitation records*

Two noise removal schemes, high noise and low noise, are applied to remove the non-geophysical signals as defined in appendix A, *a.*

### *e. The continuity check of rainfall event*

The combination of drizzle and rain data analysis is necessary to classify the rainfall event. The continuity check is designed to remove any isolated spectrum that may have passed the noise check. The assumption is that a rainfall event must last longer than a single recording interval (1 minute for rain and 3 minutes for drizzle). If no new rainfall signals are recorded within 10 minutes of a single "detection", then that detection is assumed to be false.

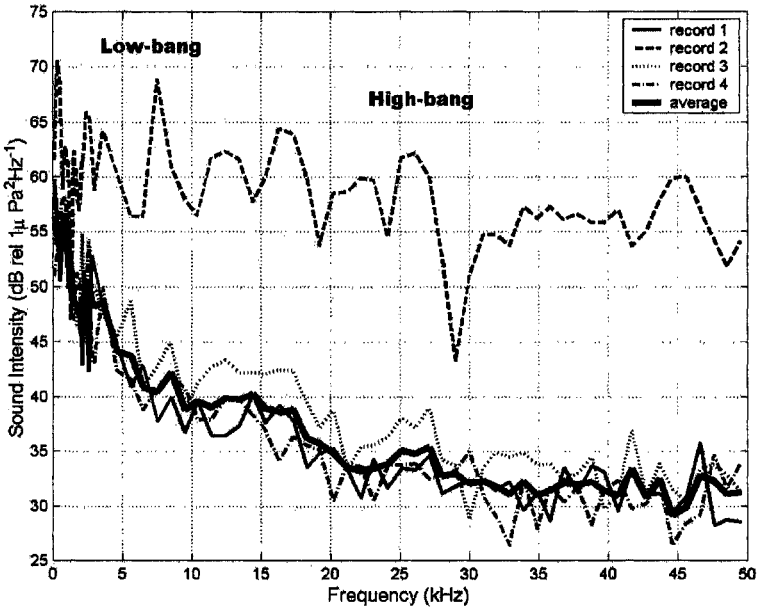


*Figure B1. The example of four spectra for precipitation detection data. Two types of transient noises are defined as high and low bangs, and removed from the averaging process to produce reliable one minute sampling interval records.*

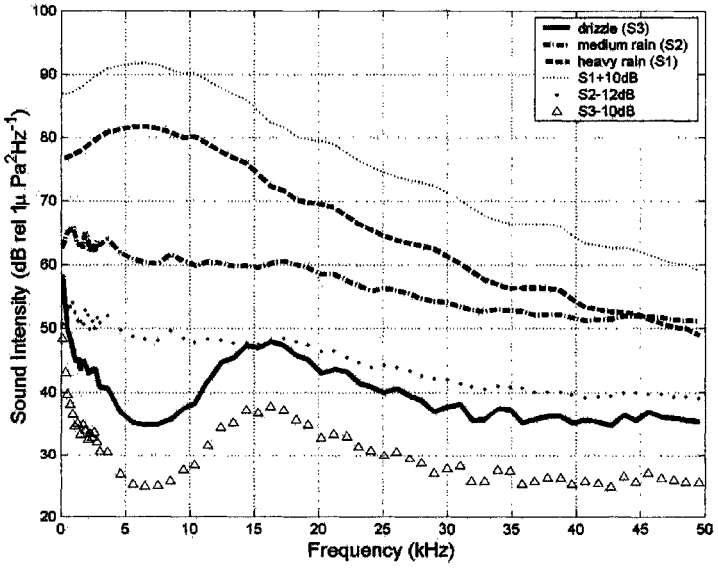


*Figure B2. The sample spectra used for identifying precipitation signals.*

# VITA

Bin-Bing Ma, A.K.A. Barry, was born in Tainan, Taiwan. He is a Lieutenant Commander of Taiwanese Navy. He served in submarine squadron for about ten years including two types of diesel-powered submarines, Guppy II and Zwaardvis-class. He earned a Bachelor degree from Republic of China (Taiwan) Naval Academy in 1988, and a Master degree of Physical Oceanography from the U.S. Naval Postgraduate School in 1996. In 2004 he earned a Doctor of Philosophy at the University of Washington in Oceanography.